

# Geodynamic evolution of Upper Cretaceous Zagros ophiolites: formation of oceanic lithosphere above a nascent subduction zone

HADI SHAFII MOGHADAM\*† & ROBERT J. STERN‡

\*School of Earth Sciences, Damghan University, Damghan, Iran

‡Geosciences Dept., University of Texas at Dallas, Richardson, TX 75083-0688, USA

(Received 30 September 2010; accepted 30 March 2011; first published online 29 June 2011)

**Abstract** – The Zagros fold-and-thrust belt of SW Iran is a young continental convergence zone, extending NW–SE from eastern Turkey through northern Iraq and the length of Iran to the Strait of Hormuz and into northern Oman. This belt reflects the shortening and off-scraping of thick sediments from the northern margin of the Arabian platform, essentially behaving as the accretionary prism for the Iranian convergent margin. Distribution of Upper Cretaceous ophiolites in the Zagros orogenic belt defines the northern limit of the evolving suture between Arabia and Eurasia and comprises two parallel belts: (1) Outer Zagros Ophiolitic Belt (OB) and (2) Inner Zagros Ophiolitic Belt (IB). These belts contain complete (if disrupted) ophiolites with well-preserved mantle and crustal sequences. Mantle sequences include tectonized harzburgite and rare ultramafic–mafic cumulates as well as isotropic gabbro lenses and isolated dykes within the harzburgite. Crustal sequences include rare gabbros (mostly in IB ophiolites), sheeted dyke complexes, pillowed lavas and felsic rocks. All Zagros ophiolites are overlain by Upper Cretaceous pelagic limestone. Limited radiometric dating indicates that the OB and IB formed at the same time during Late Cretaceous time. IB and OB components show strong suprasubduction zone affinities, from mantle harzburgite to lavas. This is shown by low whole-rock  $Al_2O_3$  and CaO contents and spinel and orthopyroxene compositions of mantle peridotites as well as by the abundance of felsic rocks and the trace element characteristics of the lavas. Similarly ages, suprasubduction zone affinities and fore-arc setting suggest that the IB and OB once defined a single tract of fore-arc lithosphere that was disrupted by exhumation of subducted Sanandaj–Sirjan Zone metamorphic rocks. Our data for the OB and IB along with better-studied ophiolites in Cyprus, Turkey and Oman compel the conclusion that a broad and continuous tract of fore-arc lithosphere was created during Late Cretaceous time as the magmatic expression of a newly formed subduction zone developed along the SW margin of Eurasia.

Keywords: Zagros, Iran, ophiolites, Tethys, subduction, Late Cretaceous, fore-arc.

## 1. Introduction

The Zagros orogenic belt (ZOB) of SW Iran extends NW–SE from eastern Turkey through northern Iraq and along SW Iran to the Strait of Hormuz and into northern Oman, accommodating  $\sim 20$  mm yr<sup>-1</sup> of convergence between Arabia and Eurasia (Reilinger *et al.* 2006). In contrast to most other parts of the Alpine–Himalaya mountain chain, convergence with Arabia has not yet obliterated the structure of the hanging-wall fore-arc. Many studies have been done on the structure, origin and geodynamic evolution of the Zagros region (e.g. Alavi, 1980, 2004, 2007; Agard *et al.* 2005; Homke *et al.* 2009). The ZOB is interpreted as the product of three major tectonic events (Alavi, 1994): (1) subduction of the Neo-Tethys Ocean beneath Central Iran during Cretaceous time; (2) emplacement of ophiolites over the Afro-Arabian passive continental margin in Turonian to Campanian time; and (3) collision of the Arabian plate with Iran beginning in mid-Cenozoic time. The ZOB is bounded to the NW by the East Anatolian strike-slip

fault and to the SE by the Oman line (Falcon, 1969). The ZOB formed because of convergence between Arabia and Eurasia, behaving essentially as a subaerial accretionary prism and provides insights into the early stages of collision (e.g. Hatzfeld *et al.* 2003; Vernant *et al.* 2004). Growth of the ZOB reflects the continuing subduction of the Arabian continental crust beneath Iran, which began 10–20 Ma (McQuarrie *et al.* 2003). Several major tectonic events occurred across the ZOB during Late Cretaceous, Late Eocene and Early to Middle Miocene times (Robertson, 2000; Agard *et al.* 2005) with reorganization at  $5 \pm 2$  Ma (Allen, Jackson & Walker, 2004). Abundant ophiolites in the ZOB define the southern Eurasian fore-arc and mark the suture with Arabia, which continues to develop. This ophiolite belt is key for reconstructing the Neo-Tethyan realm from Late Permian rifting to the beginning of collision in Miocene time. It is therefore especially important to understand how and when these ophiolites formed.

The Iranian ophiolites of Zagros are part of a 3000 km long belt that extends from Troodos, Cyprus, to Semail, Oman (Fig. 1). The ophiolites at either end of this belt are the best studied in the world (e.g. Pearce & Robinson, 2010; Dilek & Furnes,

† Author for correspondence: hadishafaii@du.ac.ir; hadishafaii@yahoo.com

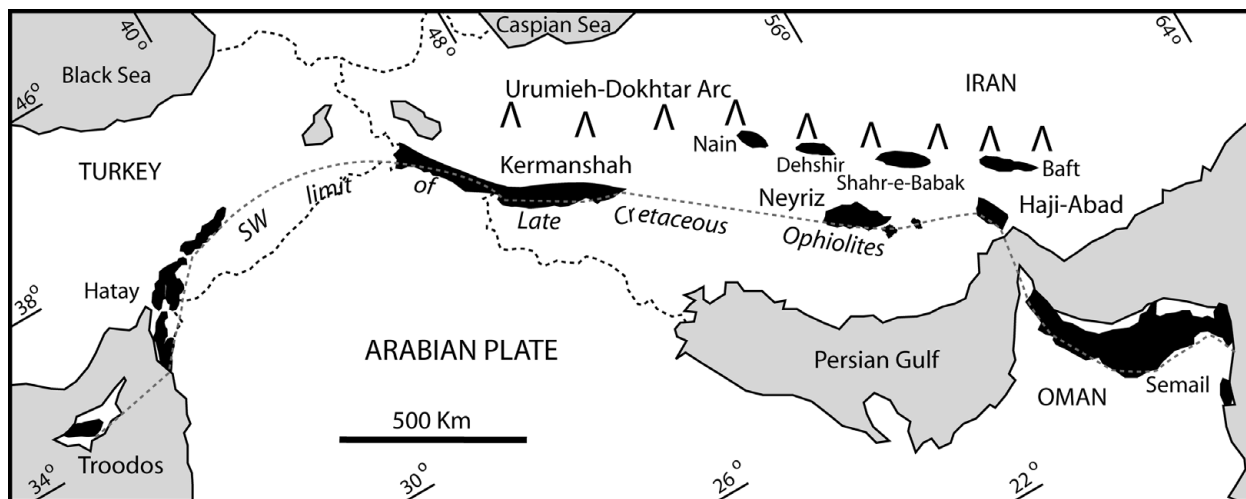


Figure 1. Location of the Zagros Ophiolitic Belt as part of the 3000 km long Upper Cretaceous ophiolite belt of SW Asia between Cyprus and Oman (modified after Blome & Irwin, 1985).

2009; Dilek, Furnes & Shallo, 2007; Garfunkel, 2006; Robertson & Mountrakis, 2006; Godard, Dautria & Perrin, 2003; Godard, Bosch & Einaudi, 2006; Robertson, 2002, 1998; Floyd, Yaliniz & Goncuoglu, 1998; Sengor, 1990; Alabaster, Pearce & Malpas, 1982, among others). In contrast, the Upper Cretaceous ophiolites of the Iranian Zagros (Fig. 2a) are poorly known. Developing a cohesive tectonic model which explains the significance of the Zagros ophiolite belt is a complex task and in particular requires a better understanding of these ophiolites.

Zagros ophiolites can be subdivided into two belts, one south of the Main Zagros Thrust (MZT) fault and the other along the SW periphery of the Central Iranian (Tauride) block (Stocklin, 1977) (Fig. 2a). Hereafter, we use 'Outer Zagros Ophiolitic Belt' (OB) and 'Inner Zagros Ophiolitic Belt' (IB) to describe the parallel belts containing the Kermanshah–Neyriz and Nain–Baft ophiolites, respectively (Fig. 2a, b). The OB includes the Kermanshah, Neyriz and Haji-Abad–Esfandagheh ophiolites, from the NW to SE (Fig. 2a, b). There are many hypotheses to explain the tectonic significance of these ophiolites. The Neyriz ophiolite has been considered both as a piece of Neo-Tethyan oceanic lithosphere generated at the foot of the north Gondwanan passive margin (e.g. Ricou, 1971, 1976; Ricou, Braud & Brunn, 1977; M. R. Jannessary, unpub. Ph.D. thesis, l'Univ. de Louis Pasteur, France, 2003) and as seafloor that was scraped off the down-going plate and incorporated into the Zagros accretionary prism (e.g. Babaie *et al.* 2006). The Kermanshah ophiolite is described as a piece of Tethyan oceanic lithosphere scraped off during NE-directed subduction underneath the Iranian block (e.g. Braud, 1970, 1978; J. Braud, unpub. Ph.D. thesis, Univ. Paris-Sud, France, 1987). The tectonic history of the Haji-Abad–Esfandagheh ophiolites is much more complex. Here, two types of ophiolites coexist: older ones (Upper Triassic–Cretaceous ophiolites) such as the Sikhoran (Ghasemi *et al.* 2002), and younger ones, the Upper

Cretaceous ophiolites, including Haji-Abad, near the MZT fault.

The IB is an ophiolitic mélangé along the SW margin of the Central Iranian block (e.g. Davoudzadeh, 1972; Stocklin, Eftekhari-Nezhad & Hushmandzadeh, 1972; Berberian & King, 1981; Arvin & Robinson, 1994; Arvin & Shokri, 1997). In addition to various hypotheses that have been considered for IB formation (see Shafaii Moghadam, Stern & Rahgoshay, 2010 for further details), these ophiolites are interpreted as para-autochthonous fragments of fore-arc lithosphere that formed when subduction began beneath Iran in Late Cretaceous time (Shafaii Moghadam, Stern & Rahgoshay, 2010). We regard all Upper Cretaceous Zagros ophiolites as well as others in the 3000 km long belt that extends from Cyprus to Oman to result from an episode of subduction initiation on the north side of the Neo-Tethys Ocean. Most Upper Cretaceous Zagros ophiolites are highly disrupted fragments in tectonic mélangé, complicating their study. Some ophiolites from northwestern Iran (such as Khoy–Maku) and Armenia are along-strike continuations of the IB and considered both as IB and OB by some geologists (e.g. Berberian & King, 1981; Khalatbary-Jafary *et al.* 2004). Although describing these ophiolites is beyond the scope of this paper, recent works on the Khoy ophiolite (e.g. Khalatbary-Jafary *et al.* 2004; Azizi *et al.* 2011) and Armenian ophiolites (e.g. Galoyan *et al.* 2009; Asatriyan *et al.* 2010) highlight that these ophiolites are geochemically, geochronologically and geodynamically different from both IB and OB ophiolites.

This paper summarizes our understanding of the geodynamic evolution of the Zagros ophiolites based on the available radiometric ages, field data and geochemistry of mantle peridotites and overlying lavas. We discuss each of the important ophiolitic massifs in both the inner and outer Zagros ophiolitic belts. This overview is intended to provide useful background for geoscientists interested in Upper Cretaceous ophiolites and tectonic

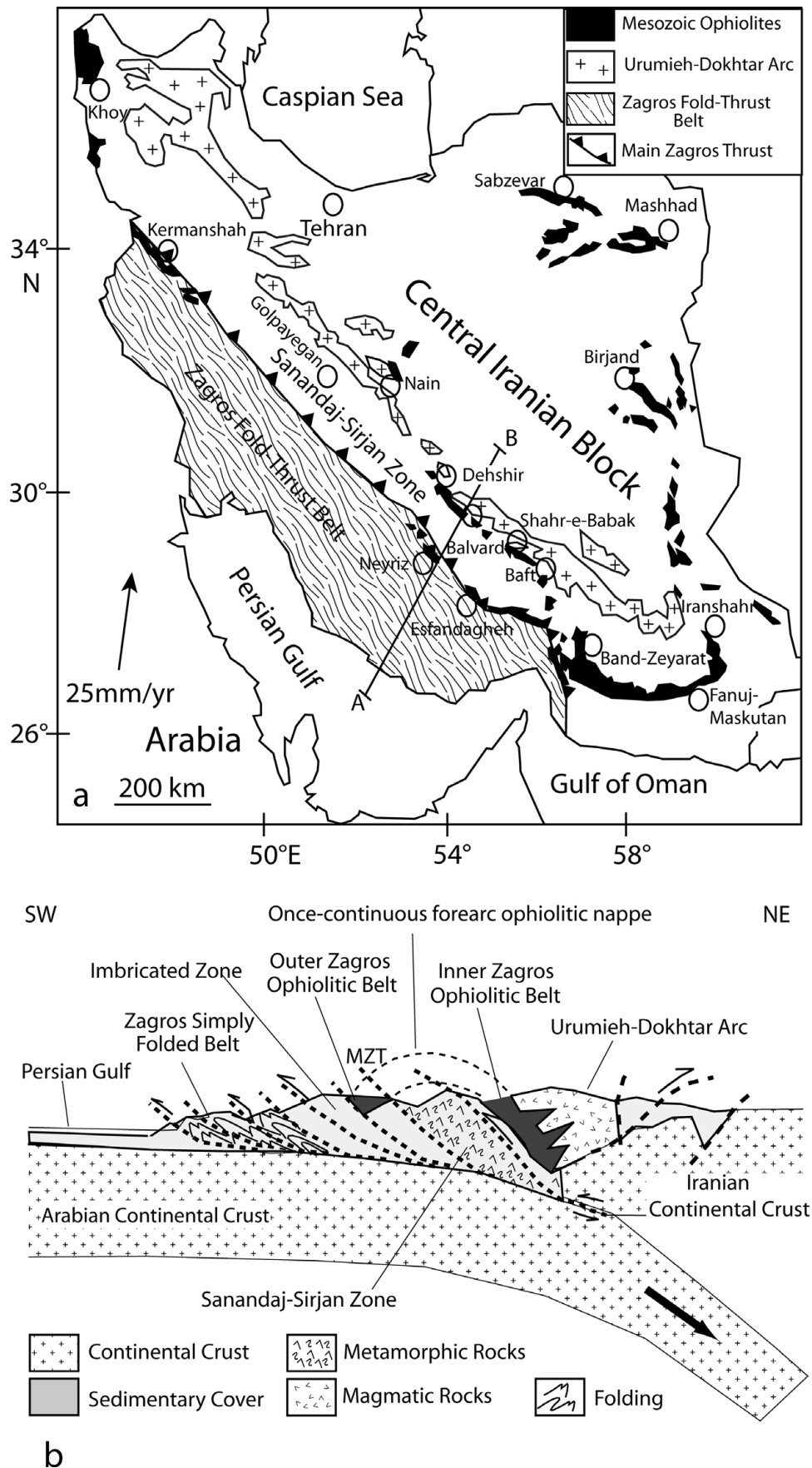


Figure 2. (a) Map showing the distribution of the inner (Nain–Dehshir–Baft–Shahr-e-Babak) and outer (Kermanshah–Neyriz–Haji-Abad) Zagros ophiolitic belts, the location of the Urumieh–Dokhtar magmatic arc (Eocene–Quaternary), and Main Zagros Thrust (MZT). (b) Schematic cross-section showing the relationship between the outer and the inner Zagros ophiolitic belts and the Zagros thrust–fold belt (after Shafäii Moghadam, Stern & Rahgoshay, 2010). Note that the Sanandaj–Sirjan Zone is shown as exhumed subducted material, as discussed in the text.

evolution of the larger Eastern Mediterranean and Persian Gulf region, and to advance discussion of the relationship between subduction initiation and ophiolite formation generally.

## 2. Tectonic evolution of the Zagros orogenic belt: previous reconstructions

The ZOB is bounded to the NW by the East Anatolian strike-slip fault. This left-lateral fault separates the ZOB from the Eastern Taurides of Turkey (Alavi, 2007). Tectonically the ZOB consists of six tectonic zones oriented parallel to the Arabian–Eurasian plate boundary, from undeformed trench fill (in the SW) to a magmatic Andean-type arc (in the NE; Alavi, 1994, 2004, 2007) (Fig. 2b): (1) Mesopotamian Foredeep/Persian Gulf; (2) Zagros fold-and-thrust belt (Zagros active orogenic wedge of Alavi, 2007); (3) Outer Zagros Ophiolitic Belt; (4) Sanandaj–Sirjan Zone (Moritz, Ghazban & Singer, 2006); (5) Inner Zagros Ophiolitic Belt; and (6) Urumieh–Dokhtar magmatic arc (Alavi, 1994). Each zone is bounded by reverse faults. These zones are further described in the next Sections.

### 2.a. Mesopotamian Foredeep/Persian Gulf

The Mesopotamian Foredeep/Persian Gulf is an elongated basin filled with sediments as old as Neoproterozoic along the northeastern subducting margin of the Arabian plate. This basin is asymmetric from NE to SW, with sediments thickening from 4.5 km on the Arabian plate to 18 km beside the MZT (Edgell, 1996). As the Arabian and Eurasian plates converged, passive margin sedimentation on the north side of Arabia evolved into a foreland basin, the Mesopotamian Foredeep, which accumulated thick, coarse clastic sediments as its depocentre migrated through time from NE to SW to its present location in the Persian Gulf (Molinaro *et al.* 2004).

### 2.b. Zagros fold–thrust belt

The Zagros fold–thrust belt (ZFTB) is the external (trenchward) deformed part of the ZOB (Alavi, 1980, 1991, 1994). The ZFTB extends SE for nearly 2000 km from southeastern Turkey through northern Syria and northeastern Iraq to western and southern Iran (Alavi *et al.* 1997). The ZFTB reflects the shortening and off-scraping of thick sediments from the northern margin of the Arabian platform, essentially behaving as the outer part of the accretionary prism for the Iranian convergent margin (Farhoudi & Karig, 1977). Convergence between Arabia and Iran has  $\sim 60^\circ$  obliquity (e.g. McClay *et al.* 2004; Vernant & Chery, 2006; Alavi, 2007); this results in a significant transpressional component of deformation in the ZOB, with dextral strike-slip faulting along NW-trending faults such as the Main Recent Fault. Because the pole of rotation for Arabia–Eurasia convergence lies in the

Eastern Mediterranean, the convergence rate increases eastward along the ZOB, from  $\sim 1.5$ – $1.8$  cm/yr in the NW (McClusky *et al.* 2000) to  $\sim 2.8$  cm/yr to the SE (Sella, Dixon & Mao, 2002). The ZFTB is bounded on the NE by the Main Zagros Thrust (Berberian & King, 1981; Berberian, 1995). The ZFTB is further subdivided across strike into three structural subzones, which largely manifest cumulative shortening increasing to the NE, which are from NE to SW: the Zagros Imbricate Zone (High Zagros); Zagros Simply Folded Belt (Falcon, 1974); and the Zagros Foredeep (which is the same as the Mesopotamian Foredeep/Persian Gulf). The Zagros Imbricate Zone or ‘crush zone’ consists of imbricated tectonic slices of Mesozoic limestones, radiolarites, ophiolites and Eocene volcanic rocks and flysch (Agard *et al.* 2005). The Zagros Simply Folded belt consists of *c.* 13–14 km of shelf deposits of Permo-Triassic to Late Cretaceous/Paleocene age similar to those of the Arabian platform followed by a more complex pattern of sedimentation up to Pliocene time (James & Wynd 1965; Berberian & King 1981). These deposits were folded into a succession of NW–SE-trending folds after Mio-Pliocene time (Agard *et al.* 2005).

### 2.c. Outer Zagros Ophiolitic Belt

The OB includes three main ophiolites, which are, from NW to SE, the Neyriz, Kermanshah and Haji–Abad. These slices are separated by the MZT from the ZFTB. Among outer belt ophiolites, only the Neyriz ophiolite has been studied in much detail. We will briefly discuss these ophiolites in Section 3.a.

### 2.d. Sanandaj–Sirjan Zone

Rocks of the 100–150 km wide Sanandaj–Sirjan Zone (SSZ) make up the metamorphic core of the Zagros (Mohajjel, Fergusson & Sahandi, 2003) and separate the inner and outer ophiolite belts. SSZ rocks span most of Phanerozoic time, including imbricated slices of marine and continental siliciclastic sediments metamorphosed under low- and medium-grade greenschist conditions (Alavi, 1994). Lavas and intrusive bodies accompany these sediments. In many interpretations, the northern continental margin of the Neo-Tethyan Ocean is represented by the SSZ (e.g. Berberian & King, 1981; Sengor, 1990). Following Stocklin (1968), several geologists consider the SSZ as a once-active margin of the Central Iranian block (e.g. Berberian & King, 1981; Sengor, 1990; Sheikholeslami *et al.* 2008; Fazlnia *et al.* 2009) with northeastward subduction of the Tethys Ocean during Late Triassic–Early Jurassic time (Berberian & King, 1981; Davoudzadeh & Schmidt, 1984) or Late Jurassic time (Mohajjel & Fergusson, 2000). Others suppose that the SSZ is an accreted microcontinent that separated from Gondwanaland during Early Jurassic time (e.g. Golonka, 2004; Agard *et al.* 2005). In some of these models the SSZ is a continental fragment

rifted from Arabia and was accreted to Eurasia during Cretaceous time (e.g. Glennie, 2000; Golonka, 2004; Agard *et al.* 2005, 2006). However, Robertson (2007) observed that the rocks of the SSZ cannot be correlated with Arabian rocks.

In the Golpayegan area, to the SE, the SSZ can be subdivided into two parts: (1) the southern part consists of rocks deformed and metamorphosed in Middle to Late Triassic time; and (2) the northwestern part, deformed in Late Cretaceous time, contains many intrusive felsic rocks of mainly Late Cretaceous–Paleocene age (Eftekharnejad, 1981; Rachidnejad *et al.* 2002; Ghasemi & Talbot, 2006). The presence north of Shahr-e-Kord (the southern part of the SSZ) of metabasites, amphibolites and eclogites with mid-ocean ridge (MORB)-like compositions suggests remnants of Neo-Tethyan oceanic lithosphere (Davoudian *et al.* 2006, 2007), thought to be exhumed subduction zone materials. Blueschists are an important component of SSZ rocks in the Haji–Abad area, where Agard *et al.* (2006) documented metamorphic conditions around 11 kbar and 520–530 °C, and laser-ablation <sup>40</sup>Ar/<sup>39</sup>Ar ages on phengite clustering at 85–95 Ma; similar rocks are found in the SSZ near Neyriz (Davoudian *et al.* 2006, 2007). These blueschist occurrences show that some SSZ rocks were subducted and later exhumed. Agard *et al.* (2006) concluded that exhumation of Haji–Abad blueschist was completed by 80 Ma. The Early Eocene uplift and therefore hiatus in overlying sediments of all Zagros ophiolites during Paleocene–Early Eocene time may be a further expression of the exhumation of the Sanandaj–Sirjan accretionary complex. This extension and exhumation of metamorphic rocks of the SSZ has been also suggested by Moritz, Ghazban & Singer (2006).

Because it separates the inner and outer belt ophiolites, the nature of the SSZ, particularly whether or not it was subducted and exhumed in Late Cretaceous–Palaeogene time, is a critical test of the Iranian fore-arc hypothesis of Shafaii Moghadam, Stern & Rahgoshay (2010). In the northern part of Chah Gaz (Zardu 1/100 000 sheet) and Balvard regions, SSZ metamorphic rocks show faulted contacts with Shahr-e-Babak and Balvard–Baft ophiolites (Dimitrijevic, 1973). We think that the metamorphic conditions of SSZ rocks and emplacement between otherwise identical Zagros ophiolite belts supports the idea that these are exhumed subducted materials, which now define an anticlinorium structurally beneath the fore-arc ophiolites (Fig. 2b), as first proposed by Alavi (2004, fig. 5). The SSZ behaves today as a fairly rigid block moving northward at ~14 mm yr<sup>-1</sup> relative to Eurasia (Vernant *et al.* 2004).

### 2.e. Inner Zagros Ophiolitic Belt

Zagros inner belt ophiolites occur in several distinct massifs named after nearby towns. These massifs can be traced along strike for 500–600 km and are, from NW to SE, the Nain, Dehshir, Shahr-e-Babak and Balvard–

Baft ophiolites. These ophiolites are organized as a pile of slices, imbricated during Late Cretaceous time, and cut by strike-slip faults. We will briefly discuss these ophiolites in Section 3.b.

### 2.f. The Urumieh–Dokhtar magmatic assemblage

The Urumieh–Dokhtar magmatic assemblage (UDMA) is a 50–80 km wide Andean-type magmatic belt of intrusive and extrusive rocks formed by northeastward subduction of Neo-Tethyan ocean floor beneath Iran (Falcon, 1974; Berberian & Berberian, 1981; Berberian & King, 1981; Berberian *et al.* 1982; Alavi, 1994; Shahabpour, 2007). This magmatic assemblage includes a thick (~4 km) pile of early calc-alkaline and latest shoshonitic as well as alkaline rocks (Alavi, 1997).

The presence of pyroclastic rocks along with Upper Cretaceous pelagic sediments just above the Baft ophiolite, along with the observation that these pyroclastic rocks thicken to the NE, suggests that the UDMA existed in Late Cretaceous time. In the Zagros Imbricate Zone, there are local thrust slivers which consist of Cretaceous–Tertiary pyroclastic/volcaniclastic strata, interpreted to be distal facies from UDMA activity deposited in a fore-arc basin and later deformed by Zagros thrusting (Alavi, 1997).

## 3. Lithology and rock units of Zagros ophiolites

The principal lithologies and mineral components of Zagros ophiolites are summarized below. Upper Cretaceous Zagros ophiolites consist of fragments that were tectonically disrupted during emplacement and younger deformation and often comprise tectonic mélange, but locally the relationships within ophiolitic units and overlying sediments and flanking units are well preserved.

### 3.a. Outer Zagros Ophiolitic Belt

#### 3.a.1. Kermanshah ophiolite

This is the NW-most outer belt ophiolite in Iran. The ophiolite trends NW–SE and is distributed in two regions, separated by the SSZ metamorphic rocks (see Fig. A1 in online Appendix 1 at <http://journals.cambridge.org/geo>). The ophiolite is exposed over ~2400 km<sup>2</sup>, essentially SW of the MZT (Fig. 2). It is bordered to the NE by SSZ metamorphic rocks and to the SW by Bisotun limestone, a ~3 km thick carbonate sequence of Late Triassic to Late Cretaceous (Cenomanian) age, as well as by the Triassic to Cretaceous Kermanshah radiolarites and then by ZFTB sedimentary rocks. The Kermanshah ophiolite is thrust over the Bisotun limestone. Initial thrusting of the Kermanshah ophiolite is thought to have occurred during Maastrichtian–Paleocene time, as evidenced by ophiolitic clasts in the Maastrichtian–Paleocene Amiran Conglomerate Formation of the ZFTB

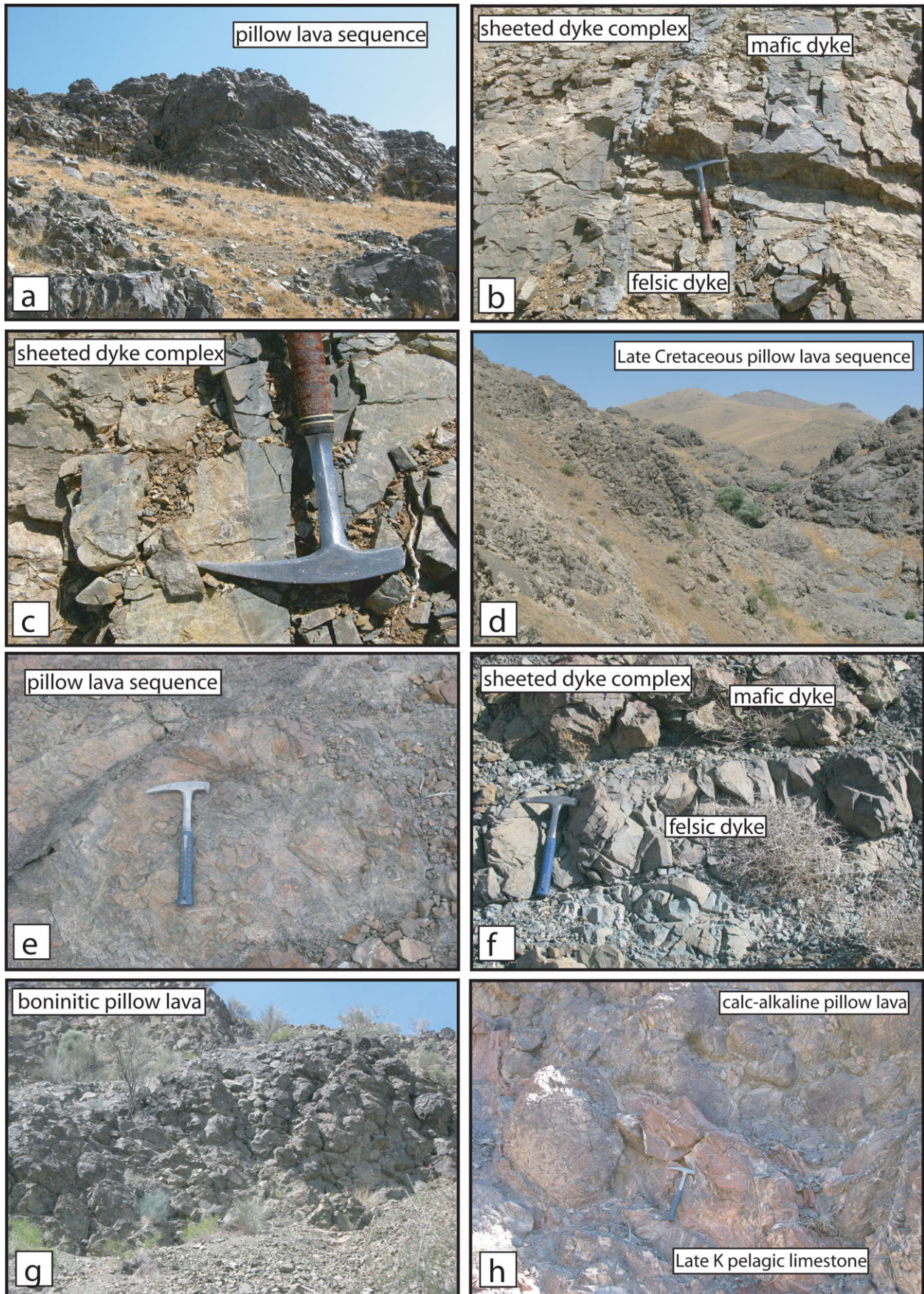


Figure 3. (Colour online) Field photographs of Zagros outer belt ophiolites (approximate positions shown in Fig. A10 in online Appendix 1 at <http://journals.cambridge.org/geo>). (a) Pillow lava sequence of the Kherran to Sartakht section (Kermanshah ophiolite). (b) Sheeted dyke complex in the Kherran to Sartakht section (Kermanshah ophiolite). Late felsic dykes injected into early mafic dykes. (c) Close-up view of contact between dykes in sheeted dyke complex (Kermanshah ophiolite). (d) Upper Cretaceous pillow

(J. Braud, unpub. Ph.D. thesis, Univ. Paris-Sud, France, 1987). This episode of erosion may also correspond to when SSZ rocks were exhumed. This thrust was reactivated in Miocene time, as indicated by the presence of Miocene flysch below the ophiolite (Agard *et al.* 2005).

Two oceanic domains, the Harsin sub-oceanic basin to the south and the Neo-Tethys to the north are proposed for the evolution of the Kermanshah ophiolite (Wrobel-Daveau *et al.* 2010). In this new model, the Harsin basin is suggested to have resulted from mantle exhumation and detachment faulting at two different times: Early Jurassic and early Late Cretaceous (Cenomanian). The later extensional regime could correlate with tectonic movements indicated by Aptian–Albian olistostromes in Neyriz oceanic sediments, the Pichakun nappe (Robin *et al.* 2010). Moreover, there may be a younger nappe stack of gabbros, intrusive rocks and pelagic sediments, emplaced during Late Eocene time on the top of the former Cretaceous ophiolite (Wrobel-Daveau *et al.* 2010).

The Kermanshah ophiolite has not been studied much. The presence of scattered dykes with island arc tholeiite (IAT) affinity is reported by Desmons & Beccaluva (1983). Some diabasic dykes yield  $^{40}\text{K}$ – $^{40}\text{Ar}$  ages of 83–86 Ma (Delaloye & Desmons, 1980). Ghazi & Hassanipak (1999) reported mantle peridotites, gabbro and both island arc tholeiitic and alkaline lavas. Recently Allahyari *et al.* (2010) described mantle peridotite, normal mid-ocean ridge basalt (N-MORB)-to enriched mid-ocean ridge basalt (E-MORB)-type gabbroic sequences and scarce pillow lavas at Sahneh (NE of Kermanshah). Not all mafic gabbros are ophiolitic, for example undated pegmatitic gabbro south of Sahneh is probably the westernmost part of a  $5 \times 10$  km E–W gabbro-volcanic belt of Eocene age shown by Allahyari *et al.* (2010).

The Upper Cretaceous Kermanshah ophiolite comprises mantle and crustal igneous rocks. The crustal sequence is distinguished by a sheeted dyke complex and a well-developed sequence of pillow lavas; crustal gabbros are missing (see Fig. A2 in online Appendix 1 at <http://journals.cambridge.org/geo>). Mantle peridotites including harzburgite, depleted lherzolite and pervasively impregnated harzburgite intruded by pegmatite gabbro lenses are found along the Harsin to Noor-Abad road. Another outcrop of depleted lherzolites and harzburgites is SSW of Sahneh (Allahyari *et al.* 2010). Harzburgites contain serpentized olivines, large orthopyroxene porphyroclasts, minor clinopyroxene and tiny grains of chromite.

Interstitial undeformed plagioclase blebs and unstrained intergranular clinopyroxene are abundant in impregnated harzburgites, where they occur as melt-crystallized phases between pyroxene and olivine porphyroclasts. These minerals and millimetre-size gabbro-noritic aggregates indicate impregnation of harzburgite by melts with the composition of the low-pressure peridotite eutectic (e.g. Piccardo *et al.* 2005; Pearce *et al.* 2000). Depleted lherzolites have minor clinopyroxene and are considered to represent residual MORB mantle (Allahyari *et al.* 2010). Ultramafic–mafic cumulate rocks are not observed.

Sheeted dyke complexes, including early basaltic and basaltic-andesitic-diabasic dykes and late dacitic-rhyolitic dykes, are found near Kherran and Sartakht villages (Fig. 3b, c). Each dyke (usually < 0.5 m, locally > 1 m thick) has been injected into others (Fig. 3c); locally plagiogranitic patches are observed as screens between dykes. Diabasic dykes are porphyritic with plagioclase phenocrysts and microlites. Magnesio-hornblende and/or clinopyroxene are also common. The felsic dykes are clearly younger as they cut the mafic dykes. Felsic dykes are composed of feldspar, quartz and amphibole phenocrysts and a cryptocrystalline to spherulitic groundmass. Relative abundances of felsic to mafic dykes are 1:3 to 1:2. A well-preserved volcanic sequence and sheeted dyke complex is found in many places e.g. near Kherran and Sartakht villages, especially near 47°E. Near the Kherran village, there is a ~200 m thick volcanic pile including (from bottom to top) poorly phyrific basaltic-andesites, basaltic lavas and pillowed basalts (Fig. 3a). Pillow lavas contain clinopyroxene, altered plagioclase microlites and tiny titanomagnetites set in an altered glassy groundmass. The volcanic pile is capped by a thin basaltic lava flow. Locally, basaltic flows contain thin plagiogranitic veins.

The base of the volcanic pile SSE of Sartakht village consists of pillowed basalts intruded by diabasic dykes that grade down into a sheeted dyke complex. Dykes include some that are andesitic and amphibole-bearing diabasic. Near Siah-Pareh village, there is a > 5 km<sup>2</sup> region composed of a thick sequence of pillow lavas and basaltic flows (Fig. 3d).

### 3.a.2. Neyriz ophiolite

The Neyriz ophiolite (see Fig. A3 in online Appendix 1 at <http://journals.cambridge.org/geo>) was first defined as the High Zagros ophiolite–radiolarite belt by Berberian & King (1981). There are three imbricated sheets, from bottom (SW) to top (NE), the Pichukan series, mélange units and ophiolite

lava sequence near Siah-Pareh village (section C of Fig. A10 in online Appendix 1 at <http://journals.cambridge.org/geo>) (Kermanshah ophiolite). (e) Close-up view of fragmented pillow lavas in Dowlat-Abad, Neyriz ophiolite. (f) Tale-Afshari sheeted dyke complex in the Neyriz ophiolite. Late felsic dyke injected into early mafic dyke. (g) Upper Cretaceous boninitic pillow lavas near Avenan village, Haji-Abad ophiolite. (h) Calc-alkaline pillow lavas with intercalation of Upper Cretaceous pelagic limestones near Chale-Mort village (Haji-Abad ophiolite).

(Ricou, 1971, 1976; L. E. Ricou, unpub. Ph.D. thesis, Univ. Paris-Sud, France, 1974; Ricou, Braud & Brunn, 1977). The Pichakun series (Ricou, 1968) consists of Upper Triassic limestone, Middle Jurassic oolitic limestone and Lower–Middle Cretaceous conglomeratic limestone, representing Neo-Tethys pelagic sediments (analogous to the Bisotun limestone and radiolarites of Kermanshah). The Pichakun series is wedged between two thrust sheets of sheared *mélange* (Pamić & Adib, 1982; Babaie *et al.* 2001). Above the Pichakun series, the *mélange* consists of exotic blocks of Permian–Triassic *Megalodon*-bearing limestone associated with radiolarites, pillow lavas with alkaline (M. Arvin, unpub. Ph.D. thesis, Univ. London, 1982) and tholeiitic (Babaie *et al.* 2006) characteristics, serpentinites and metamorphic rocks. The upper *mélange* is tectonically overlain by ophiolite slices, and both ophiolite and *mélange* thrust sheets are transported over Cenomanian–Turonian shallow water shelf/platform carbonates (Sarvak Formation; Alavi, 1994). The contact of the lower *mélange* with the underlying autochthonous Sarvak Formation is marked by a mylonitic amphibolite sole (Babaei, Babaie & Arvin, 2005).

Ophiolite thrust sheets cover about 1500 km<sup>2</sup>. These are unconformably overlain by uppermost Cretaceous anhydritic limestones of the Tarbour Formation (James & Wynd, 1965). The Neyriz ophiolite was thrust over the Pichakun and *mélange* sheets in Turonian to Maastrichtian time (e.g. Ricou, Braud & Brunn, 1977; Alavi, 1994; Babaie *et al.* 2006), exposing and allowing erosion of the ophiolite and accumulation of such clasts in Upper Cretaceous–Paleocene conglomerates (Haynes & Reynolds, 1980; Lanphere & Pamić, 1983). This episode of erosion may correspond to when SSZ rocks were exhumed, as evidenced by the presence of SSZ clasts in Upper Cretaceous–Paleocene conglomerates (Sabzehei, 1996).

The Neyriz ophiolite is composed of mantle and crustal units capped by Upper Cretaceous (Cenomanian–Turonian to lower Santonian) pelagic sediments. The mantle sequence is represented by depleted to highly impregnated harzburgites containing screens of residual dunite, podiform chromitite, pyroxenitic sills/dykes, pegmatite gabbros, gabbroic dykes/sills, isotropic melano-gabbros and diabasic-basaltic-andesitic dykes (see Fig. A2 in online Appendix 1 at <http://journals.cambridge.org/geo>). Diabasic dykes contain highly altered plagioclase and clinopyroxene. Isotropic melano-gabbros are characterized by plagioclase, orthopyroxene, clinopyroxene, brown amphibole, minor sulfides and titanomagnetite. Dunitic dykes/sills are common through the Neyriz mantle sequence. At the top of the mantle sequence there are highly impregnated peridotites including layered leucogabbro, olivine-bearing melanogabbro and pyroxenite cumulate sills and lenses. These lenses intrude mantle peridotites (see Fig. A2 in online Appendix 1 at <http://journals.cambridge.org/geo>) and contain olivine, slightly altered plagioclase,

clinopyroxene and fine-grained sulfide. Marble and skarn-type rocks are found at the contact of these intrusions with depleted harzburgite and on the top of gabbroic dykes (see Fig. A2 in online Appendix 1 at <http://journals.cambridge.org/geo>) suggesting they formed when hot peridotite intruded Upper Triassic platform limestones during continental rifting (Hall, 1980) and/or via interaction with high-temperature fluids released from gabbroic dykes intruding peridotite (M. R. Jannessary, unpub. Ph.D. thesis, l'Univ. de Louis Pasteur, France, 2003).

Coarse-grained melano-gabbros containing plagiogranitic pockets overly the mantle sequence. These rocks consist of serpentinitized olivine, plagioclase and clinopyroxene showing cumulate texture. A highly fragmented sheeted dyke complex is widespread in the Tale-Afshari region (Fig. 3f); this includes diabasic-basaltic and dacitic dykes. Although intrusive contacts between dykes are difficult to recognize owing to faulting, some intrusive contacts between dykes and dyke-in-dyke relationships are seen. Pillowed and massive lavas containing chert and Upper Cretaceous pelagic limestone are common (Fig. 3e).

### 3.a.3. Haji-Abad ophiolite

The Haji-Abad (sometimes called Esfandagheh) ophiolite covers ~2000 km<sup>2</sup>. Two ophiolites exist here; an older (more northerly) one of Late Triassic–Cretaceous age (Sikhoran–Soghan complexes; Ghasemi *et al.* 2002; Ahmadipour *et al.* 2003), and a younger, Upper Cretaceous Haji-Abad ophiolite (more southerly) near the MZT (see Fig. A4 in online Appendix 1 at <http://journals.cambridge.org/geo>). The older complex is overlain by marble and amphibolites of the Sargaz–Abshur complex and are intruded by Upper Triassic–Lower Jurassic (K–Ar dating; Ghasemi *et al.* 2002) isotropic gabbros. The injection of Middle Jurassic–Cretaceous diabasic dykes was the last igneous event experienced by the older ophiolites (Ghasemi *et al.* 2002; Ahmadipour *et al.* 2003). Older ophiolitic lavas have suprasubduction zone geochemical signatures. Formation in a back-arc basin (Ghasemi *et al.* 2002) or rift (Ahmadipour *et al.* 2003) has been suggested.

The southern Haji-Abad ophiolite formed in Late Cretaceous time and is highly faulted. The mantle sequence includes depleted harzburgite and residual dunite occasionally foliated with aligned spinel. Podiform chromitites are common within the residual dunite (see Fig. A2 in online Appendix 1 at <http://journals.cambridge.org/geo>). Porphyroclastic harzburgites contain serpentinitized olivine, bastitized orthopyroxene, occasional traces of clinopyroxene and black-brown to pale brown spinels. Dunites have highly deformed olivine porphyroclasts with deformation lamellae and inclusions of black spinel. Leucogabbroic and gabbroic dykes are common in the harzburgites. Metamorphosed diabasic dykes containing amphibole, altered plagioclase, chlorite and epidote cross-cut the mantle harzburgite. Haji-Abad ophiolite crustal

sequences are characterized by pillowed and massive lava flows (Fig. 3g, h), overlain tectonically or occasionally stratigraphically by Upper Cretaceous pelagic limestones. Small tonalitic intrusions into the crustal sequence also show fault contacts with serpentinites. A fine-grained plagiogranitic sill cross-cuts the tonalitic intrusions. Highly spilitized metavolcanics with thin layers of pelagic limestone are widespread (Fig. 3h). The Upper Cretaceous Haji–Abad ophiolite is overlain by volcanoclastic sandstone and siltstone turbidites, which are succeeded by basalt flows (see Fig. A2 in online Appendix 1 at <http://journals.cambridge.org/geo>). Basalts are commonly metamorphosed to greenschist facies, with chlorite, titanite, epidote, calcite and secondary quartz. Plagioclase is altered and clinopyroxene rims are chloritized. Greenschist-facies metamorphism may be related to a Cyprus-type massive sulfide deposit within pillow lavas in the Sheikh-Ali region (Rastad, Miralipour & Momenzadeh, 2002). Ophiolitic lavas are overlain by Upper Cretaceous pelagic limestones.

### 3.b. Inner Zagros Ophiolitic Belt

#### 3.b.1. Nain ophiolite

The Nain ophiolite is the NW-most IB massif (Fig. 2) and covers about 600 km<sup>2</sup> (see Fig. A5 in online Appendix 1 at <http://journals.cambridge.org/geo>). Davoudzadeh (1972) first described it as an Upper Cretaceous–Lower Eocene coloured *mélange*. Rahmani, Noghreyan & Khalili (2007) proposed that the Nain ophiolites formed in a suprasubduction zone tectonic environment, based on the composition of sheeted dykes.

The Nain ophiolite mantle sequence is composed of moderately depleted harzburgites with minor plagioclase lherzolite formed as a result of gabbroic impregnation. Harzburgites have porphyroclastic and/or blastomylonitic texture. Pegmatite gabbros, coarse-grained sulfide-bearing gabbros and isotropic gabbros/gabbronorites are common within the mantle sequence. Pyroxenitic, gabbroic, gabbronoritic and diabasic dykes and sills cross-cut the Nain mantle sequence (Fig. 4a and Fig. A6 in online Appendix 1 at <http://journals.cambridge.org/geo>). Pegmatite gabbros contain large clinopyroxene and plagioclase crystals. Coarse-grained gabbros locally show alternating plagioclase-rich and clinopyroxene-rich layers. Gabbronorites are cumulates, containing olivine, orthopyroxene, clinopyroxene and plagioclase crystals with minor pyrite. Isotropic gabbros have clinopyroxene, amphibole and variably altered plagioclase crystals. Slices of garnet amphibolite containing leucocratic segregations resulting from partial melting occur in this ophiolite.

The Nain ophiolite crustal sequence includes a sheeted dyke complex and overlying lavas (Fig. 4b and Fig. A6 in online Appendix 1 at <http://journals.cambridge.org/geo>). The sheeted dyke complex contains mafic and felsic microgabbroic and gab-

bronoritic dykes with mutually intrusive contacts. These dykes either intrude the host amphibole gabbros/microgabbros (Fig. 4b) and plagiogranites (e.g. near Ahmad-Abad village) or are injected into other dykes (SE of Separo village). Pillow lavas and massive lava flows overlie the sheeted dyke complex. Plagioclase microlites and clinopyroxene are primary minerals of the lavas. Once-glassy lava groundmass is altered into reddish clay.

*Globo truncana*-bearing Upper Cretaceous (Coniacian–Maastrichtian) pelagic limestones overlie the pillow lavas and are found as thin screens between pillows. Pelagic limestones are unconformably overlain by grey sandy limestones of Palaeogene age (Davoudzadeh, 1972). A basal conglomerate containing ophiolitic cobbles indicates Early Paleocene uplift and erosion of the ophiolite. Diabasic sills with boninitic affinities intrude Middle to Upper Paleocene limestones (H. Shafaii Moghadam, unpub. Ph.D. thesis, Shahid Beheshti Univ., Tehran, Iran, 2009). Small Oligo-Miocene dacitic domes with adakitic signatures cross-cut the Nain ophiolite (H. Shafaii Moghadam, unpub. Ph.D. thesis, Shahid Beheshti Univ., Tehran, Iran, 2009).

#### 3.b.2. Dehshir ophiolite

The Dehshir ophiolite is exposed discontinuously over ~150 km<sup>2</sup> near the centre of the IB (Fig. 2 and Fig. A7 in online Appendix 1 at <http://journals.cambridge.org/geo>). The lavas of this ophiolite are conformably capped by Turonian–Maastrichtian (93.5–65.5 Ma) *Globo truncana*-bearing pelagic limestones. This ophiolite was first described as part of regional geological mapping (Sabzehei, 1997). More detail is presented by Shafaii Moghadam, Stern & Rahgoshay (2010).

The Dehshir ophiolite mantle sequence includes harzburgite, clinopyroxene-bearing harzburgite and cumulate rocks including plagioclase lherzolite, clinopyroxenite, leucogabbro and pegmatite gabbro (see Fig. A6 in online Appendix 1 at <http://journals.cambridge.org/geo>). Plagioclase and clinopyroxene are the predominant cumulus phases in pegmatite gabbros. Clinopyroxene is partly converted into tremolite whereas plagioclase is altered into sericite and clay. Plagioclase occurs as large euhedral cumulus grains in leucogabbros and together with clinopyroxene displays coarse-grained granular texture. More rarely plagioclase laths are aligned, defining magmatic foliation. Olivine is interstitial between plagioclase. Accessory phases are titanomagnetite and ilmenite occurring as intercumulus grains.

Diabasic dykes and isotropic gabbros intrude the harzburgite (Fig. 4c). Diabasic dykes are fine- to medium-grained, aphyric to moderately porphyritic with clinopyroxene and plagioclase phenocrysts set in an intergranular groundmass. Plagioclase and clinopyroxene are the main constituents of isotropic gabbros and show intergranular to sub-ophitic textures.

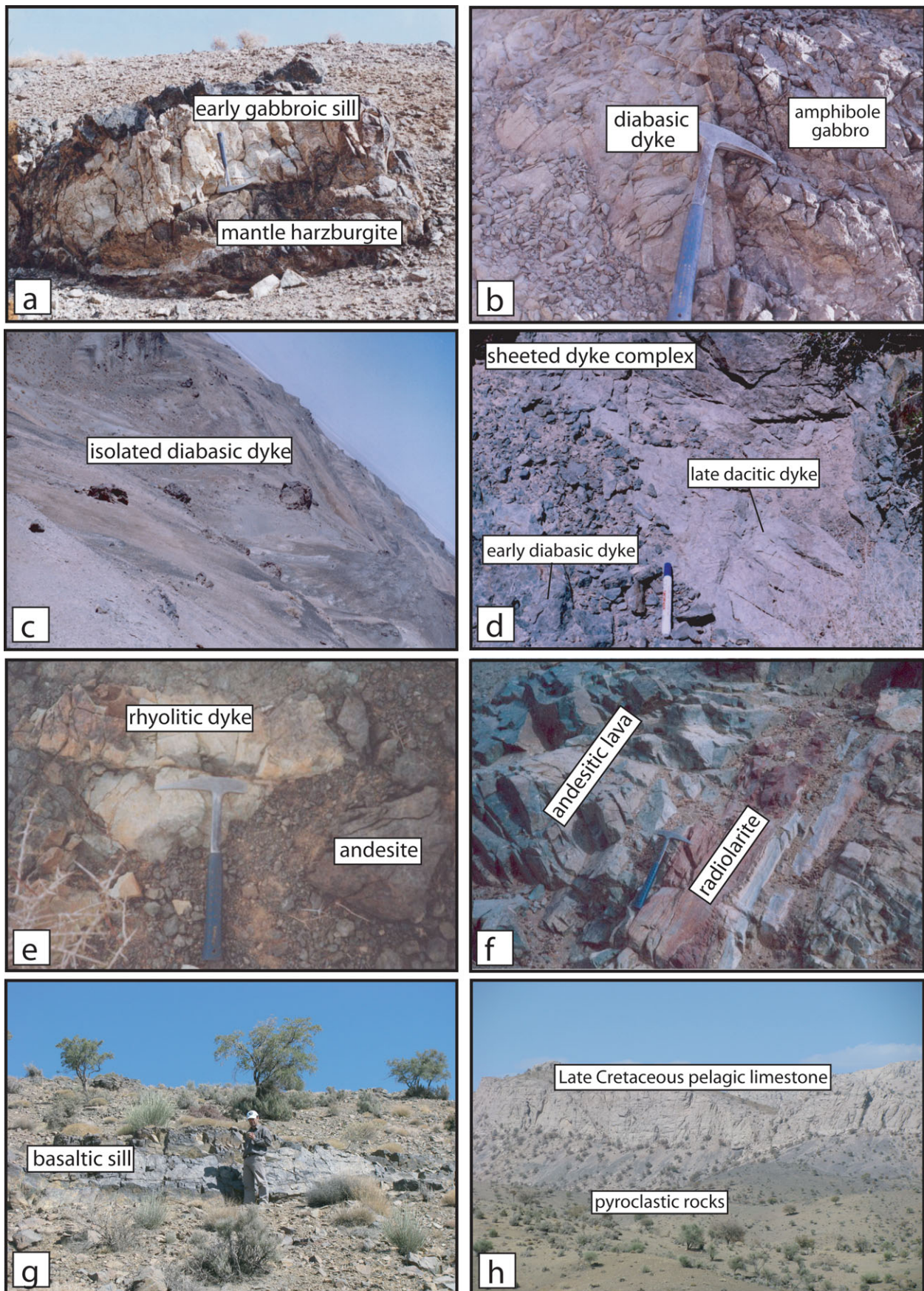


Figure 4. (Colour online) Field photographs of Zagros inner belt ophiolites (approximate positions shown in Fig. A11 in online Appendix 1 at <http://journals.cambridge.org/geo>). (a) Early rodingitized gabbroic sill in mantle harzburgite of the Nain ophiolite. (b) Injection of diabasic dyke into amphibole gabbros, host of the Nain ophiolite sheeted dyke complex. (c) Isolated diabasic dyke in mantle complex. (d) Late dacitic dykes injected into early diabasic dykes in the Dehshir ophiolite sheeted dyke complex. (e) Rhyolitic dyke injected into volcanic sequence of the Shahr-e-Babak ophiolite. (f) Interbedded andesitic lavas with Upper Cretaceous radiolarites in the Shahr-e-Babak ophiolite. (g) Basaltic sill within pyroclastic rocks of the Balvard–Baft ophiolite. (h) Pyroclastic unit of the Balvard–Baft ophiolite overlain by Upper Cretaceous pelagic limestones.

Green amphiboles (magnesian-hornblende) and disseminated ilmenites are present in isotropic gabbros.

The Dehshir ophiolite crustal section comprises pillowed basalts, basaltic and basaltic-andesitic massive flows, and a basaltic-dacitic sheeted dyke complex (Fig. 4d). Pillowed and massive lavas are moderately porphyritic, with clinopyroxene and plagioclase phenocrysts set in a glassy groundmass with plagioclase microlites. Albite microlites, K-feldspar and quartz are the main constituents of dacitic dykes in the sheeted dyke complex. Plagiogranite occurs both as dykelets injected into isotropic gabbros and as small plugs emplaced in metamorphic rocks. Plagioclase, orthoclase and anhedral quartz with accessory amphibole and biotite are found in plagiogranite.

### 3.b.3. *Shahr-e-Babak ophiolite*

The Shahr-e-Babak ophiolite lies ~100 km SE of Dehshir (Fig. 2) and covers ~500 km<sup>2</sup>. It is bounded to the west by the Dehshir–Baft fault, to the SSW by Sanandaj–Sirjan metamorphic rocks and to the NNE by the Dehaj–Sarduiyeh magmatic belt (see Fig. A8 in online Appendix 1 at <http://journals.cambridge.org/geo>), which is part of the Urumieh–Dokhtar arc (Dimitrijevic, 1973). Faulting, shearing, displacement of ophiolite units and tectonic interleaving with younger units is common. This ophiolite was first described by Dimitrijevic (1973) as a result of mapping in the Kerman region. Shahr-e-Babak comprises a complete ophiolite sequence except for a sheeted dyke complex (Ghazi & Hassanipak, 2000). Two geochemical signatures are observed: arc-like basalts, andesites and rhyodacites and ocean-island basalt (OIB)-like trachy-andesites. Ghazi & Hassanipak (2000) proposed formation in a narrow oceanic basin that opened between the Central Iranian microcontinent and the SSZ, followed by subduction to the NW.

The Shahr-e-Babak ophiolite mantle sequence is dominated by highly serpentinized harzburgites. Diabasic dykes and isotropic gabbro lenses commonly intrude harzburgite (see Fig. A6 in online Appendix 1 at <http://journals.cambridge.org/geo>). Isotropic gabbros are common within the mantle sequence as small lenses cut by plagiogranitic veins. The volcanic sequence is composed of basalt, andesite, dacite and rhyolite. These are either massive lava flows or are interbedded (associated with diabasic mafic rocks) with Campanian–Maastrichtian pelagic sediments (Fig. 4f). Massive and pillowed lavas overlie the interbedded volcanic sequence. Rhyolitic dykes and sills cross-cut andesite and basalt near Chah-Bagh village (Fig. 4e). Shallow dioritic-granitic plutons intrude the massive lavas (see Fig. A6 in online Appendix 1 at <http://journals.cambridge.org/geo>).

Basalts contain altered plagioclase phenocrysts and microlites associated with clinopyroxene. Plagioclase (albite-oligoclase) is the predominant mineral in andesites, < 2% in aphyric andesite and > 20% in

porphyritic andesite. Clinopyroxene and amphibole (edenitic to pargasitic hornblende) are also common in andesite. Plagioclase microlites with fine-grained quartz are present in the groundmass of these rocks. Coarse-grained plagioclase and quartz are the main constituents of dacites, with less abundant sanidine and apatite. Spherulitic intergrowth of albite, fine-grained polycrystalline to cryptocrystalline quartz and chlorite is characteristic of rhyolitic lavas.

Coniacian–Maastrichtian pelagic limestones overlie the basaltic-dacitic rocks of the Shahr-e-Babak volcanic sequence (Fig. 4e). Younger sediments record a hiatus during Paleocene to Early Eocene time, an unconformity overlain by Eocene conglomerate, which grades upwards into *Nummulites*-bearing limestones and then into coarse- to medium-grained sandstones. Ophiolitic cobbles are common in Eocene conglomerates (Dimitrijevic, 1973), demonstrating that the ophiolite was exposed and eroded at this time.

### 3.b.4. *Balvard–Baft ophiolite*

The Balvard–Baft ophiolite defines a 5–10 km wide WNW-trending belt, covering 800 km<sup>2</sup> (see Fig. A9 in online Appendix 1 at <http://journals.cambridge.org/geo>). This ophiolite extends NW towards Shahr-e-Babak and SE to the Dare–Pahn and Haji–Abad ophiolites (Fig. 2). The first report on the Balvard–Baft ophiolite was by Dimitrijevic (1973) as a result of mapping of the Kerman region. Two types of basaltic pillow lavas and lava flows are recognized in the Baft and the Gogher (Balvard) regions (Arvin & Robinson, 1994; Arvin & Shokri, 1997): (1) tholeiites similar to N-MORB and (2) transitional tholeiites, geochemically intermediate between E-MORB and IAT, clearly produced by melting of a subduction-modified mantle.

The Balvard–Baft mantle sequence consists of harzburgite, minor lherzolite with diabasic dykes, and pockets of isotropic and pegmatitic gabbro. Harzburgite has porphyroclastic texture, with coarse, deformed orthopyroxene. Serpentinized olivine, clinopyroxene and dark brown spinel are other peridotite constituents. Plagioclase and clinopyroxene are the predominant cumulus phases in pegmatitic gabbros, with traces of olivine and spinel (< 3%). Plagioclase and clinopyroxene are the main constituents of the isotropic gabbros, with accessory magnetite and ilmenite.

Mafic to felsic rocks including pillow lavas, basaltic-andesitic-dacitic lava flows, and basaltic-andesitic-dacitic sills in pyroclastic rocks (Fig. 4g) are the Balvard–Baft ophiolite crustal units. Pillowed and massive lavas are porphyritic, with coarse-grained, euhedral to subhedral plagioclase and subhedral to anhedral clinopyroxene phenocrysts set in an altered glassy groundmass with plagioclase microlites. Basaltic lava flows are characterized by plagioclase and clinopyroxene whereas hornblende and plagioclase are dominant in andesites and dacites. Basaltic-andesitic and dacitic sills in pyroclastic rocks contain altered pla-

gioclase laths set in a groundmass of altered glass and plagioclase microlites. Clinopyroxene phenocrysts are present, except in dacites, altered to uralite and chlorite especially around their margins. Some lavas are nearly aphyric with 1–2 % plagioclase phenocrysts and pilotaxitic texture. Pyroclastic rocks and hyaloclastites rest unconformably over the basaltic lava flows (Fig. 4h). They are composed of volcanic breccias, agglomerates, tuff, tuffaceous sandstones and lutites, pillow cold breccias and andesitic hyaloclastites with basaltic-andesitic and pillow fragments. Volcaniclastic rocks are overlain by Turonian–Maastrichtian (93.5–65.5 Ma) pelagic limestones. The Balvard–Baft ophiolite is in fault or unconformable contact with Middle to Upper Eocene sedimentary–volcanic sequences related to the Urumieh–Dokhtar arc (Srdic *et al.* 1972; Mijalkovic, Cvetic & Dimitrijevic, 1972). These sediments consist of sandstone, marl and *Nummulites*-bearing limestone turbidites, with interbedded basaltic-andesitic lava flows above a basal conglomerate. The Early Eocene appears to have been a time of uplift and erosion of the ophiolite, as evidenced by ophiolitic clasts in Middle Eocene basal conglomerate.

### 3.c. Summary of similarities and differences between inner and outer belt ophiolites

Major lithological variations in Zagros ophiolites are summarized in Table 1. As can be seen from the above summaries, mantle rocks of both inner and outer Zagros ophiolites are dominated by depleted harzburgites with gabbroic–diabasic dykes. Lherzolite and gabbro are subordinate but common. Boninitic dykes are restricted to the Nain (inner belt) ophiolite. Large chromite pods and residual to cumulate dunitic lenses are restricted to the outer Zagros Neyriz and Haji–Abad ophiolites. Although gabbroic impregnations are present in almost all inner and outer belt ophiolites, they are especially common in the Nain massif. Pegmatitic and isotropic gabbro lenses are common in the mantle sequence of all ophiolites; however, gabbronorites are found only in Nain harzburgites.

Crustal sequences of both inner and outer belt ophiolites are dominated by lavas, both pillowed and massive. Sheeted dyke complexes are found in both inner (Nain, Dehshir) and outer (Kermanshah, Neyriz) belt ophiolites. More-evolved felsic rocks including dacitic–rhyolitic lavas and plagiogranites are common in all ophiolites. Gabbros are generally minor parts of most crustal sections. Lenses of cumulate rocks are common in these ophiolites but crustal cumulates are present only in the Neyriz and Haji–Abad (OB) ophiolites. Isotropic gabbros are common in the Zagros IB crustal sequence and rare in the OB.

Overlying sedimentary sequences also are similar and distinctive. Pyroclastic rocks with basaltic to dacitic sills are abundant only for the Balvard–Baft ophiolite, but are also found at Shahr-e-Babak; these are not found in OB ophiolites, indicating that IB ophiolites were closer to the evolving Urumieh–Dokhtar arc. All

inner and outer belt ophiolites are associated with overlying Upper Cretaceous pelagic limestones, except for the Neyriz ophiolite where the pelagic sediments are interbedded with lavas. Pelagic sediment interlayers are also common in the Shahr-e-Babak and Balvard–Baft ophiolites. The age of the pelagic limestones varies from Cenomanian–Turonian (99.6–89.3 Ma) to Early Santonian (85.8–83.5 Ma) in the Neyriz and Turonian (93.5–89.3 Ma) to Maastrichtian (70.6–65.5 Ma) in the Kermanshah OB ophiolites, and from Coniacian–Maastrichtian (89.3–65.5 Ma) in the Nain and Turonian–Maastrichtian (93.5–65.5 Ma) in the Dehshir and Baft IB ophiolites (Table 1). All sedimentary successions record a Paleocene–Eocene unconformity with ophiolitic clasts, indicating that the Zagros ophiolites were exposed and eroded by that time.

### 4. Geochemical evolution of the Zagros ophiolite lavas and dykes

In this section we summarize the principal geochemical properties of the Zagros Upper Cretaceous ophiolite magmas, as preserved in lavas and dykes, using major, trace and rare earth element (REE) concentrations. We also try to reconstruct the magmatic evolution of the ophiolites, as reconstructed from lavas or dykes. We understand that caution is needed when considering ophiolitic dykes, because some are much younger than the ophiolite, for example Kermanshah has Eocene–Miocene dioritic–gabbroic intrusions and felsic dykes (e.g. Leterrier, 1985). We have been careful to avoid sampling such younger dykes or intrusions. Data on Zagros IB ophiolites come from H. Shafaii Moghadam (unpub. Ph.D. thesis, Shahid Beheshti Univ., Tehran, Iran, 2009) except for Dehshir, which comes from Shafaii Moghadam, Stern & Rahgoshay (2010). For the Neyriz ophiolite we used data from M. R. Jannessary (unpub. Ph.D. thesis, l'Univ. de Louis Pasteur, France, 2003). Major and trace element analyses for the Kermanshah and Haji–Abad ophiolites were carried out using inductively coupled plasma atomic emission spectrometry (ICP-AES) and ICP mass spectrometry at the Centre de Geochimie de la Surface, Strasbourg (France) and ACME Lab (Canada), respectively. Whole-rock compositional data are reported in online Appendix 2 at <http://journals.cambridge.org/geo>.

Despite the often-disrupted nature of the Upper Cretaceous Zagros ophiolites, the relationships between lava units and analysed samples for intact fragments of both inner and outer Zagros ophiolitic belts are shown for the OB (see Fig. A10 in online Appendix 1 at <http://journals.cambridge.org/geo>) and IB (see Fig. A11 in online Appendix 1 at <http://journals.cambridge.org/geo>). For chemostratigraphy within each ophiolite, our sampling was based on the intact ophiolitic fragments, where original, unfaulted contacts between units are clear (as shown in Figs A2 and A6 in online Appendix 1 at <http://journals.cambridge.org/geo>) and not from mélange units.

Table 1. Summary of outer and inner Zagros ophiolitic belt characteristics

		Age of overlying sediments	Geochemical evolution of lavas	Crustal thickness (m)			Mafic dyke/felsic dyke ratio in sheeted dyke complex	Isotopic dating (Ma)
				Lavas	Gabbro/plagiogranite	Sheeted dyke complex		
Outer Zagros Ophiolitic Belt	Kermanshah ophiolite	Turonian–Maastrichtian	IAT to calc-alkaline	~ > 2000*	–	~ > 1000	~ 2/1–3/1	83–86, diabasic dyke, K–Ar <sup>1</sup>
	Neyriz ophiolite	Cenomanian–Turonian to Early Santonian	MORB to boninite	~ > 100–200	gabbro ~ 400–500	~ > 100–200	~ 1/2	92–93, gabbro, Ar–Ar <sup>2</sup> 86–93, plagiogranite, Ar–Ar <sup>3</sup> 99, amphibolites, Ar–Ar <sup>4</sup>
	Haji–Abad ophiolite	Cenomanian	MORB to boninite Rare E-MORB-type pillow lava	~ > 2000	–	–	–	?
Inner Zagros Ophiolitic Belt	Nain ophiolite	Coniacian–Maastrichtian	IAT to boninite	~ 700–800	Isotropic gabbro & plagiogranite ~ 1000	~ 300–400	~ 3/1	93, gabbro, K–Ar <sup>5</sup>
	Dehshir ophiolite	Turonian–Maastrichtian	MORB to IAT/boninite	~ max. 100–200	Isotropic gabbro ~ 100–200	~ 100	~ 1/3	94–67, gabbro, K–Ar <sup>5</sup>
	Balvard–Baft ophiolite	Turonian–Maastrichtian	MORB/IAT to boninite/calc-alkaline Rare E-MORB-type pillow lava	~ 300–400	–	Pyroclastic rocks > 2000	–	94–72, gabbro, K–Ar <sup>5</sup>

\* Crustal thickness except overlying sediments.

<sup>1</sup>Delaloye & Desmons (1980); <sup>2</sup>Babaie *et al.* (2006); <sup>3</sup>Lanphere & Pamic (1983); <sup>4</sup>Jannessary (2003); <sup>5</sup>Shafaii Moghadam *et al.* (2009).

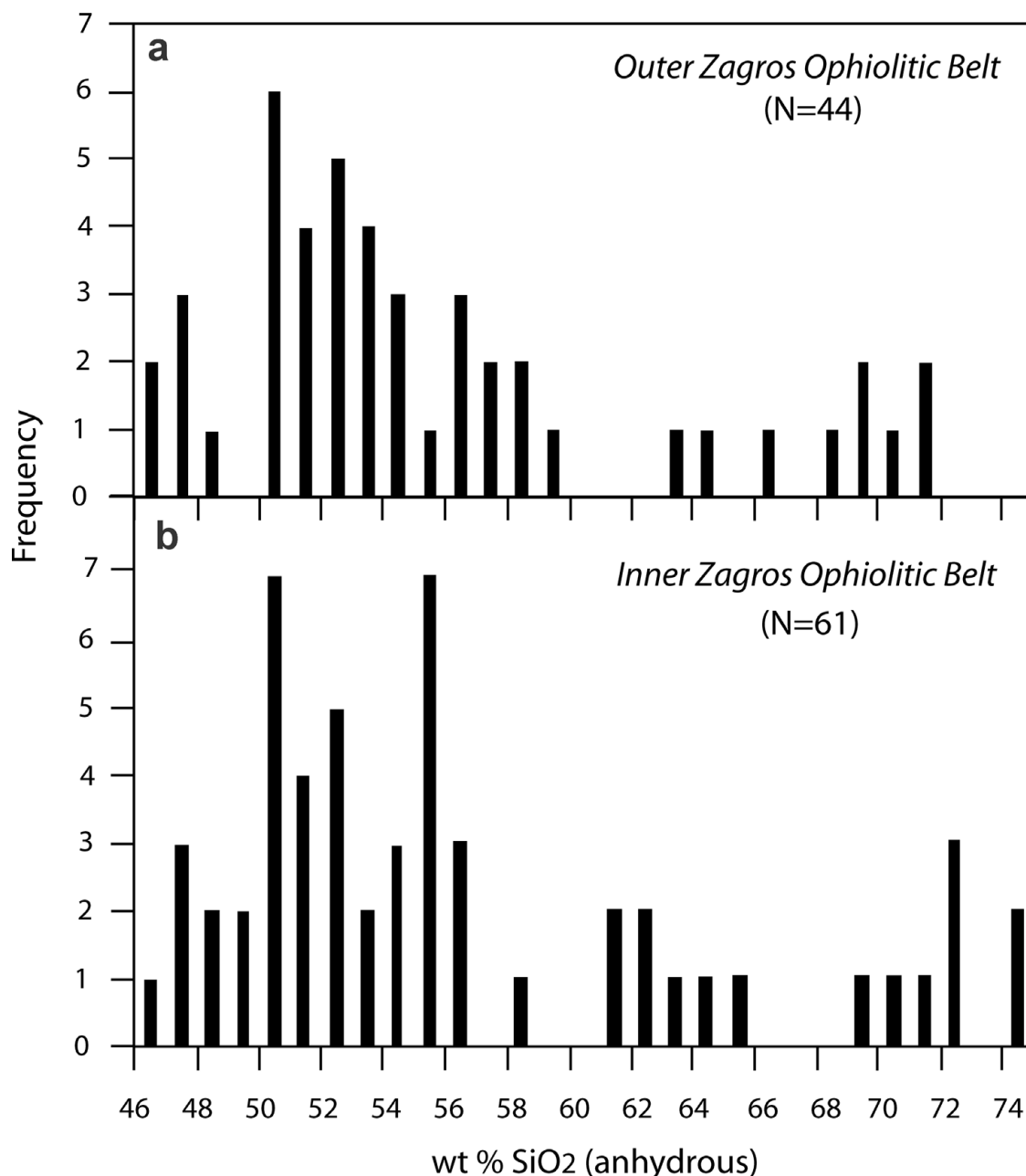


Figure 5. Histograms of wt % SiO<sub>2</sub> (recalculated 100 % anhydrous) for Zagros ophiolite lavas and dykes from sheeted dyke complex. Highly altered samples with high LOI content are not plotted. Most samples have 50–56 wt % SiO<sub>2</sub> but there is a significant proportion of samples with > 60 wt % SiO<sub>2</sub>.

#### 4.a. Outer Zagros Ophiolitic Belt

Lavas and dykes from the OB ophiolites are dominated by mafic (50–54 wt % SiO<sub>2</sub>) samples but also include a significant proportion of felsic material (up to 72 wt % SiO<sub>2</sub>), as shown by a histogram of SiO<sub>2</sub> contents (Fig. 5a). This is a much wider range in SiO<sub>2</sub> than observed at mid-ocean ridges, which are entirely basalts and basaltic-andesites.

##### 4.a.1. Kermanshah ophiolite

The Kermanshah ophiolite magmatic succession is characterized by a sheeted dyke complex with mafic and felsic dykes, as well as by massive and pillowed

lavas. To reconstruct the magmatic chemostratigraphy of this well-preserved ophiolite, we studied four sections along the Kherran to Sartakht road, near Sartakht village and near Siah-Pareh village.

Along the Kherran to Sartakht road there is a volcanic pile with sparsely phyrlic basaltic-andesites at the bottom grading upwards into porphyritic basalts with plagiogranitic veins and then into pillowed lavas (Fig. 3a and Fig. A10a in online Appendix 1 at <http://journals.cambridge.org/geo>). This sequence is capped by a thin basaltic flow. These lavas are basaltic with 49.6–52 wt % SiO<sub>2</sub>. They have high FeO/MgO, and in the FeO/MgO v. SiO<sub>2</sub> diagram plot in the high-Fe tholeiitic field (Fig. 6). Mg no. (= 100 Mg/(Mg + Fe)) of these lavas varies from 43.4 to 66.4, indicating some

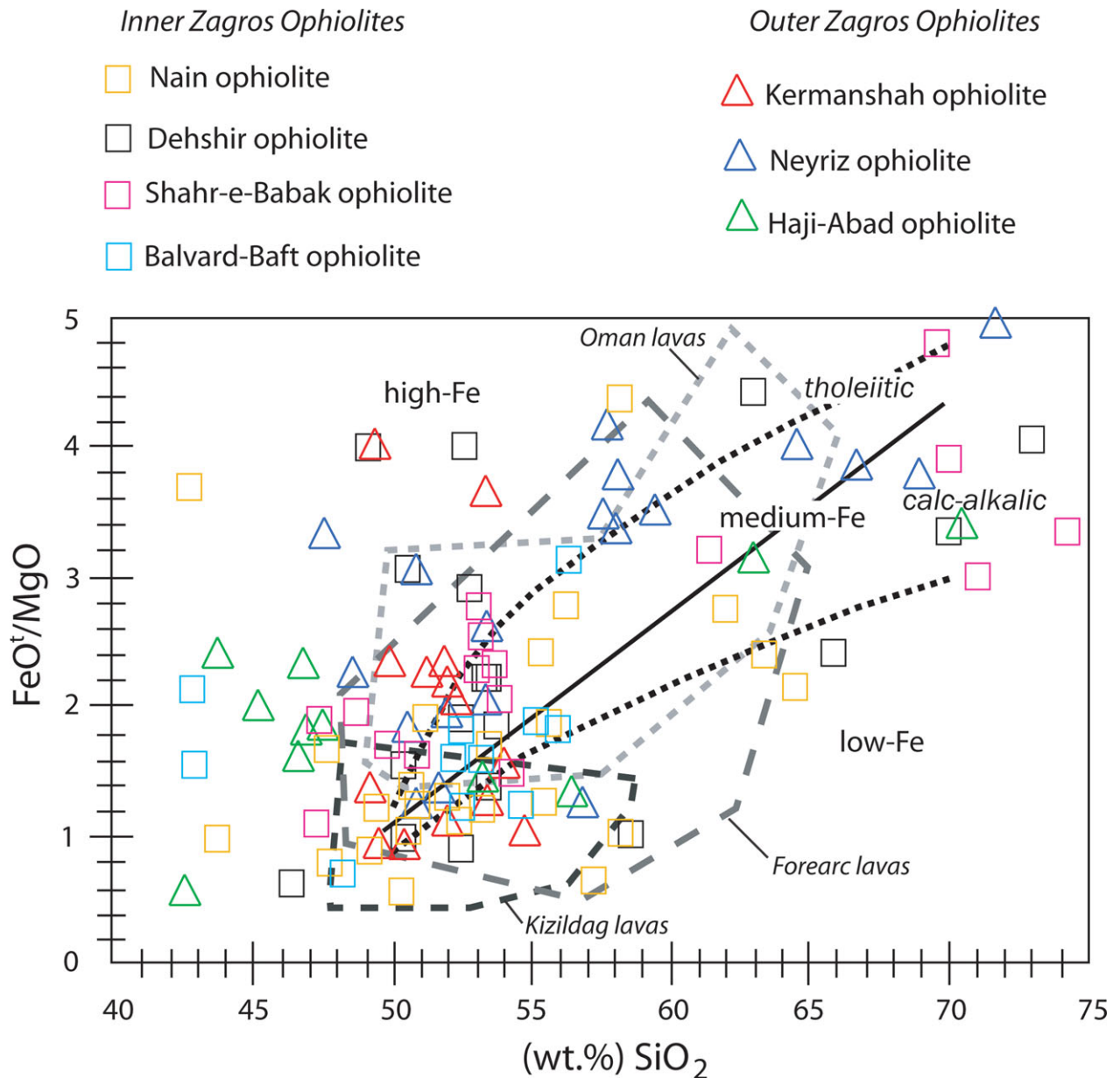


Figure 6. (Colour online)  $\text{FeO}^t/\text{MgO}$  v.  $\text{SiO}_2$  (volatile free, normalized to 100 % total) for Zagros OB and IB magmatic rocks. Boundaries between tholeiitic and calc-alkaline suites (thin solid line) and between low-, medium- and high-Fe suites (thick, dashed lines) are from Miyashiro (1974) and Arculus (2003), respectively. For comparison compositional fields from the Kizildag ophiolite, Turkey (Dilek & Thy, 2009), Oman (Godard, Dautria & Perrin, 2003) and IBM fore-arc lavas (Reagan *et al.* 2010) are shown.

are primitive.  $\text{TiO}_2$  and Zr contents vary from  $\sim 1$  to 1.9 wt% (Fig. 7) and 69 to 166 ppm, respectively. Sample KH09-24 has higher Zr content along with lower Mg no.

On REE plots, samples KH09-17 (poorly phryic basaltic flow), KH09-19 (basaltic flow) and KH09-20 (pillow lava) have flat to slightly depleted REE patterns ( $\text{La}_N/\text{Yb}_N = 0.75\text{--}1.1$ ) (Fig. 8a). These samples show similar REE patterns except for slight Eu enrichment in KH09-17 and KH09-19, with REE contents similar to N-MORB (e.g.  $\text{La} = 2.2\text{--}4.1$  ppm,  $\text{Yb} = 2.1\text{--}2.6$  ppm versus N-MORB = 2.5 ppm La, 3.05 ppm Yb; Sun & McDonough, 1989). Sample KH09-24 is LREE enriched ( $\text{La}_N/\text{Yb}_N = 2.4$ ) similar to calc-alkaline lavas (Fig. 8a). The N-MORB-normalized trace element patterns for Kermanshah basaltic rocks

show strong depletion in Nb–Ta relative to light REEs (LREEs) ( $\text{Nb}/\text{La} = 0.5\text{--}0.9 \times \text{N-MORB}$ ) (Fig. 8b). These basalts are enriched in large-ion-lithophile elements (LILEs) (e.g. Rb, Ba, U, K, Pb) relative to LREEs. All basaltic rocks in this sequence are IAT except KH09-24 which displays a calc-alkaline affinity. IAT and calc-alkaline lavas interfinger in this sequence.

A sheeted dyke complex near Kherran village contains older diabasic dykes intruded by younger andesitic-dacitic-rhyolitic dykes (Fig. 3b, c and Fig. A10 in online Appendix 1 at <http://journals.cambridge.org/geo>). All mafic dyke samples (KH09-26, KH09-36 and KH09-37) are basalts and basaltic-andesites, with 51 to 54 wt%  $\text{SiO}_2$ . These lavas have lower  $\text{FeO}/\text{MgO}$  and plot in the medium-Fe tholeiitic to low-Fe

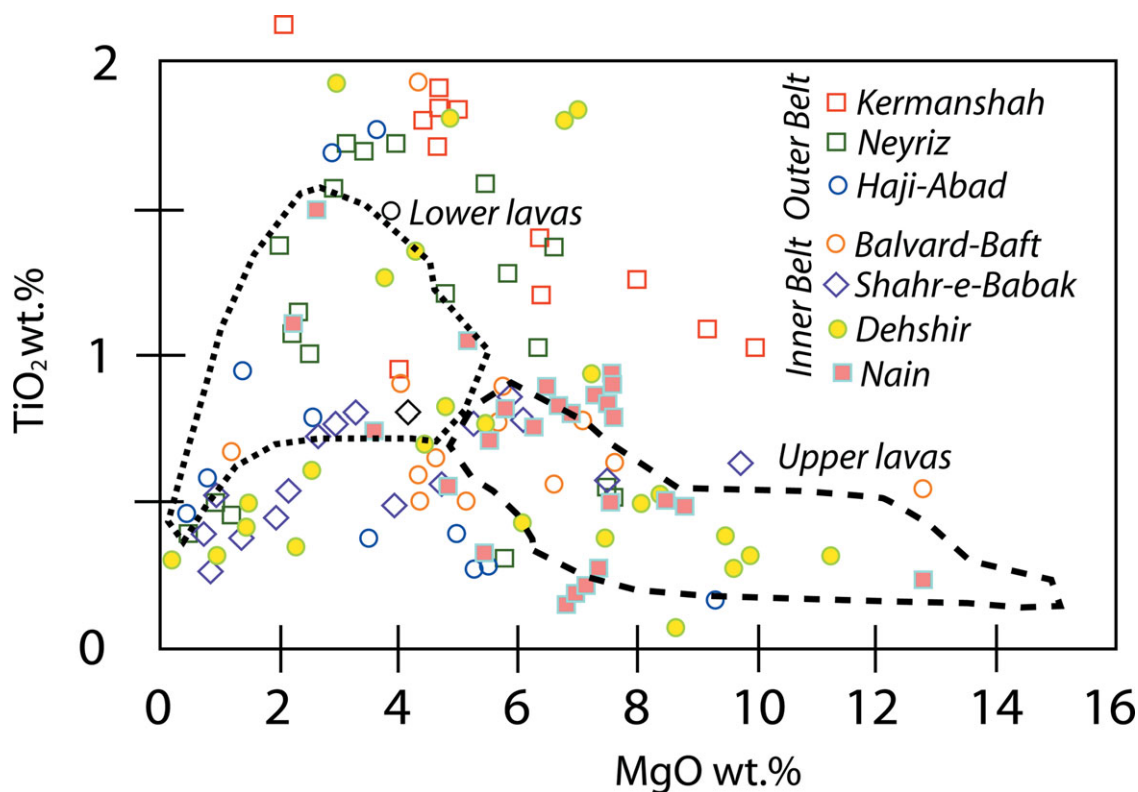


Figure 7. (Colour online) Major element variations ( $\text{TiO}_2$  v.  $\text{MgO}$ ) of OB and IB mafic rocks and comparisons to Troodos upper and lower lavas (modified after Dilek & Thy, 2009). Troodos upper and lower lava fields are outlined by dashed and dotted lines, respectively.

calc-alkaline fields (Fig. 6). They are fractionated, with low Mg no. (44 to 53.9) and elevated  $\text{TiO}_2$  (1.7 to 2.8 wt %) (Fig. 7) and Zr (212 to 316 ppm). These mafic lavas are LREE enriched (Fig. 8a) with  $\text{La}_N/\text{Yb}_N$  ranging from 2.8 to 3.3. Depletion in Nb–Ta and enrichment in Rb, Ba, Th, U, K and Pb relative to N-MORB (e.g.  $\text{Nb}/\text{La} = 0.55\text{--}0.7 \times \text{N-MORB}$  and  $\text{Th}/\text{La} = 5.6\text{--}6.3 \times \text{N-MORB}$ ) are characteristic of these mafic dykes (Fig. 8b). Felsic dykes have higher  $\text{SiO}_2$  (53–56 wt %) and Zr contents (426–474 ppm). They contain 5.6–5.9 wt %  $\text{Na}_2\text{O}$ , which may be magmatic because alteration is not severe, as shown by low loss on ignition (LOI: 0.4–0.8 wt %).

Kherran dykes show REE patterns that are concave upwards from La to Eu (Fig. 8a), with a slight increase from heavy REEs (HREEs) to middle REEs (MREEs) ( $\text{Dy}_N/\text{Yb}_N = 1.1\text{--}1.3 \times \text{chondrite}$ ) and low  $\text{La}_N/\text{Sm}_N$  (0.7–0.96) but with  $\text{La}_N/\text{Yb}_N = 0.98\text{--}2.2$ . These patterns may be attributed to crystal fractionation of basaltic melt to form felsic magmas. Like the mafic rocks, felsic dykes show slight negative Nb–Ta (and Ti) and positive Rb, Ba, Th, K, U and Pb anomalies relative to N-MORB (e.g.  $\text{Nb}/\text{La} = 0.88 \times \text{N-MORB}$ , except KH09-31 with  $\text{Nb}/\text{La} = 2.5 \times \text{N-MORB}$  and  $\text{Th}/\text{La} = 28.5\text{--}7.3 \times \text{N-MORB}$ ) (Fig. 8b). In this section, earlier mafic dykes are calc-alkaline grading into later felsic dykes that probably are fractionated arc tholeiites or products of amphibolite melting.

A well-preserved pillow lava sequence near Siah-Pareh village is > 100 m thick (Fig. A10c in online

Appendix 1 at <http://journals.cambridge.org/geo> and Fig. 3d). To characterize the melt evolution with time, we sampled from the bottom to the top of this pillow sequence. These are fractionated basalts, with relatively constant  $\text{SiO}_2$  (~52 wt %) and low Mg no. (44–47). These lavas have lower  $\text{FeO}/\text{MgO}$  and are similar to low-Fe calc-alkaline lavas (Fig. 6). They are characterized by high  $\text{TiO}_2$  (~1.8 wt %) and Zr (~200 ppm), similar to lower Troodos lavas (Fig. 7). REE patterns (Fig. 8a) do not change systematically from the bottom to the top of the pillow sequence. The lavas have similar REE patterns, enriched in LREEs ( $\text{La}_N/\text{Yb}_N = 2.2\text{--}2.9$ ) and LILEs (e.g.  $\text{Th}/\text{La} = 28.5\text{--}7.3 \times \text{N-MORB}$ ), and depleted in Nb–Ta (e.g.  $\text{Nb}/\text{La} = 0.5\text{--}0.6 \times \text{N-MORB}$ ), typical features of calc-alkaline rocks.

A sheeted dyke complex overlain by pillow lavas is found between Sartakht and Siah-Pareh villages (see Fig. A10d in online Appendix 1 at <http://journals.cambridge.org/geo>). These lavas are fractionated basalts and basaltic-andesites, with variable  $\text{SiO}_2$  (49–54 wt %), Mg no. (31–59) and calc-alkaline signature (Fig. 6). They vary from more primitive (KH09-75 and KH09-79 with  $\text{MgO} = 6.41$  wt %,  $\text{TiO}_2 = 1.22\text{--}1.4$  wt % and  $\text{Zr} = 125\text{--}138$  ppm, respectively) to more evolved (KH09-82 and KH09-76 with  $\text{MgO} = 2.89\text{--}3.34$  wt %,  $\text{TiO}_2 = 2.46\text{--}2.51$  wt % and  $\text{Zr} = 230\text{--}255$  ppm, respectively) (Fig. 7). All lavas are LREE enriched, with  $\text{La}_N/\text{Yb}_N$  between 3 and 3.6 (Fig. 8a). Depletion in Nb–Ta (e.g.  $\text{Nb}/\text{La} = 0.5\text{--}0.7$

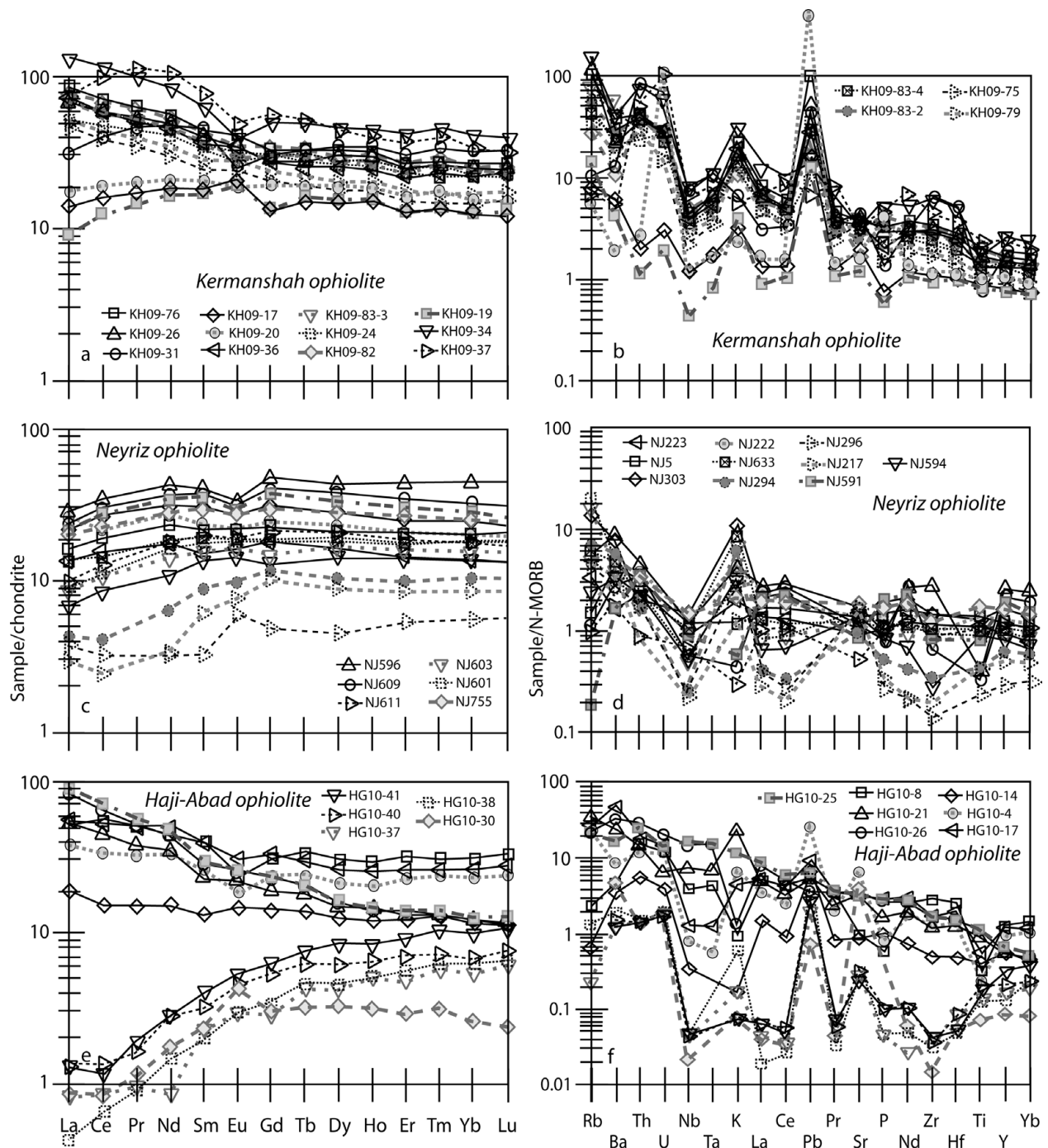


Figure 8. Chondrite-normalized rare earth element patterns (chondrite abundances are from McDonough & Sun, 1995) and normal mid-ocean ridge basalt (N-MORB)-normalized multi-element patterns (N-MORB concentrations are from Sun & McDonough, 1989) for rock units of outer belt ophiolites. (a, b) Kermanshah ophiolite; (c, d) Neyriz ophiolite; and (e, f) Haji-Abad ophiolite.

$\times$  N-MORB) and enrichment in LILEs (e.g.  $\text{Th/La} = 5.3\text{--}6.5 \times$  N-MORB), similar to calc-alkaline series, characterizes these lavas.

Kermanshah lavas display both tholeiitic and calc-alkaline trends in terms of  $\text{FeO/MgO}$  v.  $\text{SiO}_2$  (Fig. 6), with dispersion in  $\text{FeO/MgO}$  and  $\text{SiO}_2$  contents. Such dispersion along with the presence of tholeiitic and calc-alkaline lavas was considered by Miyashiro (1973) to be typical of arc magmas. The Kermanshah lavas have high  $\text{TiO}_2$  contents with a primary to evolved nature, evidenced by their  $\text{MgO}$  content

(Fig. 7). Kermanshah lavas have high  $\text{Ti/V}$ , ranging from 35 in arc tholeiites to 104 in calc-alkaline lavas. In spite of LILE enrichments and Nb–Ta depletions, characteristics indicating arc-like compositions, these ratios fall into the MORB and within-plate fields of Shervais (1982) (Fig. 9a).

Reconstruction of Kermanshah ophiolitic lava chemostratigraphy indicates that lava compositions do not show major changes in the sections described above, only interfingering of IAT and calc-alkaline lavas in the Kherran to Sartakht road section.

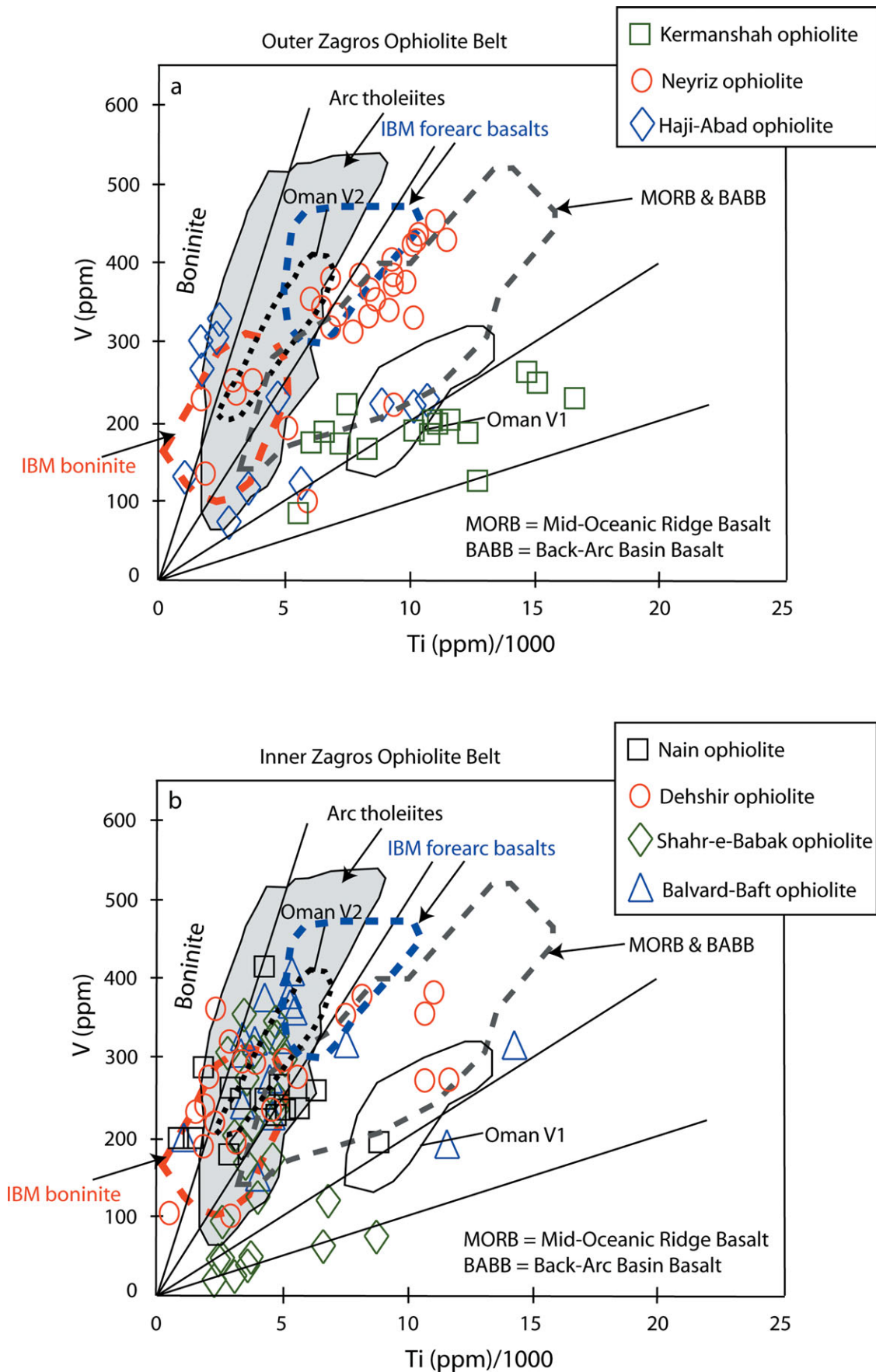


Figure 9. (Colour online) Ti v. V diagram (after Shervais, 1982) for Zagros outer belt (a) and inner belt (b) ophiolites. For comparison, fields for the V1 (lower, Geotimes unit) and V2 (upper, Lasail unit) lavas of Oman ophiolite (data from Alabaster, Pearce & Malpas, 1982) and for Mariana fore-arc basalts and boninites (Reagan *et al.* 2010) are shown.

#### 4.a.2. Neyriz ophiolite

The volcanic and hypabyssal sequence of the Neyriz ophiolite is represented by mafic and felsic dykes in a sheeted dyke complex, massive and pillowed lavas, and dykes in mantle peridotite. Despite several studies on the Neyriz ophiolite (e.g. Babaie *et al.* 2006; M. R. Jannessary, unpub. Ph.D. thesis, l'Univ. de Louis Pasteur, France, 2003), we know little about its chemostratigraphical evolution, probably because the crustal sequence is highly faulted. Here we try to combine our field observations plus geochemical data from M. R. Jannessary (unpub. Ph.D. thesis, l'Univ. de Louis Pasteur, France, 2003). We selected three volcanic sequences for closer scrutiny: (1) isolated diabasic to andesitic dykes injected into mantle harzburgites (NJ755, NJ633, NJ294, NJ296, NJ217), (2) Dowlat-Abad pillowed and massive lavas with intercalated pelagic sediments (NJ223, NJ5, NJ303, NJ222) (Fig. 3e and Fig. A10e in online Appendix 1 at <http://journals.cambridge.org/geo>) and (3) Tale-Afshari sheeted dyke/lava sequence with felsic and mafic dykes (NJ591, NJ594, NJ596, NJ609, NJ603, NJ601) (Fig. 3f and Fig. A10f in online Appendix 1 at <http://journals.cambridge.org/geo>). Unfortunately we cannot separately discuss the lava and dyke geochemistry because these are not distinguished.

Dykes intruding mantle rocks vary from basaltic (diabasic) to andesitic with 45 to 54 wt% SiO<sub>2</sub> (Fig. 5a). These dykes are mostly tholeiitic with high FeO/MgO (Fig. 6). These dykes display variable enrichment in TiO<sub>2</sub> (0.3–2.2 wt%) and Zr (10–92 ppm). In the TiO<sub>2</sub> v. MgO diagram, TiO<sub>2</sub>-rich dykes resemble lower lavas of Troodos while TiO<sub>2</sub>-poor dykes show similarity to Troodos upper lavas (Fig. 7). They are geochemically divided into (1) IAT-like dykes that are enriched in bulk REEs (NJ633 and NJ755; La = 3.3–4.8 ppm, Yb = 3.2–4.3 ppm versus N-MORB = 2.5 ppm La, 3.05 ppm Yb; Sun & McDonough, 1989) but are LREE depleted (La<sub>N</sub>/Yb<sub>N</sub> = 0.8), have modest negative Nb anomalies (Nb/La = 0.8 × N-MORB) and are enriched in LILEs relative to LREEs (e.g. Th/La = 1.7–1.8 × N-MORB) (Fig. 8c, d); and (2) boninitic dykes, which are depleted in bulk REEs (NJ294, NJ296, NJ217) with La = 0.7–1 ppm and Yb = 1–1.8 ppm (versus N-MORB = 2.5 ppm La, 3.05 ppm Yb; Sun & McDonough, 1989), are LREE depleted (La<sub>N</sub>/Yb<sub>N</sub> = 0.3–0.7), have negative Nb anomalies (Nb/La = 0.6–0.8 × N-MORB) and are enriched in positive LILEs relative to LREEs (e.g. Th/La = 3–4.6 × N-MORB) (Fig. 8c, d). Boninitic dykes also have lower Zr and TiO<sub>2</sub> contents.

Dowlat-Abad pillow lavas (Fig. 3e and Fig. A10e in online Appendix 1 at <http://journals.cambridge.org/geo>) are andesitic to dacitic with variable SiO<sub>2</sub> (56–68 wt%; Fig. 5a) and Zr contents (67–106 ppm). They have high FeO/MgO (Fig. 6) and moderate TiO<sub>2</sub> (1.4–1.7 wt%) (Fig. 7a). They have approximately flat REE patterns (Fig. 8c) with La<sub>N</sub>/Yb<sub>N</sub> = 0.7–1.3, Nb depletion (Nb/La = 0.5–0.8 × N-

MORB) and LILE enrichment (e.g. Ba/La = 1.2–8.9 × N-MORB), transitional between N-MORB and IAT (similar to fore-arc basalts).

Tale-Afshari lavas and dykes include both more- and less-evolved samples (M. R. Jannessary, unpub. Ph.D. thesis, l'Univ. de Louis Pasteur, France, 2003). Less-evolved lavas are characterized by low SiO<sub>2</sub> (50–55 wt%), Zr (20–65 ppm) and higher MgO (2.4–6.4 wt%). Lower MgO (0.5–2.5 wt%) and higher Zr (48–205 ppm) and SiO<sub>2</sub> (63–70 wt%) contents of more-evolved samples confirm these represent fractionated magmas. They are mostly tholeiitic (Fig. 6) and similar to lower lavas of Troodos (Fig. 7). More-evolved types have higher bulk REE concentrations (e.g. La = 5.2–6.6 ppm, Yb = 4.8–7.4 ppm versus N-MORB = 2.5 ppm La, 3.05 ppm Yb; Sun & McDonough, 1989) with LREE depletion (La<sub>N</sub>/Yb<sub>N</sub> = 0.6–0.8) and negative Nb anomalies (Nb/La = 0.4–0.5 × N-MORB). These types of lavas show negative Eu anomalies (Eu/Eu\* = 0.7–0.8) indicating plagioclase differentiation. The less-evolved types do not show negative Eu anomalies and are characterized by lower bulk REE contents (e.g. La = 1.6–2.3 ppm, Yb = 2.3–3.1 ppm v. N-MORB = 2.5 ppm La, 3.05 ppm Yb; Sun & McDonough, 1989). These types also show LREE depletion (La<sub>N</sub>/Yb<sub>N</sub> = 0.5–0.6) and significant Nb anomalies (Nb/La = 0.5–0.8 × N-MORB). Both Tale-Afshari lava types have an IAT signature, indicating formation in a suprasubduction zone environment. Most Neyriz lavas are medium- to high-Fe tholeiitic (Fig. 6), characterized by low MgO and high TiO<sub>2</sub> contents resembling Troodos lower lavas (Fig. 7). Some boninitic samples, with lower FeO/MgO and TiO<sub>2</sub> abundances, are similar to Troodos upper lavas (Fig. 7). On a Ti v. V diagram (Shervais, 1982) (Fig. 9a), some plot as IAT while others have slightly higher TiO<sub>2</sub> content, transitional between MORB and IAT.

#### 4.a.3. Haji-Abad ophiolite

Haji-Abad ophiolitic lavas vary in composition from tholeiitic to calc-alkalic (Fig. 6) and from moderately high to very low TiO<sub>2</sub> contents. Three volcanic sequences are distinguished: (1) older E-MORB-type pillow lavas, (2) calc-alkaline volcanic rocks and (3) younger boninitic lavas. E-MORB type pillow lavas (HG10-21, HG10-25 & HG10-26) are found near the MZT, especially near Sheikh-Ali village (see Fig. A4 in online Appendix 1 at <http://journals.cambridge.org/geo>). These older, E-MORB-type lavas are highly altered with relatively high LOI contents (7.9–10.6 wt%) and variably fractionated Mg no. (47–53). They are high-Fe tholeiitic (Fig. 6) similar to Troodos lower lavas (Fig. 7). These lavas have moderately high TiO<sub>2</sub> (1.5–1.8 wt%) (Fig. 7) and plot in the MORB field on a Ti v. V diagram (Shervais, 1982), similar to V1 Oman lavas (Fig. 9a), thought to be the first lavas to erupt. Haji-Abad E-MORB lavas are LREE enriched (La<sub>N</sub>/Yb<sub>N</sub> = 4.3–7.2) (Fig. 8e) and have positive Nb anomalies (Nb/La = 1.4–1.7 ×

N-MORB). They are enriched in LILEs (e.g. Th/La = 2.5–3.1 × N-MORB) (Fig. 8f).

Calc-alkaline lavas are massive or pillowed and are associated with pelagic limestone layers in the Chale–Mort to Haji–Abad tectonic mélange; they are also stratigraphically overlain by pelagic limestones (see Fig. A10g in online Appendix 1 at <http://journals.cambridge.org/geo>). Sample HG10-17 is from a lava flow on top of the turbidite sequence. These lavas are acidic andesite to dacite in composition with SiO<sub>2</sub> and TiO<sub>2</sub> ranging from 60 to 69 wt% (except sample HG10-14 that is characterized by SiO<sub>2</sub> leaching during alteration and a high content of LOI; 10.8 wt%) and 0.47 to 0.95 wt%, respectively. They are more-evolved lavas, with Mg no. indicating significant fractionation, from 33 to 43. In the FeO/MgO against SiO<sub>2</sub> diagram, these lavas plot in the tholeiitic field (Fig. 6) similar to Troodos lower lavas (Fig. 7). These lavas are slightly enriched in LREEs (La<sub>N</sub>/Yb<sub>N</sub> = 1.6–2.2) and LILEs (e.g. Th/La = 2.6–3.2 × N-MORB and Pb/La = 1.1–5.7 × N-MORB). They are strongly depleted in Nb (Nb/La = 0.3–0.8 × N-MORB) and TiO<sub>2</sub> (0.5–0.9 wt%), as expected for subduction-related igneous rocks.

Late boninitic magmatism is represented by pillowed and massive lavas. They are basaltic to basaltic andesite in composition with variable SiO<sub>2</sub> (41–54 wt%) and Mg no. (43.8–76.9). The low SiO<sub>2</sub> content of some lavas may partly reflect alteration, as indicated by high LOI (4.2–6.2 wt%). These lavas have very low Zr (4.7–6.1 ppm) and TiO<sub>2</sub> (0.3–0.4 wt%) contents and FeO/MgO and are similar to Troodos upper lavas (Figs 6, 7). Their low Ti and V contents plot in the boninitic field of the Shervais (1982) discrimination diagram (Fig. 9a). Haji–Abad boninitic lavas also are highly depleted in bulk REEs (e.g. La = 0.1–0.3 ppm, Yb = 0.9–1.2 ppm v. N-MORB = 2.5 ppm La, 3.05 ppm Yb; Sun & McDonough, 1989). They are strongly LREE depleted (La<sub>N</sub>/Yb<sub>N</sub> = 0.1–0.2) (Fig. 8e), with large negative Nb anomalies (e.g. Nb/Th ~ 0.1 × N-MORB) and are strongly enriched in LILEs relative to LREEs (e.g. Th/La = 13.9–41.7 × N-MORB). These boninites are similar to the Ca-boninites of Falloon & Crawford (1991). A late microgabbroic dyke injected into the Haji–Abad mantle sequence (HG10-30) is compositionally similar to boninitic lavas. The dyke has low contents of bulk REEs (e.g. La = 0.2 ppm and Yb = 0.5 ppm), TiO<sub>2</sub> (0.2 wt%) and Zr (2.5 ppm). This dyke is very depleted in LREEs (La<sub>N</sub>/Yb<sub>N</sub> = 0.3) and Nb (Nb/La = 0.5 × N-MORB), similar to boninites. This may be a feeder dyke for the boninitic lavas.

We tentatively conclude that Haji–Abad magmatism evolved from early E-MORB to boninitic.

#### 4.b. Inner Zagros Ophiolitic Belt

The composition of IB ophiolitic lavas and dykes is similar to that of OB rocks, including a wide range in SiO<sub>2</sub> contents, extending to much higher values than seen in modern mid-ocean ridge lavas (Fig. 5b). IB

lavas and dykes are bimodal in SiO<sub>2</sub> content, with two modes: (1) between 50 and 56 wt% and (2) > 61 wt%. This type of chemical variability among the IB lavas as well as OB lavas, in the sense of silica distribution, resembles that of island arc magmatic sequences (Miyashiro, 1973; Pearce & Robinson, 2010).

##### 4.b.1. Nain ophiolite

Crustal rock units in the Nain ophiolite consist of massive and pillowed lavas, a sheeted dyke complex and amphibole gabbros, which also serve as a root zone for the sheeted dyke complex. Diabasic-gabbroic-noritic dykes and isotropic gabbro lenses are widespread within the Nain mantle sequence. To better constrain the chemostratigraphic evolution of the Nain ophiolite, we sampled two sequences where age relationships are clear: (1) a sheeted dyke complex with overlying pillow lavas and underlying gabbros and plagiogranites (see Fig. A11a in online Appendix 1 at <http://journals.cambridge.org/geo>), and (2) intrusions in mantle peridotite, including early rodingitized diabasic-gabbroic dykes/sills and late chloritized diabasic dykes (see Fig. A11b in online Appendix 1 at <http://journals.cambridge.org/geo>). The sheeted dyke complex includes earlier diabasic and later dacitic-rhyolitic-noritic dykes. In the root zone of this complex, the diabasic dykes intrude gabbros, microgabbros, amphibole gabbros and plagiogranite (see Fig. A11a in online Appendix 1 at <http://journals.cambridge.org/geo>). Dykes intrude each other at higher levels. A pillow lava sequence overlies the dyke complex and is covered by pelagic sediments.

Nain ophiolitic dykes are classified into earlier IAT and later boninitic dykes. The FeO/MgO of these dykes mostly distribute in medium-Fe tholeiitic to low-Fe calc-alkaline domains (Fig. 6). These dykes have variable and low contents of TiO<sub>2</sub> (0.2–0.8 wt%) and Zr (17.5–32.5 ppm). Their low TiO<sub>2</sub> content is similar to Troodos low-Ti upper lavas (Fig. 7). One early IAT dyke (BAH-14) is LREE depleted (La<sub>N</sub>/Yb<sub>N</sub> = 0.54) (Fig. 10a). This dyke contains less REE than N-MORB (e.g. La = 1.56 ppm, Yb = 2.07 ppm versus N-MORB = 2.5 ppm La, 3.05 ppm Yb; Sun & McDonough, 1989). It is highly depleted in Nb–Ta (e.g. Nb/La = 0.31 × N-MORB) and enriched in LILEs relative to LREEs (e.g. Th/La = 2.8 × N-MORB) (Fig. 10b). Later boninitic-IAT and boninitic dykes are represented by samples BS05-16 and BS05-13, respectively. BS05-16 shows a LREE-depleted pattern (La<sub>N</sub>/Yb<sub>N</sub> = 0.45) whereas BS05-13 has a U-shaped REE pattern (Fig. 10a, b), with La<sub>N</sub>/Yb<sub>N</sub> = 1.05, typical of boninites (Crawford, Falloon & Green, 1989). These dykes are depleted in REEs relative to N-MORB (e.g. La = 1.24–0.85 ppm, Yb = 0.85–1.36 ppm v. N-MORB = 2.5 ppm La, 3.05 ppm Yb; Sun & McDonough, 1989). A negative Nb anomaly is common for these dykes (e.g. Nb/La = 0.3–0.9 × N-MORB). Late andesitic-dacitic dykes (BS05-12, BS05-8 A) intrude diabases in the Nain sheeted dyke complex. These dykes have

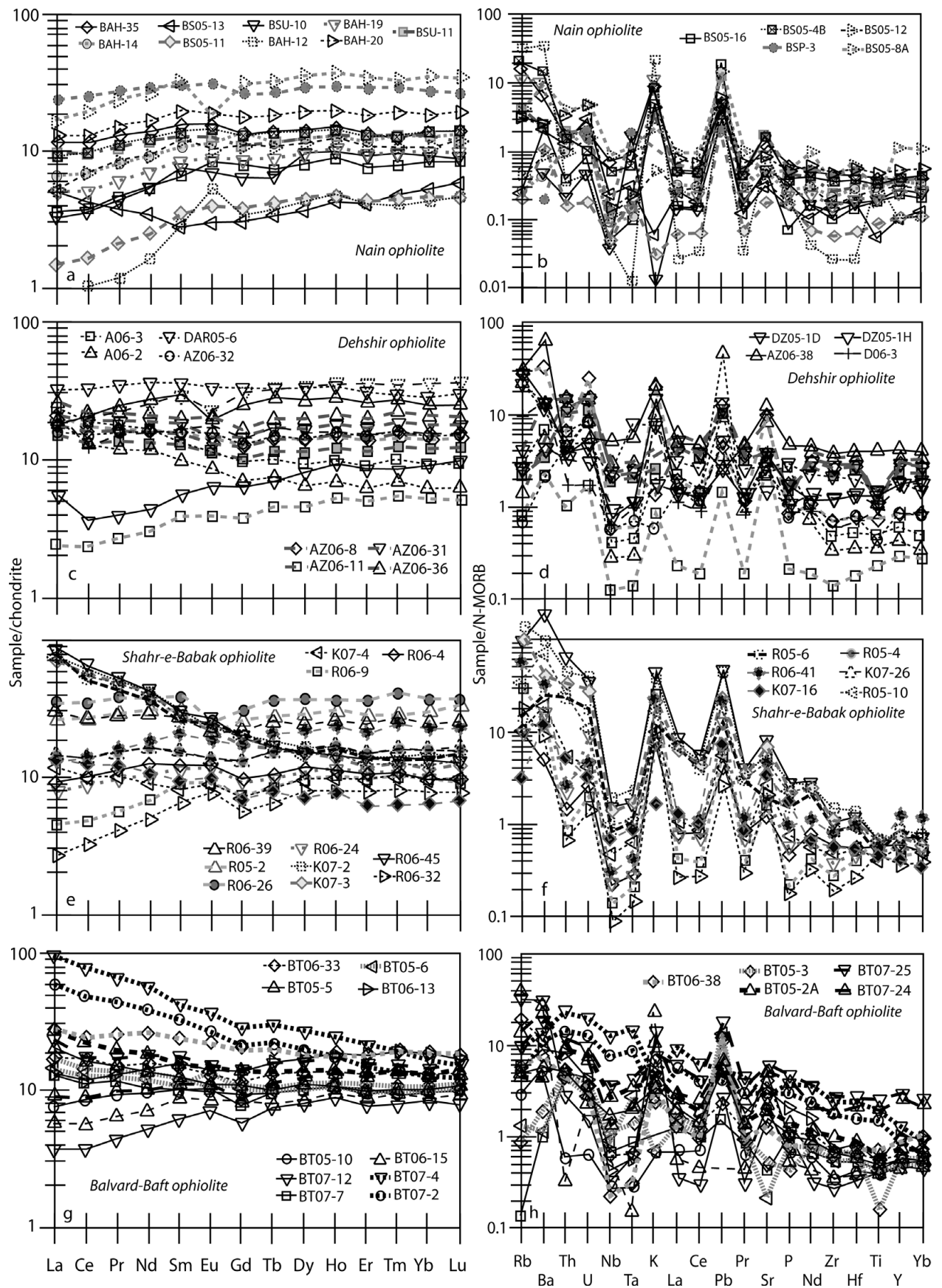


Figure 10. Chondrite-normalized rare earth element patterns (chondrite abundances are from McDonough & Sun, 1995) and normal mid-ocean ridge basalt (N-MORB)-normalized multi-element patterns (N-MORB concentrations are from Sun & McDonough, 1989) for rock units of inner belt ophiolites. (a, b) Nain ophiolite; (c, d) Dehshir ophiolite; (e, f) Shahr-e-Babak ophiolite; and (g, h) Balvard-Baft ophiolite.

55–64 wt % SiO<sub>2</sub> and 0.5–0.7 wt % TiO<sub>2</sub>, with low Zr contents (26–51 ppm). These plot in the calc-alkaline field on the FeO/MgO versus SiO<sub>2</sub> diagram (Fig. 6). Felsic dykes are characterized by depleted LREEs ( $La_N/Yb_N = 0.5$ ) and Nb–Ta (e.g.  $Nb/La = 0.5–0.96 \times N\text{-MORB}$ ) (Fig. 10a, b), similar to IAT trace element patterns. Sample BS05-8 A shows a negative Eu anomaly, suggesting that this was a highly fractionated melt in equilibrium with cumulate or residual plagioclase.

Pillowed tholeiitic lava (BAH-35) found above the sheeted dyke sequence has higher TiO<sub>2</sub> (0.9 wt %) and Zr (61 ppm) relative to dykes. This lava has a flat REE pattern ( $La_N/Yb_N = 0.9$ ) and is enriched in LILEs relative to LREEs (e.g.  $Ba/La = 7.7 \times N\text{-MORB}$ ). Th/La is higher than that of N-MORB ( $Th/La = 2.25 \times N\text{-MORB}$ ), and Ba is even more enriched ( $Ba/Th = 3.4 \times N\text{-MORB}$ ). Nb–Ta is depleted relative to K and U (e.g.  $U/Nb = 2.9 \times N\text{-MORB}$ ), although Nb content of the Nain pillow lava is slightly higher than that of N-MORB ( $Nb = 2.63$  versus  $N\text{-MORB} = 2.33$  ppm Nb; Sun & McDonough, 1989).

Geochemically, most gabbros below the Nain sheeted dyke complex are LREE-depleted IAT ( $La_N/Yb_N = 0.77–0.16$ ), except samples BAH-12 and BS05-11 which are boninitic (Fig. 10a, b). Most gabbros are depleted in Nb compared to LREEs ( $Nb/La = 0.23–1.6 \times N\text{-MORB}$ ) (Fig. 10b). BAH-12 and BS05-11 have very low REE contents (e.g.  $La = 0.16–0.34$  ppm,  $Yb = 0.72–0.73$  ppm versus  $N\text{-MORB} = 2.5$  ppm La, 3.05 ppm Yb; Sun & McDonough, 1989), indicating derivation from highly depleted mantle.

Dykes and sills intruding mantle peridotites, including a gabbroic dyke (BSP-3) and diabasic dykes (BSU-10 & BSU-11), are variably altered, from a rodingitized dyke with high LOI (9.5 wt %) to diabasic dykes with lower LOI (2.1–2.6 wt %). They are characterized by low TiO<sub>2</sub> (0.5–0.8 wt %) and Zr (21–62 ppm). These dykes are LREE-depleted (Fig. 10a) ( $La_N/Yb_N = 0.9–0.4$ ) with negative Nb–Ta ( $Nb/La = 0.3–0.2 \times N\text{-MORB}$ ) and positive LILE anomalies ( $U/La = 2.9–2.8 \times N\text{-MORB}$ ). The gabbroic dyke (BSP-3) is more differentiated (e.g.  $La = 2.73$  ppm versus  $N\text{-MORB} = 2.5$  ppm La; Sun & McDonough, 1989) and the diabasic dyke BSU-10 is boninitic with low REE contents (e.g.  $La = 0.8$  ppm versus  $N\text{-MORB} = 2.5$  ppm La; Sun & McDonough, 1989).

Most Nain lavas scatter in the FeO/MgO v. SiO<sub>2</sub> diagram (Fig. 6). All Nain ophiolite rock units are depleted in immobile Nb and HREEs (Fig. 10b), demonstrating a subduction-related source for genesis of these magmas. On a Ti v. V diagram (Shervais, 1982), lavas show IAT or boninitic affinities (Fig. 9b) and otherwise resemble Troodos upper pillow lavas (Fig. 7). Injection of late boninitic and noritic dykes into early tholeiitic dykes indicate that Nain magmas evolved from early IAT into late boninites as the ophiolite formed. A similar conclusion is reached for dykes intruding mantle peridotites, where late boninitic and non-altered noritic dykes are found.

#### 4.b.2. Dehshir ophiolite

Detailed geochemical data and interpretations were presented by Shafaii Moghadam, Stern & Rahgoshay (2010); here we focus on the chemostratigraphy of ophiolite magmatic units. Fine-grained isotropic gabbros, pillow basalts, basaltic lava flows and basaltic-andesitic-dacitic dykes (in a sheeted dyke complex and intruding amphibole gabbros) are the magmatic rocks of the Dehshir ophiolite. These magmatic rocks belong to both the calc-alkaline and tholeiitic series (Fig. 6). Some samples are similar to Troodos lower lavas, with higher TiO<sub>2</sub> contents, while others resemble Troodos upper lavas (Fig. 7).

Pillow lavas above the sheeted dyke complex (AZ06-32, DAR05-6) (Fig. 4c) and harzburgites (A06-2, A06-3) in the Ardan region (see Fig. A11d in online Appendix 1 at <http://journals.cambridge.org/geo>) show either flat REE patterns ( $La_N/Yb_N = 1.1–1.2$ ) or are LREE enriched ( $La_N/Yb_N = 2.7–3.3$ ) typical of IAT and calc-alkaline series, respectively (Fig. 10c). On an N-MORB-normalized trace element diagram, these lavas are depleted in Nb ( $Nb/La \sim 0.2–0.7 \times N\text{-MORB}$ ) and enriched in Pb, U, Ba and Th (e.g.  $Th/La \sim 1–3 \times N\text{-MORB}$ ) (Fig. 10d).

The sheeted dyke complex includes early basalts and late dacitic dykes (see Fig. A11c in online Appendix 1 at <http://journals.cambridge.org/geo>). An early basaltic dyke (sample AZ06-38) in the sheeted dyke complex has a nearly flat REE pattern (Fig. 10c) with  $La_N/Yb_N = 0.8$ . It shows no high-field-strength element (HFSE) depletion ( $Nb/La = 1.1 \times N\text{-MORB}$ ) and geochemically is similar to N-MORB. Late dacites in the sheeted dyke complex have nearly flat REE patterns ( $La_N/Yb_N = 1.2–1.3$ ). Relative to N-MORB, these rocks are depleted in Nb, Ta, P and Ti, whereas U, Th and Pb show positive anomalies (Fig. 10d). Felsic dykes show trace element similarities with low-K tholeiitic or calc-alkaline rock series. Dacitic dykes are distinguished by very low Sr/Y and  $La_N/Yb_N$  (3.9–10 and 1.2–1.3, respectively), typical of low-pressure basalt fractionates or amphibolite melts (Shafaii Moghadam, Stern & Rahgoshay, 2010).

Isotropic gabbros beneath the sheeted dyke complex (samples D06-3 & DZ05-1 H) (Fig. 4c) have flat to LREE-depleted patterns ( $La_N/Yb_N = 1.7–0.4$ ) with strong Nb depletion ( $Nb/La = 0.2–0.5 \times N\text{-MORB}$ ). An andesitic dyke (DZ05-1D) intruding gabbro has low REE contents relative to N-MORB (e.g.  $La = 0.8$  ppm and  $Yb = 1.5$  ppm v.  $N\text{-MORB} = 2.5$  ppm La, 3.05 ppm Yb; Sun & McDonough, 1989), with LREE and Nb depletion ( $La_N/Yb_N = 0.4$ ;  $Nb/La = 0.4 \times N\text{-MORB}$ ), similar to boninite. On a Ti v. V diagram (Shervais, 1982), Dehshir lavas show MORB to boninitic affinities (Fig. 9b).

A diabasic dyke in mantle harzburgite (AZ06-29; see Fig. A11d in online Appendix 1 at <http://journals.cambridge.org/geo>) is slightly LREE enriched ( $La_N/Yb_N = 1.6$ ) but is strongly depleted in Nb

and Ta (e.g. Nb/La  $\sim 0.3 \times$  N-MORB), typical of calc-alkaline series. Dyke sample A06-1 is compositionally similar to overlying pillow lavas. Another diabasic dyke (AZ06-29, Fig. 10c, d) is depleted in total REEs (La = 0.6 ppm, Yb = 0.8 ppm versus N-MORB = 2.5 ppm La, 3.05 ppm Yb; Sun & McDonough, 1989), LREE-depleted ( $La_N/Yb_N = 0.5$ ) and is strongly depleted in Nb (Nb/La =  $0.5 \times$  N-MORB).

Although disruption of rock units during and after ophiolite emplacement prohibits reconstructing Dehshir ophiolitic lava chemostratigraphy in detail, the data of Shafäii Moghadam, Stern & Rahgoshay (2010) indicate that basalt lava compositions vary from MORB and IAT to calc-alkaline and boninitic with time (see Fig. A11c, d in online Appendix 1 at <http://journals.cambridge.org/geo>). For example, the base of pillow lavas (see Fig. A11c in online Appendix 1 at <http://journals.cambridge.org/geo>) is IAT (sample AZ06-32) and is intruded by basaltic-dacitic dyke swarms. Early basaltic dykes (sample AZ06-38) are N-MORB and are intruded by late dacitic dykes with a suprasubduction zone chemical signature. We saw no evidence in the field for a break between the MORB/IAT (lower) and the upper (IAT/boninite) sequences in the form of an unconformity or intervening sedimentary sequence.

#### 4.b.3. Shahr-e-Babak ophiolite

Basaltic to rhyolitic lava sheets interbedded with Upper Cretaceous pelagic sediments (limestones, radiolarites, marly limestones) (Fig. 4f and Fig. A11f in online Appendix 1 at <http://journals.cambridge.org/geo>) are the main components of the Shahr-e-Babak ophiolite crustal sequence. Lavas are basaltic, andesitic, dacitic and rhyolitic together with minor pyroclastic rocks. Rhyolitic dykes and sills cross-cut this rock assemblage. To constrain the geochemical signatures of this sequence, we selected interbedded mafic (R06-9, R06-45, R05-6, R06-32 and R06-24), andesitic (R06-41) and dacitic samples (R06-39). A rhyolitic dyke (R06-26) injected into the lavas is also discussed (Fig. 4e and Fig. A11f in online Appendix 1 at <http://journals.cambridge.org/geo>). Interbedded lavas have SiO<sub>2</sub> and Mg no. ranging from 47 to 70 wt% and 62 to 27, respectively. The rhyolitic dyke is more evolved with 74 wt% SiO<sub>2</sub> and a Mg no. of 22. These lavas mostly have higher FeO/MgO and are mildly tholeiitic (Fig. 6) with some calc-alkaline samples. Their variable TiO<sub>2</sub> contents overlap with both lower and upper Troodos lavas (Fig. 7). These lavas display two REE patterns (Fig. 10e): (1) slightly to highly LREE enriched and (2) LREE depleted. LREE-enriched samples show  $La_N/Yb_N = 1.3$  for dacitic lava (sample R06-39) and  $La_N/Yb_N = 6.1-7.1$  for some mafic lavas (samples R05-6 and R06-45). HFSE depletion and LILE enrichment relative to LREEs is typical for these lavas (e.g. Nb/La =  $0.1-0.3 \times$  N-MORB, Th/La  $\sim 2.5-7.3 \times$  N-MORB and U/La  $\sim 2.4-$

$3.9 \times$  N-MORB). Some mafic lavas show calc-alkaline to shoshonitic affinities. LREE-depleted samples have  $La_N/Yb_N = 0.4-0.9$  and are depleted in Nb-Ta relative to LREEs (Nb/La  $\sim 0.3 \times$  N-MORB), similar to IAT. Samples R06-32 and R06-9 are exceptional, with low concentrations of REEs (e.g. La = 0.7-1.1 ppm, Yb = 1.5-1.2 ppm versus N-MORB = 2.5 ppm La, 3.05 ppm Yb; Sun & McDonough, 1989) similar to boninites. A rhyolitic dyke has a nearly flat REE pattern,  $La_N/Yb_N = 1.1$  (Fig. 10e), negative Eu anomaly, depletion in Nb (Nb/La  $\sim 0.3 \times$  N-MORB) and LILE enrichment (Th/La  $\sim 2.5 \times$  N-MORB), confirming formation as a low-pressure fractionate of IAT magma or amphibolite melt.

Based on field observations, it seems that calc-alkaline-shoshonitic lavas are younger than tholeiites. Lavas are interbedded with Upper Cretaceous pelagic sediments. Upper Cretaceous calc-alkaline-shoshonitic lavas are sometimes confused with Eocene shoshonitic basaltic-dacitic lavas, but some features distinguish them: (1) Upper Cretaceous ones are interbedded with Upper Cretaceous pelagic sediments with no evidence of injection into pelagic limestones, and (2) dacitic-rhyolitic lavas associated with ophiolites are tholeiitic compared to Eocene calc-alkaline dacites.

Shahr-e-Babak ophiolite pillow lavas (see Fig. A11e in online Appendix 1 at <http://journals.cambridge.org/geo>) occur as isolated patches in fault contact with massive lava flows. Massive and pillowed lavas are variably evolved (Fig. 5) with SiO<sub>2</sub> and Mg no. ranging from 50 to 74 wt% and 31 to 54, respectively. These lavas are tholeiitic (Fig. 6) and resemble Troodos lower lavas (Fig. 7) with slightly higher TiO<sub>2</sub> content ( $\sim 0.7$  wt%). A pillow lava sample (R06-4) is slightly LREE-depleted ( $La_N/Yb_N = 0.9$ ) with negative Nb anomaly relative to LREEs (Nb/La  $\sim 0.3 \times$  N-MORB) resembling IAT (Fig. 10e, f). Overlying basaltic to dacitic lava flows, as well as interbedded rock units discussed above, are classified as: (1) those with flat REE patterns ( $La_N/Yb_N = 0.9-1.3$ ) and Nb depletions (Nb/La  $\sim 0.2-0.3 \times$  N-MORB), similar to IAT, and (2) those with LREE-enriched patterns ( $La_N/Yb_N = 2.3-6.5$ ) and strong Nb depletions (Nb/La  $\sim 0.1-0.5 \times$  N-MORB) resembling calc-alkaline to shoshonitic lavas. Both types are overlain by Upper Cretaceous pelagic limestones.

Nb depletion is especially conspicuous for Shahr-e-Babak lavas compared with other inner and outer belt ophiolitic lavas; calc-alkaline rocks have more Nb than tholeiitic-boninitic lavas (Fig. 10f). On a Ti v. V diagram (Shervais, 1982), the Shahr-e-Babak lavas scatter in the fields of boninite to MORB (Fig. 9b); felsic lavas have very low V and Ti concentrations.

Although disruption and faulting of the Shahr-e-Babak ophiolite prohibits chemostratigraphic reconstruction of lava stratigraphy, our field observations for individual sections suggest that lava compositions changed from IAT/boninite into calc-alkaline-shoshonitic with time.

#### 4.b.4. Balvard–Baft ophiolite

Crustal rock units in the Balvard–Baft ophiolite consist of massive and pillowed lavas, overlain by pyroclastic rocks. Basaltic to dacitic sills are common within the pyroclastic rocks (Fig. 4g and Fig. A11h in online Appendix 1 at <http://journals.cambridge.org/geo>). Upper Cretaceous pelagic limestones rest unconformably on the pyroclastic rocks (Fig. 4h). Isotropic gabbro lenses are common within the Balvard–Baft mantle sequence. To better constrain the chemostratigraphic evolution of the Balvard–Baft ophiolite, we studied two sequences: (1) an isotropic gabbro lens including early diabasic and late gabbroic dykes NNW of Baft (see Fig. A11g in online Appendix 1 at <http://journals.cambridge.org/geo>), and (2) a volcanic sequence (Cheshmeh–Baghal sequence) grading upwards into pyroclastic rocks and capped by Upper Cretaceous pelagic limestones (Fig. 4h and Fig. A11h in online Appendix 1 at <http://journals.cambridge.org/geo>). Mafic samples of the Balvard–Baft ophiolite have 40 wt % (most altered basaltic sample) to 54 wt % SiO<sub>2</sub> and 23 to 72 Mg no. They are characterized by medium-Fe, mildly tholeiitic to calc-alkaline signatures (Fig. 6). Most have low TiO<sub>2</sub> content and plot in upper lava field of the Troodos ophiolite (Fig. 7).

An isotropic gabbro sample (BT05-5) is LREE enriched ( $La_N/Yb_N = 2.2$ ) (Fig. 10g) with slight Nb depletion relative to LREEs ( $Nb/La \sim 0.8 \times N\text{-MORB}$ ) (Fig. 10h) similar to T-MORB. Early diabasic dykes (sample BT05-2 A) cross-cut isotropic gabbros and are enriched in LREEs ( $La_N/Yb_N = 2.2$ ) and LILEs (e.g.  $Th/La \sim 3.6 \times N\text{-MORB}$ ) without a negative Nb anomaly ( $Nb/La \sim 1.1 \times N\text{-MORB}$ ). These dykes are compositionally transitional between transitional mid-ocean ridge basalts (T-MORB) and calc-alkaline lavas. Late gabbroic dykes (BT05-3 & BT05-6) also are enriched in LREEs ( $La_N/Yb_N = 1.6\text{--}1.7$ ) and Th ( $Th/La \sim 3.1 \times N\text{-MORB}$ ) and are somewhat depleted in Nb ( $Nb/La \sim 0.7 \times N\text{-MORB}$ ), similar to calc-alkaline series. This suggests that magmas evolved from MORB to calc-alkaline with time. Other isotropic gabbros in the Balvard–Baft mantle sequence (e.g. BT06-33) show calc-alkaline affinities with LREE enrichment ( $La_N/Yb_N = 1.5$ ) and Th ( $Th/La \sim 3.2 \times N\text{-MORB}$ ) and Nb depletion ( $Nb/La \sim 0.3 \times N\text{-MORB}$ ) (Fig. 10g, h).

E-MORB-type pillow lavas were first reported by Arvin & Robinson (1994) in the Balvard–Baft ophiolite. Pillow lavas at the base of the ophiolite volcanic sequence are LREE enriched ( $La_N/Yb_N \sim 5\text{--}6$ ), lack Nb depletion ( $Nb/La \sim 1.4 \times N\text{-MORB}$ ) and are similar to E-MORB. Overlying massive lavas (samples BT06-13 & BT06-15) are LREE and Nb depleted ( $La_N/Yb_N \sim 0.7\text{--}0.8$ ;  $Nb/La \sim 0.2 \times N\text{-MORB}$ ) (Fig. 10g, h), similar to IAT. Sample BT06-15 is also depleted in bulk REEs (e.g.  $La = 1.4$  ppm,  $Yb = 1.4$  ppm versus  $N\text{-MORB} = 2.5$  ppm  $La$ , 3.05 ppm  $Yb$ ; Sun & McDonough, 1989), resembling boninite. Lava flows are overlain by thick pyroclastic

rocks with basaltic to dacitic sills. Basaltic sills (BT07-24 and BT06-25) have geochemical affinities with IAT, including approximately flat REE patterns ( $La_N/Yb_N \sim 0.8\text{--}1.8$ ), Nb depletion ( $Nb/La \sim 0.4\text{--}0.5 \times N\text{-MORB}$ ) and Th enrichment ( $Th/La \sim 2.6\text{--}5.1 \times N\text{-MORB}$ ) (Fig. 10g, h). A pillow fragment in volcanic breccias (BT06-38) is calc-alkaline with LREE enrichment ( $La_N/Yb_N \sim 1.5$ ) and strong negative Nb anomaly ( $Nb/La \sim 0.2 \times N\text{-MORB}$ ). Geochemical evolution from MORB to IAT and then into calc-alkaline and boninitic is characteristic of the lava sequence at Cheshmeh–Baghal. On a Ti v. V diagram (Shervais, 1982) (Fig. 9b), Balvard–Baft lavas plot mostly in the IAT field but also in MORB and boninite fields.

#### 4.c. Inner and outer belt ophiolitic peridotite: constraints from whole-rock CaO and Al<sub>2</sub>O<sub>3</sub> contents

Peridotite compositions are sensitive indicators of tectonic setting (e.g. Bonatti & Michael, 1989). Some major oxides such as Al<sub>2</sub>O<sub>3</sub> and CaO are especially useful for evaluating the degree of melting and peridotite depletion (Ishii *et al.* 1992; Pearce *et al.* 1992). Modal abundance of clinopyroxene in mantle peridotite covaries with CaO and Al<sub>2</sub>O<sub>3</sub> contents. Most mantle rocks of both inner and outer belt ophiolites are harzburgites with low modal pyroxene abundances and low Al<sub>2</sub>O<sub>3</sub> and CaO contents. Depleted lherzolites occur sporadically in some ophiolites. These peridotites mostly plot in the Mariana fore-arc field on an Al<sub>2</sub>O<sub>3</sub> v. CaO diagram (Fig. 11), similar to Oman peridotites. Some peridotites from the Haji–Abad, Dehshir and Balvard–Baft ophiolites, as well as some Oman peridotites, have higher pyroxene modal content and plot in the abyssal peridotite field of Pearce *et al.* (1992). As is clear in Figure 11, most OB and IB Zagros and Oman peridotites are residues after > 15% partial melting (RMM20). For comparison we also plotted Kermanshah peridotite data from Allahyari *et al.* (2010). These are considered depleted abyssal peridotite having high Al<sub>2</sub>O<sub>3</sub> and CaO contents. These peridotites, especially lherzolites show scatter in the Al<sub>2</sub>O<sub>3</sub> v. CaO diagram (Fig. 11), having CaO and Al<sub>2</sub>O<sub>3</sub> contents that are mostly lower than depleted MORB mantle (e.g. Workman & Hart, 2005). In contrast, ZOB peridotites are compositionally similar to fore-arc peridotites.

#### 4.d. Pyroxene composition of inner and outer belt peridotites

Depleted mantle harzburgite has pyroxenes with higher Mg no. and lower TiO<sub>2</sub> and Al<sub>2</sub>O<sub>3</sub> abundances than fertile lherzolite. OB and IB peridotites usually have Opx with Mg no. > 90.1, except for Dehshir, where Opx Mg no. = 85–90. OB and IB peridotite orthopyroxenes have low Al<sub>2</sub>O<sub>3</sub> (< 4 wt %) and CaO (< 2.2 wt %), except for some Nain and Haji–Abad Opxs with slightly higher Al<sub>2</sub>O<sub>3</sub> content, resembling depleted

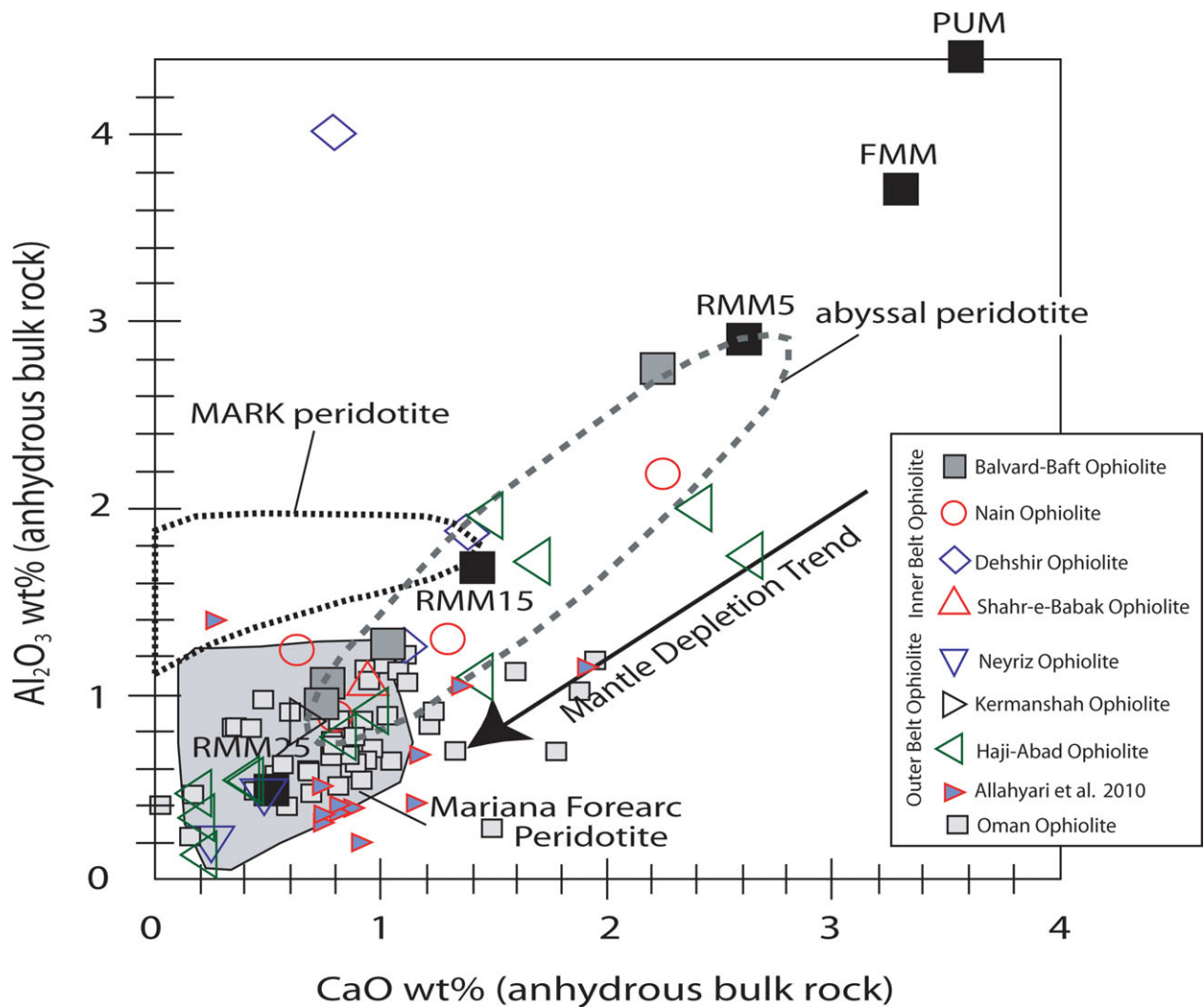


Figure 11. (Colour online)  $\text{Al}_2\text{O}_3$  v.  $\text{CaO}$  compositional plot (volatile free, normalized to 100 % total) for Zagros inner and outer belt ophiolitic peridotites. Fields for abyssal and fore-arc peridotites are from Pearce *et al.* (1992). MARK peridotite data is from Casey (1997). Data for Oman ophiolite harzburgites (Godard, Jousset & Bodinier, 2000; Girardeau *et al.* 2002) are shown for comparison. The composition of primitive upper mantle (PUM), fertile MORB mantle (FMM) and mantle residue after 5 to 25 % partial melting are from Pearce & Parkinson (1993). Data for the Kermanshah ophiolite from Allahyari *et al.* (2010) are shown for comparison.

harzburgites from modern fore-arcs (Fig. 12a).  $\text{Al}_2\text{O}_3$  and  $\text{TiO}_2$  contents of most OB and IB peridotite clinopyroxenes are similar to the very low values found in Cpx from highly depleted fore-arc peridotites (Ishii *et al.* 1992) (Fig. 12b). Most OB and IB harzburgite Cpxs are chemically distinct from those of moderately depleted abyssal peridotites, which have significantly higher  $\text{Al}_2\text{O}_3$  and  $\text{TiO}_2$  contents (e.g. Hébert, Adamson & Komor, 1990; Johnson, Dick & Shimizu, 1990). Some Cpxs from Haji-Abad, Neyriz and Kermanshah harzburgites have higher  $\text{TiO}_2$  content, indicating compositional changes due to re-equilibration of Cpx with percolating melts.

#### 4.e. Spinel composition from inner and outer belt peridotites

Spinel Cr no. ( $=100\text{Cr}/(\text{Cr} + \text{Al})$ ) is a sensitive indicator of partial melting of host peridotite (e.g. Dick & Bullen, 1984; Johnson, Dick & Shimizu, 1990). With increasing degree of partial melting, decreasing activity

of aluminium in the peridotite leads to an increase in Cr no. of spinel (Hellebrand *et al.* 2001; Hellebrand, Snow & Muhe, 2002). Fore-arc mantle peridotite is composed of depleted harzburgite, characterized by spinels with Cr no.  $> 50$  and low  $\text{TiO}_2$  contents (Bloomer & Hawkins, 1983; Parkinson & Pearce, 1998; Stern, 2010). Spinels from the IB and OB peridotites (also spinel data from Allahyari *et al.* 2010 on the Kermanshah ophiolite), as well as spinels from the Oman peridotite, show chemical variations following both the MORB and fore-arc trends of Dick & Bullen (1984), with most of them plotting in the fore-arc field (Fig. 13a). The  $\text{TiO}_2$  content of most spinels is less than 0.2 wt % similar to those of fore-arc harzburgites and boninites (Tamura & Arai, 2006) (Fig. 13b). Some spinels, especially Haji-Abad spinels, display higher  $\text{TiO}_2$  abundance ( $\text{TiO}_2 > 0.2$  wt %), interpreted to be the result of melt-mantle interaction during melt percolation (Cannat *et al.* 1997). These spinels are found in very depleted harzburgites of the Haji-Abad mantle sequence.

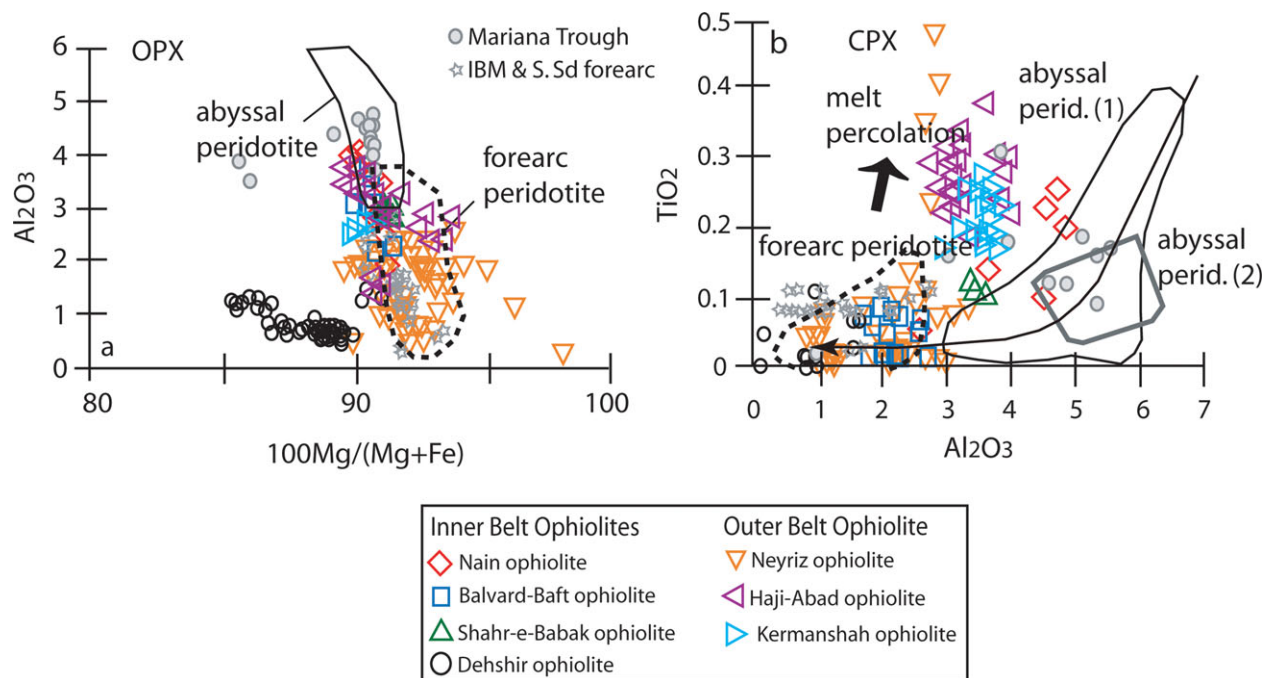


Figure 12. (Colour online) Composition of OB and IB harzburgite pyroxenes. (a) Orthopyroxene Al<sub>2</sub>O<sub>3</sub> v. Mg no. composition diagram. Fields for abyssal peridotites (Johnson, Dick & Shimizu, 1990) and fore-arc peridotites (Ishii *et al.* 1992) are shown for comparison. (b) Clinopyroxene TiO<sub>2</sub> against Al<sub>2</sub>O<sub>3</sub> for OB and IB harzburgites. Comparative fields are shown for abyssal peridotites (abyssal peridotite 1: Hébert, Adamson & Komor, 1990; abyssal peridotite 2: Johnson, Dick & Shimizu, 1990) and fore-arc peridotites (Ishii *et al.* 1992). The long thin arrow shows changes expected for residual clinopyroxene due to progressive partial melting of peridotite. Short thick arrow shows compositional changes due to re-equilibration of Cpx with percolating melt. Izu–Bonin–Mariana (IBM) and South Sandwich fore-arc harzburgite data are from Parkinson & Pearce (1998) and Pearce *et al.* (2000), respectively; Mariana Trough (back-arc basin peridotite) data are from Ohara *et al.* (2002). For comparison we have also plotted data on the Kermanshah peridotite from Allahyari *et al.* (2010).

## 5. Discussion

In this Section we discuss three aspects of the Upper Cretaceous Zagros ophiolites: compositional variations, comparison with other Upper Cretaceous ophiolites between Cyprus and Oman and modern fore-arcs, and the tectonic setting of Upper Cretaceous Zagros ophiolites.

### 5.a. Summary of Upper Cretaceous Zagros ophiolite compositional variations

Geochemical evolution of both the OB and IB ophiolites is summarized in Table 1. OB and IB mantle harzburgites, as well as Oman peridotites, have low CaO and Al<sub>2</sub>O<sub>3</sub> abundances similar to Mariana fore-arc peridotite (Pearce *et al.* 1992). Fore-arc peridotites are typically more depleted than abyssal peridotites, except for some lherzolites from the South Sandwich fore-arc (Pearce *et al.* 2000; Arai & Ishimaru, 2008). Opx and Cpx from OB and IB harzburgites have low CaO, Al<sub>2</sub>O<sub>3</sub> and TiO<sub>2</sub> contents, resembling those of depleted harzburgites from modern fore-arcs and different from moderately depleted abyssal peridotites. OB and IB mantle harzburgites, like Oman harzburgites, are dominated by Cr-rich spinels, mostly with Cr no. > 50 and low TiO<sub>2</sub> content, similar to spinel from fore-arc harzburgites. In fertile abyssal lherzolites, spinels with Cr no. < 30 are dominant (Dick & Bullen,

1984), while spinel in fore-arc peridotites may cover a slightly wider range, 40 < Cr no. < 80 (Arai, 1994).

OB and IB lavas and dykes, as well as other Upper Cretaceous Tethyan ophiolites such as Troodos (Pearce & Robinson, 2010) have variable SiO<sub>2</sub> contents; most lavas have 50–56 wt % SiO<sub>2</sub> but a significant proportion has up to 75 wt % SiO<sub>2</sub> (Fig. 5). The abundance of silica-rich lavas is not seen at mid-ocean ridges and is an important argument for a suprasubduction zone origin for Zagros ophiolites. Compositional data for lavas and isotropic gabbros from both IB and OB ophiolites scatter on the FeO<sup>1</sup>/MgO versus SiO<sub>2</sub> diagram of Arculus (2003) (Fig. 6). Although some of this scatter may reflect alteration, mostly it indicates that tholeiitic and calc-alkaline magmas coexisted, although most lavas plot in the tholeiitic, medium- to high-Fe field. Oman V1 and V2 lavas, when compared to IB and OB lavas, are mostly high-Fe tholeiites, while other Tethyan Upper Cretaceous ophiolites such as the Kizildag (Turkey) are mostly low- to medium-Fe types, probably manifesting differing magmatic H<sub>2</sub>O contents, low for tholeiites and high for calc-alkaline series (Arculus, 2003). Our Al<sub>2</sub>O<sub>3</sub>/TiO<sub>2</sub> v. TiO<sub>2</sub> data from OB and IB lavas as well as Kizildag and Oman ophiolites and Izu-Bonin-Mariana (IBM) fore-arc basalts range from MORB-like to IAT to boninites (Fig. 14a). The first lavas in Tethyan ophiolites as well as IBM fore-arc basalts tend to be MORB-like, with higher TiO<sub>2</sub> and Zr

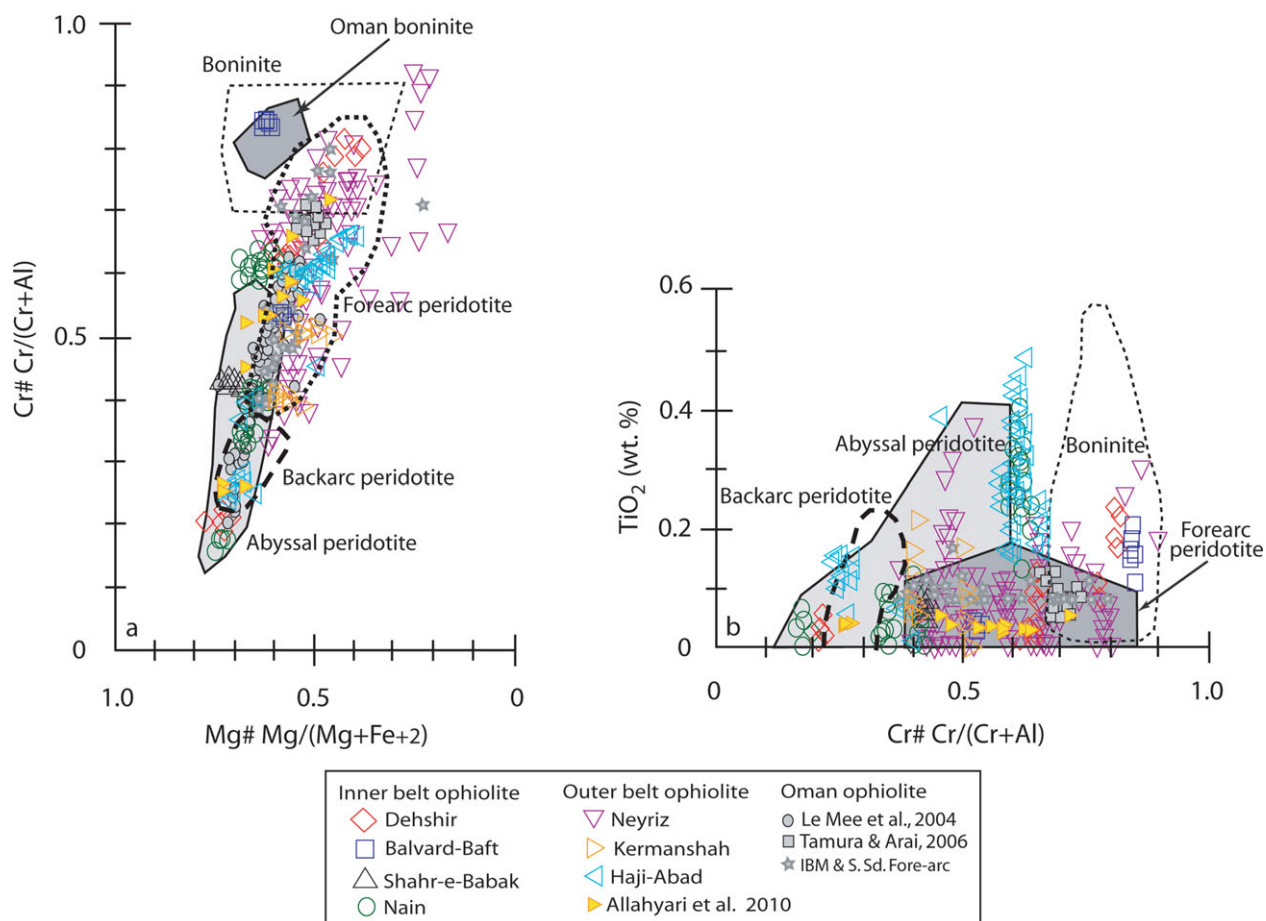


Figure 13. (Colour online) (a) Cr no. v. Mg no. diagram (modified after Dick & Bullen, 1984) for spinels in OB and IB harzburgites. (b) Diagram (after Tamura & Arai, 2005, 2006) showing TiO<sub>2</sub> against Cr no. of spinels, in order to discriminate between various types of peridotites and links to boninite. Note that spinels plot in fields for both MORB peridotites and fore-arc peridotites. Some data show affinity to boninite. IBM and South Sandwich fore-arc harzburgite data are from Parkinson & Pearce (1998) and Pearce *et al.* (2000), respectively; Mariana Trough (back-arc basin) peridotite are from Ohara *et al.* (2002); Oman harzburgite data are from Le Mée, Girardeau & Monnier (2004) and Tamura & Arai (2006).

contents (Fig. 14b), compared to younger calc-alkaline or boninitic lavas.

Furthermore, most ZOB lavas and dykes show trace element characteristics of subduction-related magmas (IAT, boninite and calc-alkaline) such as Nb–Ta depletion and LILE enrichments but there are some with trace element patterns like those of MORB. Where magmatic successions can be reconstructed, there is often a change from earlier tholeiitic melts (MORB and/or IAT) that are less affected by subduction-related geochemical inputs to those that are more affected, such as boninitic and/or calc-alkaline lavas or intrusions. E-MORB type pillow lavas are also found in the Balvard–Baft and Haji–Abad ophiolites, while N-MORB basalts occur in the Dehshir ophiolite. Late boninitic lavas and dykes are common in most inner and outer belt ophiolites but are especially conspicuous in the Nain, Haji–Abad, Balvard–Baft and Dehshir. Late-stage high-K calc-alkaline to shoshonitic magmatism is common in the Kermanshah and Shahr-e-Babak ophiolites. This magmatic evolution, from bottom to top, appears to have been continuous; there is no evidence in any of the ophiolites for

a hiatus between lower MORB/IAT-like and upper calc-alkaline/boninite sequences in the form of an unconformity or intervening sedimentary sequence. This evolution is similar to that seen in the IBM fore-arc (Reagan *et al.* 2010).

The Th/Yb versus Nb/Yb diagram is useful for further exploring the petrogenesis and tectonic setting of OB and IB igneous rocks (Fig. 14c). In this diagram, Yb is used to normalize Nb and Th to remove the effects of partial melting, fractional crystallization and crystal accumulation (Pearce & Peate, 1995; Pearce *et al.* 1995). Th and Nb have similar melt-crystal distribution coefficients (Leat *et al.* 2004), but Th is added by high-temperature fluid release from subducted sediments to mantle magma sources above subduction zones, whereas Nb is not. Most, but not all, OB and IB mafic rocks are displaced from the mantle array, defined by MORB and OIB owing to higher concentrations of the subduction-mobile element Th (Fig. 14c). These relations reinforce the conclusion that most OB and IB melts were derived from subduction-modified MORB-like asthenospheric mantle. The Oman V1 (Geotimes unit) and V2 (Lasail unit) lavas follow the Zagros

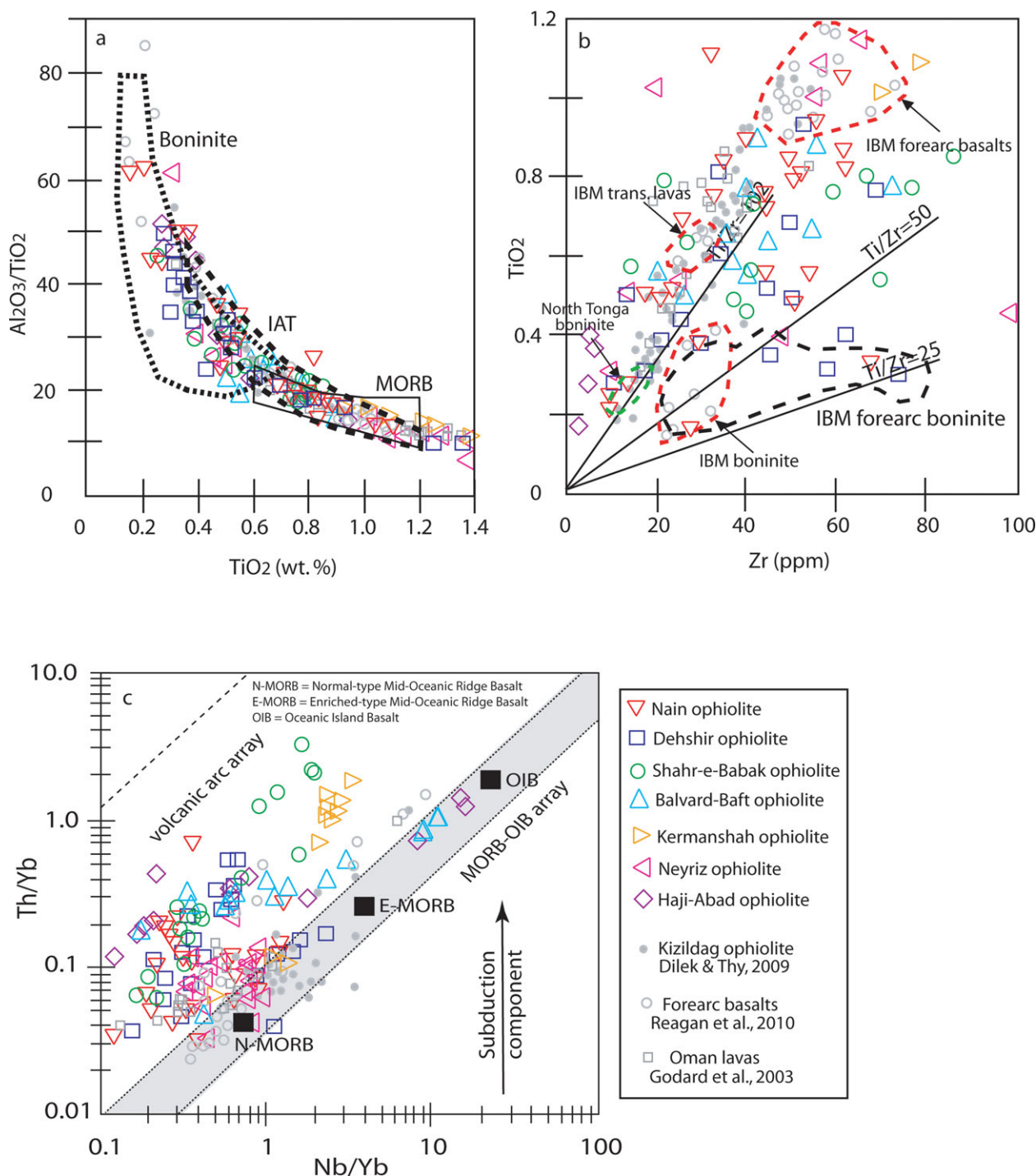


Figure 14. (Colour online) (a)  $Al_2O_3/TiO_2$  versus  $TiO_2$  and (b) Zr versus  $TiO_2$  variations for OB and IB magmatic rocks (modified after Bağcı, Parlak & Hock, 2008). North Tonga boninites from Falloon & Crawford (1991); IBM fore-arc boninites from Arculus *et al.* (1992). (c) Th/Yb v. Nb/Yb diagram (after Leat *et al.* 2004) for OB and IB ophiolites. Most OB and IB mafic rocks have high Th/Yb and plot above the mantle array near the volcanic arc array, with some exceptions that are MORB-like. For comparison data from the Kizildag ophiolite, Turkey (Dilek & Thy, 2009), Oman lavas (Godard, Dautria & Perrin, 2003) and IBM fore-arc lavas (Reagan *et al.* 2010) are shown.

ophiolite trends with lower Th (and maybe higher Yb) content, while Kizildag ophiolite (Turkey) lavas mostly plot along the MORB–OIB array. Nevertheless, MORB-like tholeiites are common and cannot easily be ascribed to a different tectonic setting; instead, these are probably associated with fore-arc spreading when subduction began.

Low concentrations of incompatible elements and low Nb/Yb imply that tholeiitic melts issued from depleted N-MORB mantle, with the interesting exception of E-MORB/OIB-type lavas in the Balvard–Baft and Haji–Abad ophiolites. Involvement of convecting asthenosphere and/or extremely depleted mantle with more extensive hydrous fluid input generated

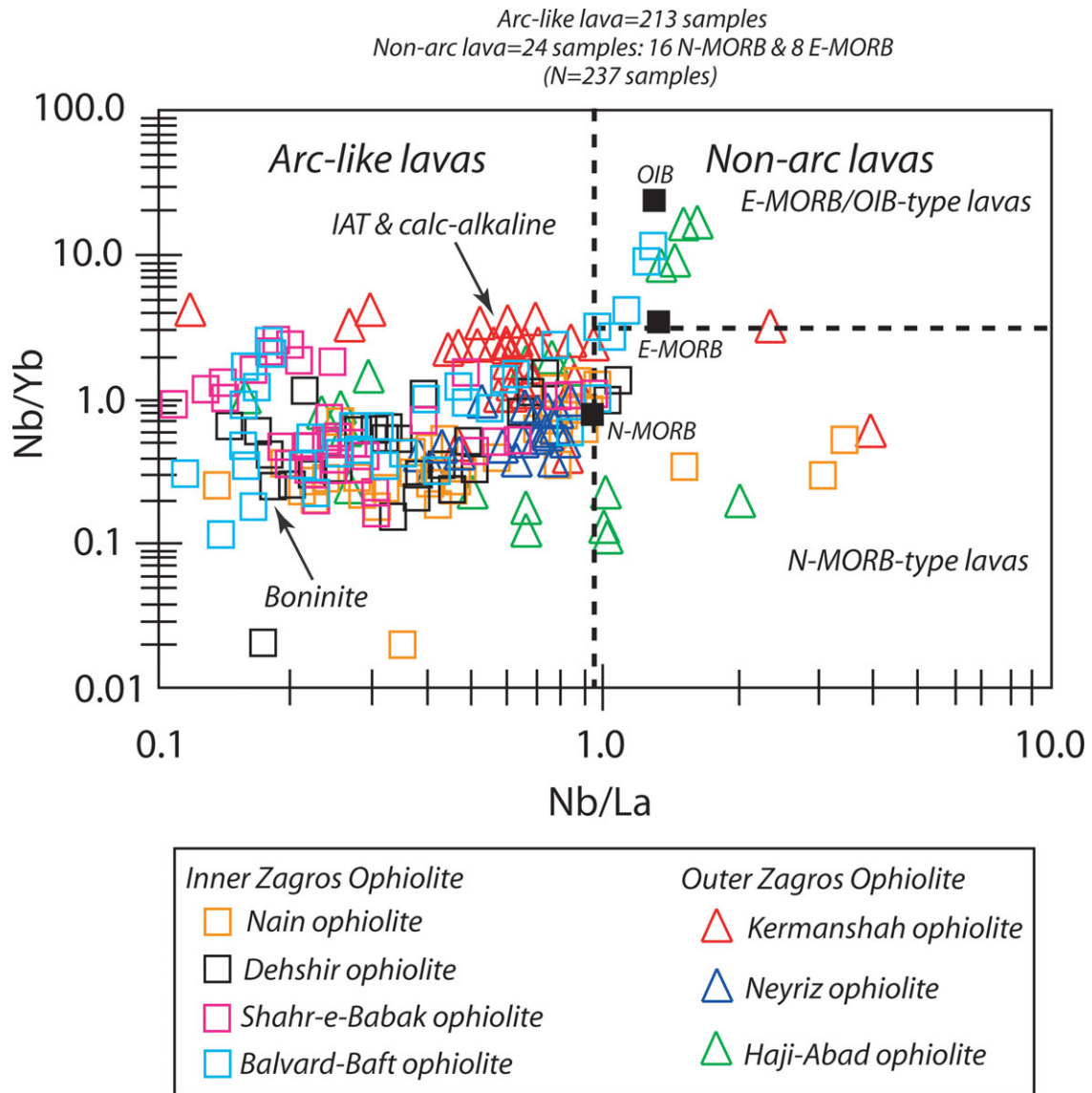


Figure 15. (Colour online) Nb/Yb v. Nb/La diagram to discriminate between arc-like and non-arc lavas and dykes in the Upper Cretaceous Zagros ophiolites. Nearly all samples (90 %) indicate arc-like characteristics while only 10 % of lavas have a tendency towards non-arc geochemical characteristics.

IAT/calc-alkaline and boninitic magmas, respectively (Ishizuka *et al.* 2006). Some pillow lavas from the Balvard–Baft and Haji–Abad ophiolites are geochemically between E-MORB and OIB-type lavas. There are two possible explanations for the genesis of these lavas: (1) they formed during the early stage of oceanic formation (in Late Permian time), as suggested by Allahyari *et al.* (2010) for the genesis of E-MORB type gabbros in Kermanshah ophiolites. In addition, Ghazi & Hassanipak (1999) and M. Arvin (unpub. Ph.D. thesis, Univ. London, 1982) reported Triassic OIB-type lavas from Kermanshah and Neyriz ophiolites. Therefore, it may be that these E-MORB/OIB-type lavas correlate with the alkaline lavas of the Oman (Robertson, 2007) and that they formed during the rifting/early oceanization phase of north Gondwana. However, the Balvard–Baft and Haji–Abad E-MORB/OIB-type pillow lavas are associated with Upper Cretaceous pelagic limestones and are

not likely to be Triassic; and (2) the Haji–Abad and Balvard–Baft E-MORB/OIB-type lavas are in fact the first lavas to erupt when the Tethyan oceanic plate began to sink beneath the Eurasian plate as subduction began in Late Cretaceous time. They were generated from subduction component-free mantle, perhaps flowing in from beneath Eurasia to fill space created by the initial sinking of the Tethyan plate, as hypothesized by Stern & Bloomer (1992). Such a model is also suggested for the early MORB-like lavas from the IBM fore-arc (Reagan *et al.* 2010). To approximate the proportion of ophiolitic lavas and dykes that are arc-like rather than non-arc-like (MORB and E-MORB) we plotted all Zagros ophiolitic lavas and dykes on a Nb/Yb v. Nb/La diagram (Fig. 15). Arc lavas are represented by Nb/La < 0.95 while a Nb/Yb ratio > 3 discriminates between N-MORB and E-MORB. A total of 237 analyses were plotted; 213 samples (90 %) have the low Nb/La indicating arc affinities

(Fig. 15), whereas only 24 samples (10%) are characterized by non-arc geochemical signatures. Among non-arc lavas, only 8 samples (3%) plot in the E-MORB field and 16 samples (7%) plot in the N-MORB field. This diagram emphasizes the overwhelming arc-like affinities of lavas and dykes in the Zagros Upper Cretaceous ophiolites.

### 5.b. Comparison with Oman–Turkey, Troodos ophiolites and the IBM fore-arc

Upper Cretaceous Tethyan ophiolites south of the Tauride platform (including the Central Iranian block) were emplaced onto the northern edge of Arabia, including Troodos (Cyprus), Kizildag (Turkey), Baer-Bassit (Syria) and Zagros (Dilek & Thy, 2009). All these Upper Cretaceous Tethyan ophiolites are about the same age; 90–94 Ma for Troodos plagiogranite (U–Pb zircon; Mukasa & Ludden, 1987); 95 Ma for Oman plagiogranite (U–Pb zircon; Hacker, Mosenfelder & Gnos, 1996); 91–92 Ma for Kizildag plagiogranite (U–Pb zircon; Dilek & Thy, 2009); 92–93 Ma for OB Neyriz hornblende gabbros ( $^{40}\text{Ar}$ – $^{39}\text{Ar}$ ; Babaie *et al.* 2006) and 93 Ma for IB gabbros (K–Ar; Shafaii Moghadam *et al.* 2009). The tight clustering of ages for ophiolites along the ~3000 km belt implies a common origin.

The Troodos ophiolite crustal sequence contains gabbros (3–6 km thick, Mackenzie *et al.* 2006), a sheeted dyke complex (800 m thick) and overlying lavas and sediments (750 m–1.5 km thick). Lower pillow lavas are IAT while upper lavas are boninitic (Thy & Xenophontos, 1991; Dilek & Thy, 2009). Kizildag ophiolite (Turkey) crustal rocks include cumulate rocks (165–700 m thick), isotropic gabbros (2–2.5 km thick), a sheeted dyke complex and lavas (1.3 km thick) with geochemical evolution from MORB to boninite (Bageci, Parlak & Hock, 2008; Dilek & Thy, 2009). In the Oman ophiolite, the crustal sequence starts with layered gabbros (2.0–2.5 km thick) grading upwards into isotropic gabbros (500–1000 m thick). The Oman sheeted dyke complex is 400–1600 m thick and the overlying lava sequence is 1.0–1.7 km thick. Chemostratigraphy for Oman lavas shows that these lavas change from MORB-like (Geotimes unit) upwards into depleted IAT and boninitic (Lasail unit) (Alabaster, Pearce & Malpas, 1982; Ernewein, Pflumino & Whitechurch, 1988). Our compiled data (Table 1) indicates that the Zagros ophiolites are similar to most other Upper Cretaceous Tethyan ophiolites in terms of age, lithological components (other than having little gabbro) and geochemical evolution. These ophiolites are also remarkably similar to 45–50 Ma lithosphere of the IBM fore-arc in terms of peridotite compositions and the magmatic evolution of the volcanic and sheeted dyke complex (Stern, 2004). The first lavas in the IBM fore-arc are older MORB-like basalts (fore-arc basalts) with low Ti/V (14–16, compared to Pacific MORB with Ti/V = 26–32) grading upwards into younger boninites (Reagan *et al.* 2010).

The IBM fore-arc and many ophiolitic lava sequences change systematically from MORB-like early lavas to late lavas that are boninitic, but there is a lot of variability from ophiolite to ophiolite and between IBM fore-arc and Tethyan Upper Cretaceous ophiolites. The scatter amongst the analysed Zagros ophiolitic samples in REE- and extended trace element plots indicates variable geochemical signatures (MORB, calc-alkaline, boninite, IAT) within OB and IB magmas. This could reflect the life cycle of suprasubduction zone ophiolites (Shervais, 2001). Such variability in geochemical signatures is also found amongst fore-arc lavas (e.g. Ishizuka *et al.* 2006; Macpherson & Hall, 2001; Pearce *et al.* 1992; Taylor *et al.* 1992) mostly reflecting variable contributions of subducted fluid and sediment to the rapidly evolving magma source (Stern, 2004).

The  $\text{TiO}_2$  versus MgO diagram (based on Dilek & Thy, 2009) compares Zagros lavas (Fig. 7) and those from other Tethyan ophiolites with those of modern fore-arcs (Fig. 16). Troodos upper pillow lavas as well as Oman Geotimes units have lower  $\text{TiO}_2$  and higher MgO abundances than the lower pillow lavas of these ophiolites (Fig. 16a). Zagros ophiolitic lavas scatter similarly between low and high  $\text{TiO}_2$  end-members, with Nain lavas mostly having lower and Kermanshah lavas mostly higher  $\text{TiO}_2$  contents (Fig. 7). IBM fore-arc basalts (Reagan *et al.* 2010) have higher MgO contents than Troodos lower lavas, and IBM fore-arc boninites of Ishizuka *et al.* (2006) have lower MgO contents than Troodos upper lavas (Fig. 16b).

Most Zagros OB and IB lavas fall into the IAT and boninite fields on a Ti v. V diagram (Fig. 9a, b), similar to both depleted Oman Lasail lavas (V2 lavas) and IBM fore-arc lavas (Reagan *et al.* 2010). Some Zagros ophiolite lavas are more MORB-like, and some are compositionally intermediate between tholeiitic lavas of the Oman Geotimes (V1) and depleted lavas of the Lasail (V2) units. Neyriz lavas are similar to MORB-like IBM fore-arc basalts, whereas most other Zagros lavas are more akin to IBM boninites or are transitional between these two end-members. The Kermanshah calc-alkaline lavas are exceptional in having high  $\text{TiO}_2$  with low V abundance. Felsic lavas from Zagros ophiolites have much lower Ti and V abundances and plot in the lower left corner of the diagram.

### 5.c. Tectonic setting of Zagros ophiolite formation

Several different tectonic models have been considered for the tectonic environment where Upper Cretaceous Zagros ophiolites formed. These hypotheses are here briefly described before we present our model.

#### 5.c.1. Suggested tectonic models for the OB

Several hypotheses have been proposed for the tectonic evolution of the OB (e.g. Berberian & King, 1981; Desmons & Beccaluva, 1983; Glennie, 2000; Stampfli *et al.* 2001). According to some geologists,

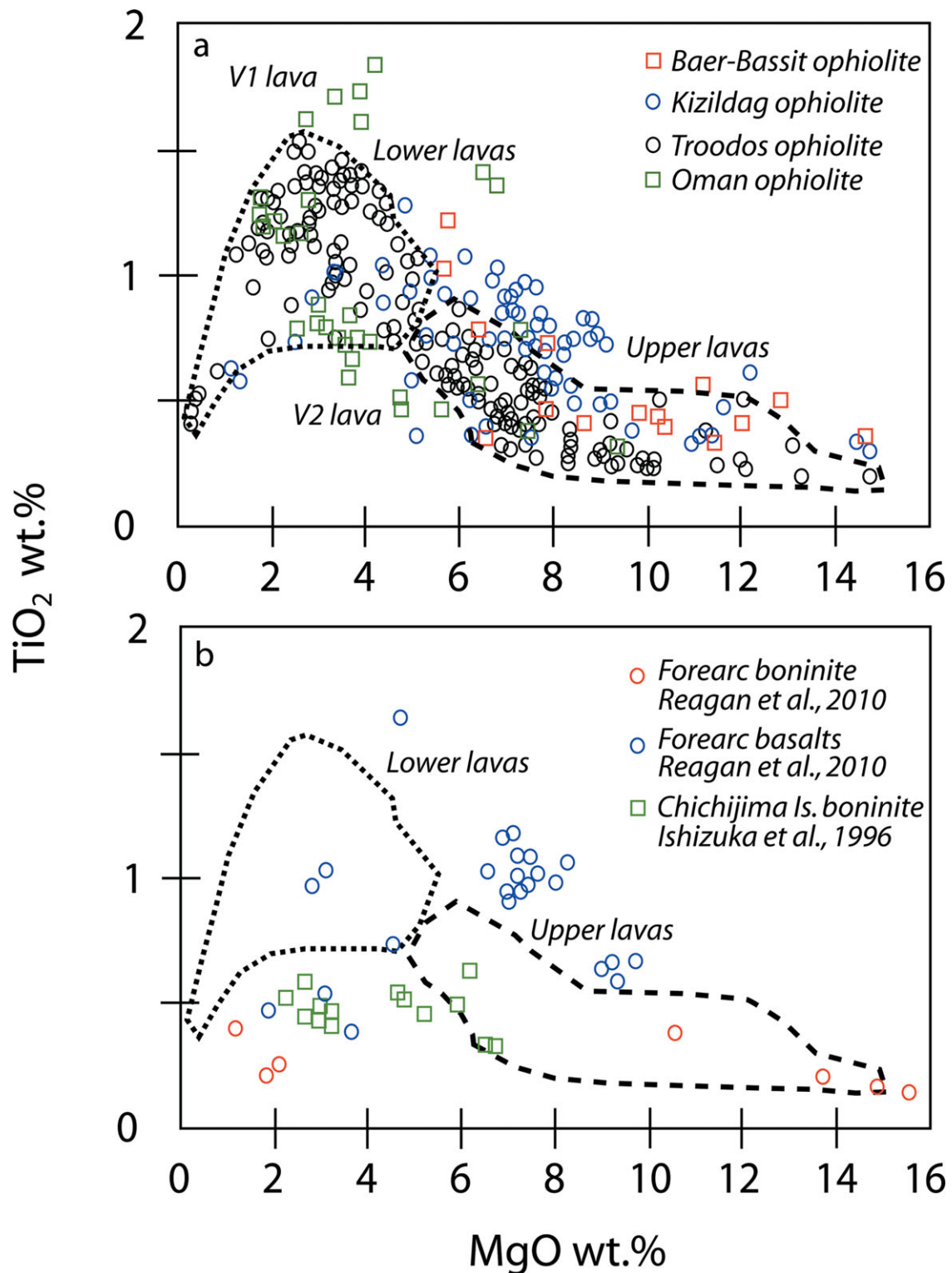


Figure 16. (Colour online) (a) Major element variations (TiO<sub>2</sub> v. MgO) of mafic rocks of Upper Cretaceous Tethyan ophiolites from Troodos, Kizildag, Oman and Baer-Bassit (modified after Dilek & Thy, 2009). (b) Major element variations (TiO<sub>2</sub> v. MgO) of Chichijima Island boninites (Ishizuka *et al.* 2006) and IBM fore-arc lavas (Reagan *et al.* 2010) are also shown for comparison. Troodos upper and lower lava fields are outlined by dashed and dotted lines, respectively.

Neo-Tethyan oceanic lithosphere was consumed in a NE-dipping subduction zone beneath the SSZ margin during Early Jurassic time (Dercourt *et al.* 1986). In one school of thought, the Neyriz ophiolite is considered both as a piece of Neo-Tethyan oceanic lithosphere generated at the foot of the north Gondwana passive

margin (e.g. Ricou, 1971, 1976; M. R. Jannessary, unpub. Ph.D. thesis, l'Univ. de Louis Pasteur, France, 2003) and/or as material that was scraped off the down-going plate and incorporated into the Zagros accretionary prism (e.g. Babaie *et al.* 2006). Otherwise the Kermanshah ophiolite may be described as a piece

of Tethyan oceanic lithosphere scraped off during NE-directed subduction underneath the Iranian block in Early Cretaceous time (e.g. Agard *et al.* 2005; Braud, 1970, 1978; J. Braud, unpub. Ph.D. thesis, Univ. Paris-Sud, France, 1987). An intraoceanic arc origin is also suggested for the Kermanshah ophiolite by Ghazi & Hassanipak (1999) and Desmons & Beccaluva (1983). All these models, except Jannessary's model for the Neyriz ophiolite, consider a suprasubduction zone for the evolution of the outer belt ophiolites.

### 5.c.2. Previous tectonic models for the IB

The IB is described as ophiolitic *mélange*, originated from a Neo-Tethyan oceanic branch that existed between the SSZ and the Lut blocks (e.g. Davoudzadeh, 1972; Stocklin, Eftekhar-Nezhad & Hushmandzadeh, 1972; Berberian & King, 1981; Arvin & Robinson, 1994; Arvin & Shokri, 1996). In many interpretations the Nain–Baft ophiolite belt represents a suture on the site of a small Mesozoic ocean basin (e.g. Stampfli & Borel, 2002; Agard *et al.* 2006; Shafaii Moghadam *et al.* 2009) with a number of microcontinents. However, there is no agreement as to how such microcontinents and ocean basins should be reconstructed in space and time, or in the rift processes (Robertson, 2007). Why did the Nain–Baft (IB) oceanic branch open? Do we have the evidence of rifted margins including turbidites, deep-water radiolarites and platform carbonates along with plume-related alkaline lavas older than Late Cretaceous in the Nain–Baft ophiolites? These types of deposits and lavas are reported from all eastern Tethyan ophiolites, such as the Hawasina window of Oman, and are suggested to show pulses of rifting, responsible for opening the Neo-Tethys. These types of rocks are not found for the Nain–Baft ophiolites. Some geologists prefer a model whereby the IB marks the position of a Campanian back-arc basin (e.g. Stampfli & Borel, 2002; Agard *et al.* 2006; Shafaii Moghadam *et al.* 2009). This back-arc basin represented a narrow seaway with discontinuous oceanic crust (Shafaii Moghadam *et al.* 2009). A back-arc basin model is also proposed for ophiolites on the northern margin of the Tauride microcontinent (Stampfli & Borel, 2002). In this model, the SSZ was also considered similar to the Tauride block of Robertson (2007). As for the SSZ, both flanks of the Tauride block are marked by ophiolites, the trace of the North Tethyan Ocean to the north and that of the South Tethyan Ocean to the south, although there is evidence of Triassic rifting and continental breakup along the northern margin of the Tauride–Anatolide platform (see Yilmaz *et al.* 1997 and Robertson, 2007 for more information).

Another possible explanation for the mixture of MORB and suprasubduction zone basaltic rocks in the Zagros ophiolites is that these formed in one or two back-arc basins (e.g. Stampfli & Borel, 2002; Agard *et al.* 2006; Shafaii Moghadam *et al.* 2009). We do not think this is a good explanation, for a

number of reasons. First, there is no arc to the south of the Zagros ophiolites, so for the back-arc basin hypothesis to be correct either the arc to the south was completely removed somehow or the back-arc basin was associated with a S-dipping subduction zone. Tectonic evolution from a S-dipping subduction zone in Late Cretaceous time to a N-dipping one today requires that a collision occurred sometime between then and now, causing the subduction zone polarity reversal, from S-dipping to N-dipping. There is no evidence for this; instead, it appears that a magmatic arc has been present at about where the Urumieh–Dokhtar arc is through much of Late Cretaceous time and all of Cenozoic time. Second, boninites are common in fore-arcs and rare in back-arc basins (Bedard *et al.* 1998). Peridotite compositions are also diagnostic. Upper Cretaceous Zagros ophiolitic peridotites include ultra-depleted harzburgites (and minor depleted lherzolites) that are not reported from back-arc basins (back-arc basin peridotites are moderately depleted, like MOR peridotites (Ohara, 2006)); such depleted harzburgites are only found in modern intraoceanic fore-arcs.

### 5.c.3. A fore-arc tectonic model for the evolution of the Upper Cretaceous Zagros ophiolites

Considered together, the data we have reviewed for the Zagros Upper Cretaceous ophiolites, along with what is known for the better-studied Troodos and Oman ophiolites, compels us to conclude that a long, broad and continuous tract of oceanic lithosphere was created at about the same time during Late Cretaceous time along the southern margin of Eurasia. This tract extended beyond Iran through Syria and Turkey as far as Cyprus to the west and Oman to the east (Fig. 1). The similarity of ages for igneous rocks and overlying sediments, both along (from Cyprus to Oman) and across (inner to outer belt) the ophiolite belt indicates that a successful model should explain all of these occurrences.

All Zagros ophiolites are dominated by components with strong suprasubduction zone affinities, especially for the most diagnostic lithologies of mantle harzburgite, diabasic dykes and lavas. Most volcanic sections have mixtures of arc-like and MORB-like compositions with some E-MORB/OIB-type pillow lavas. Where age relationships can be resolved, MORB-like lavas usually are older and arc-like lavas are younger. It is important to appreciate that MORB-like basalts do not require a mid-ocean ridge tectonic environment, only that asthenospheric mantle melted to ~10% due to decompression, without a discernible input from subducted sediments or crust. Tectonic models with two distinct phases (for example, a MOR setting followed by an arc setting) might be appropriate if there was any evidence for a significant hiatus between MORB-like lower basalts and arc-like upper basalts and boninites, but this is nowhere observed in any Upper Cretaceous Zagros ophiolitic lava section, or in any of the other Upper Cretaceous ophiolites from Cyprus to Oman. Instead, we interpret the volcanic succession to

have formed in a single tectonic environment, albeit one that was rapidly evolving. This reflected melting and progressive depletion of originally fertile asthenospheric mantle as a new subduction zone formed on the SW flank of Eurasia. Melting was first due to decompression alone and then due to an influx of water and sediment melts when the foundering lithosphere reached a certain depth and true subduction started. This interpretation is partly based on comparing our results with those of recent Shinkai 6500 diving on the inner wall of the Mariana Trench, which found MORB-like basalts (called fore-arc basalts) at the base of the volcanic succession, followed upsection by boninitic lavas (Reagan *et al.* 2010). Reagan *et al.* (2010) interpreted the lower MORB-like lavas as first stage melts of asthenospheric mantle that were generated when foundering of Pacific lithosphere to initiate the IBM subduction zone occurred in Eocene time. This model was applied to Tethyan ophiolites, including Troodos and Semail, by Whattam & Stern (2009). The geochemical data we have summarized for both Upper Cretaceous Zagros ophiolites, plus the observation that some IB ophiolites are conformably overlain by arc-derived pyroclastic rocks compels the conclusion that both the OB and IB formed over a subduction zone, at least for the later part of their early history. It is more controversial whether the MORB-like lavas of these ophiolites formed in the same setting, earlier during subduction initiation, or are remnant pieces of older oceanic crust, as seems to be the case for the Khoy and Haji-Abad ophiolites, where older tracts are juxtaposed with Upper Cretaceous ophiolites. We note that in these cases, the evidence for greater age of the older fragments is clear, whereas no such evidence exists for other Zagros OB and IB ophiolites. Consequently, we prefer to interpret MORB- and OIB-like igneous rocks in the Upper Cretaceous Zagros ophiolites as forming at about the same time as those with clear suprasubduction zone affinities.

It is also controversial whether or not the IB and OB are remnants of two distinct Late Cretaceous oceanic basins (as most other workers prefer) or a single disrupted one (as we prefer). Understanding the tectonic history of the SSZ is key for resolving this controversy, as discussed above. Our preferred hypothesis is that Zagros IB and OB ophiolites are remnants of a once-continuous tract of fore-arc lithosphere that formed during a Late Cretaceous episode of subduction initiation on the SW flank of Eurasia. We further argue that SSZ rocks were subducted several tens of kilometres deep before being exhumed beneath the Zagros fore-arc and disrupted it to yield the two ophiolite belts and the present configuration shown in Figure 2b. We reiterate that there is evidence that SSZ rocks were deeply subducted. They contain blueschist (e.g. Agard *et al.* 2006) and other evidence of high *P/T* metamorphism, but much more work is needed to test this idea. Furthermore, we hypothesize that the Paleocene–

Eocene unconformity found above all Zagros ophiolites could mark the main episode of Sanandaj–Sirjan exhumation.

The fore-arc/subduction initiation model for the Zagros ophiolites is most consistent with diagnostic lithologies, boninite and harzburgite. Boninites are unusually high-degree melts of Cpx-poor peridotite. They are often found as parts of fore-arc crust, where they are thought to form when subduction begins. Boninites are rarely found in back-arc basins (Bedard *et al.* 1998). Back-arc basin boninite has recently been discovered erupting in the northernmost Lau Basin (Michael *et al.* 2009), but this is a restricted, unusual tectonic setting, where the Lau Basin spreading axis intersects a transform margin. Peridotite compositions are also key. Upper Cretaceous Zagros ophiolitic peridotites include ultra-depleted harzburgites (and minor depleted lherzolites) that today are only found in modern intraoceanic fore-arcs. Harzburgites are residues after unusually extensive melting, to the point of Cpx exhaustion. At some point in their evolution, the shallow upper mantle beneath the Upper Cretaceous Zagros ophiolites experienced much more extensive melting (to the point of Cpx exhaustion) than is found anywhere else in the modern Earth (Bonatti & Michael, 1989; Neumann & Simon, 2009). Because the mantle beneath modern fore-arcs is cold and rarely melts, this catastrophic melting must have occurred under very special conditions, most likely when subduction began. A much larger volume of magma is produced when a subduction zone first forms than for mature arcs (Stern & Scholl, 2010). Such voluminous melt generation mostly yields abundant tholeiite magma and harzburgitic residual mantle, sometimes along with boninite. This is consistent with the observation that boninites and very depleted peridotites are produced during subduction initiation and are common in the IBM fore-arc (Ishizuka *et al.* 2006; Reagan *et al.* 2010).

The tectonic scenario that we prefer for the Upper Cretaceous Zagros ophiolites and other Upper Cretaceous ophiolites from Cyprus to Oman is that these formed along the southern margin of Eurasia during a subduction initiation event, as summarized in Figure 17. This interpretation implies that these ophiolites are not accreted fragments but formed essentially where they are today on the southern margins of Eurasia. They are not far-travelled, exotic fragments of oceanic lithosphere but are partially preserved fragments of an oceanic fore-arc that formed when subduction began along this margin in Late Cretaceous time. This inference links Zagros, Cyprus and Oman ophiolites as examples of subduction initiation magmatic activity and precludes models for their formation at a normal MOR, a small Red Sea-like basin, a back-arc basin or anywhere except at a strongly extensional, incipient convergent margin. Such a model is also consistent with the observation that Zagros ophiolites formed when relative plate motions in the region changed dramatically (Garfunkel, 2006).

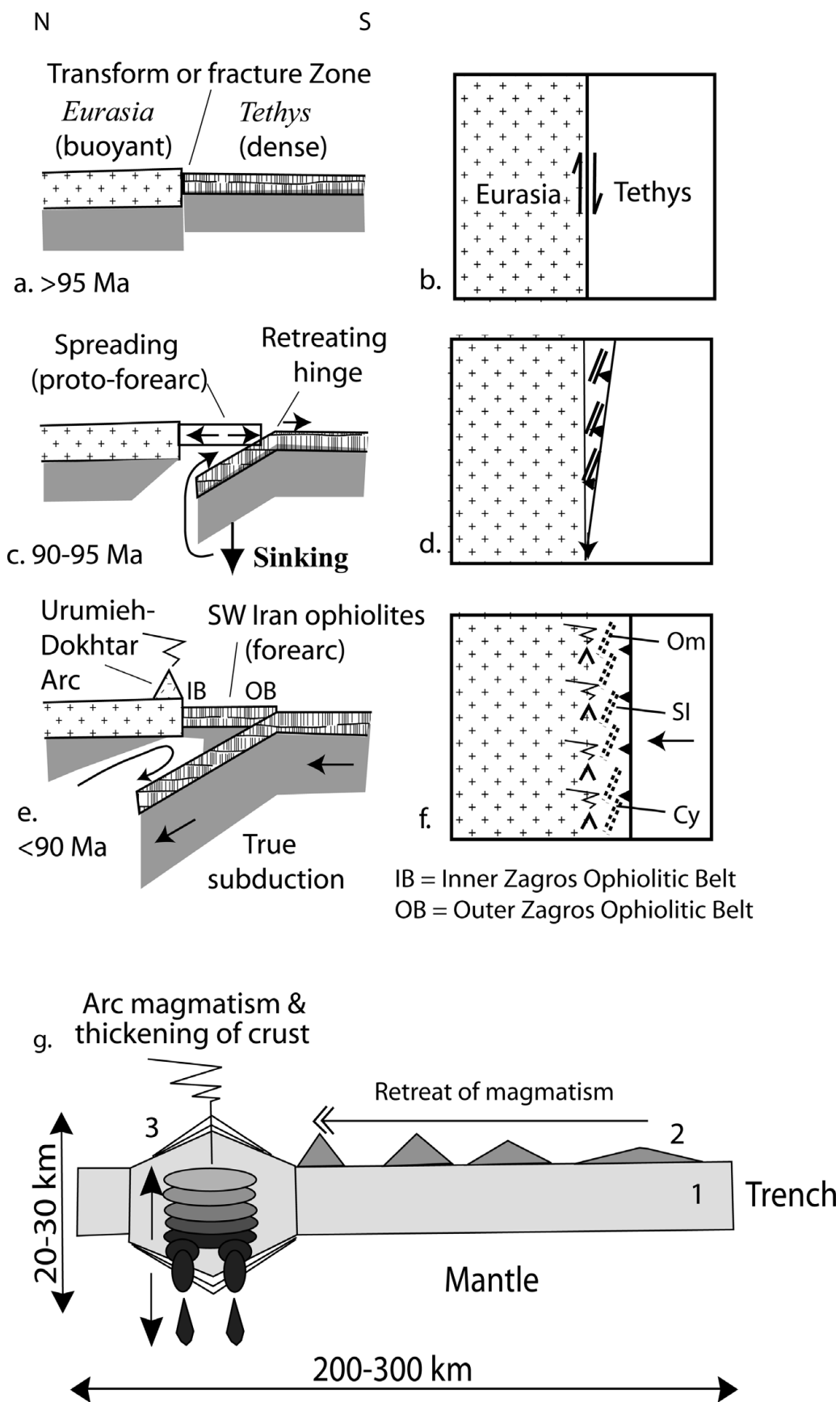


Figure 17. Generation of the Upper Cretaceous Zagros ophiolites as a proto-fore-arc formed during subduction initiation, modified after Stern (2004). Left panels are sections perpendicular to the evolving plate boundary and right panels are map views. (a) and (b) show the initial (> 95 Ma) configuration. Two lithospheres of differing density (buoyant Eurasia, dense Tethys) are juxtaposed across a transform fault or fracture zone. (c, d) Old, dense lithosphere sinks asymmetrically, with maximum subsidence nearest the transform fault or fracture zone. Asthenosphere flows over the sinking lithosphere and propagates along the transform/fracture zone. Strong

## 6. Conclusions

The OB and IB Zagros Upper Cretaceous ophiolites as well as similar-aged ophiolites in Turkey, Cyprus and Oman are coeval and represent remnants of a Late Cretaceous oceanic fore-arc formed along the southern margin of Eurasia. Our compilation indicates that the Zagros ophiolites and other Upper Cretaceous Tethyan ophiolites of SW Asia are broadly similar in terms of age, lithological components and geochemical evolution. Nearly all Zagros ophiolite components show strong suprasubduction zone affinities, especially for the most diagnostic lithologies of mantle harzburgite, arc thoeiite and boninite, excepting some MORB-like pillow lavas. Most volcanic sections have mixtures of arc-like and MORB-like compositions.

Along with other Tethyan ophiolites in the region of similar age, Zagros ophiolites are interpreted to represent autochthonous fore-arc lithosphere that formed by seafloor spreading along the southern margin of Eurasia during Late Cretaceous time. This fore-arc lithosphere was once continuous, both across the two Zagros ophiolite belts (OB and IB) as well as from Cyprus to Oman. This fore-arc has been disrupted by continued shortening, especially since collision began with Arabia in mid-Cenozoic time, as well as by tectonic underplating beneath the fore-arc and subsequent exhumation to form the SSZ, which now separates the Zagros IB and OB. Zagros ophiolites and correlatives from Cyprus to Oman constitute a tract of oceanic lithosphere that formed along the southern margin of Eurasia when subduction began, forming the subduction zone that has continued operating until today. This subduction zone is responsible for the Urumieh–Dokhtar arc and has since swallowed all of the Neo-Tethys between Afro-Arabia and Eurasia. The Zagros orogen has evolved as a convergent plate margin since subduction began ~95 Ma, with the Persian Gulf representing a trench that is being progressively filled from the NW, the Zagros fold-and-thrust belt representing a still-growing accretionary prism.

**Acknowledgements.** HSM's research on Zagros IB ophiolites has been supported financially by the French CNRS (contribution of the UMR 7516 'Institut de Physique du Globe', Strasbourg, France) and the Cultural Service of the French Embassy at Tehran. We are deeply indebted to Dr Blanchy, Dr Duhamel and Dr Lambert. We are most thankful to the University of Strasbourg for producing analyses on the IB and would like to thank Prof. Mohamad Rahgoshay,

Prof. Hubert Whitechurch and Dr Raymond Montigny for helping HSM interpret IB ophiolites for his Ph.D. research. Financial support for the OB ophiolite studies from the Research Council of Damghan University (grant number 88/GEO/64/127 to HSM) is acknowledged. We sincerely thank Prof. Pour-Mousavi from Damghan University for his excellent support of this research programme. This paper greatly benefited from the comments of Dr Mark Allen, Dr Guy Simpson and two anonymous reviewers.

## References

- AGARD, P., MONIE, P., GERBER, W., OMRANI, J., MOLINARO, M., MEYER, B., LABROUSSE, L., VRIELYNCK, B., JOLIVET, L. & YAMATO, P. 2006. Transient, synobduction exhumation of Zagros blueschists inferred from P-T, deformation, time, and kinematic constraints: implications for Neo-Tethyan wedge dynamics. *Journal of Geophysical Research* **111**, B11401, doi: 10.1029/2005JB004103, 28 pp.
- AGARD, P., OMRANI, J., JOLIVET, L. & MOUTHEREAU, F. 2005. Convergence history across Zagros (Iran): constraints from collisional and earlier deformation. *International Journal of Earth Sciences* **94**, 401–19.
- AHMADIPOUR, H., SABZEHI, M., WHITECHURCH, H., RASTAD, E. & EMAMI, M. H. 2003. Soghan complex as an evidence for paleosubduction center and mantle diapirism in Sanandaj-Sirjan zone (south-east Iran). *Journal of Sciences, Islamic Republic of Iran* **14**, 157–72.
- ALABASTER, T., PEARCE, J. A. & MALPAS, J. 1982. The volcanic stratigraphy and petrogenesis of the Oman ophiolite. *Contributions to Mineralogy and Petrology* **81**, 168–83.
- ALLAHYARI, K., SACCANI, E., POURMOAFI, M., BECCALUVA, L. & MASOUDI, F. 2010. Petrology of mantle peridotites and intrusive mafic rocks from the Kermanshah ophiolitic complex (Zagros belt, Iran): implication for the geodynamic evolution of the Neo-Tethyan oceanic branch between Arabia and Iran. *Ophioliti* **35**, 71–90.
- ALAVI, M. 1980. Tectonostratigraphic evolution of the Zagrosides of Iran. *Geology* **8**, 144–9.
- ALAVI, M. 1991. Sedimentary and structural characteristics of the Paleo-Tethys remnants in northeastern Iran. *Geological Society of America Bulletin* **103**, 983–92.
- ALAVI, M. 1994. Tectonics of the Zagros orogenic belt of Iran: new data and interpretations. *Tectonophysics* **229**, 211–38.
- ALAVI, M. 2004. Regional stratigraphy of the Zagros fold-thrust belt of Iran and its proforeland evolution. *American Journal of Science* **304**, 1–20.
- ALAVI, M. 2007. Structures of the Zagros fold-thrust belt in Iran. *American Journal of Science* **307**, 1064–95.

extension in the region above the sinking lithosphere leads to seafloor spreading, forming infant arc crust of the proto-fore-arc. This forms the Zagros ophiolites, ~93 Ma ago. (d) shows that this process is asynchronous along the margin; ophiolite ages indicate that subduction propagated from E (Oman) to W (Cyprus) between 95 and 90 Ma. (e, f) Beginning of down-dip motion of the lithosphere marks when true subduction starts (< 90 Ma). Strong extension in the fore-arc and trenchward migration of asthenosphere ends, cooling the sub-fore-arc mantle, which becomes lithosphere; further addition of water leads only to serpentinization. The locus of igneous activity retreats ~200 km away from the trench, to the region above where asthenospheric advection continues, forming the Urumieh–Dokhtar arc. This fore-arc today defines the Oman (Om), SW Iran (SI), and Cyprus (Cy) ophiolites. (g) A detailed view of how magmatism in the arc evolves with time: (1) infant arc crust of the fore-arc ophiolite forms by seafloor spreading during the first c. 5 Ma of subduction zone evolution; (2) retreat of magmatic activity away from the trench (Tr) during the second c. 5 Ma; (3) focusing of magmatic activity at the position of the active magmatic arc, resulting in crustal thickening and delamination.

- ALAVI, M., VAZIRI, H., SEYED-EMAMI, K., & LASEMI, Y. 1997. The Triassic and associated rocks of the Nakhlak and Aghdarband areas in central and northeastern Iran as remnants of the southern Turonian active continental margin. *Geological Society of America Bulletin* **109**, 1563–75.
- ALLEN, M., JACKSON, J. & WALKER, R. 2004. Late Cenozoic reorganization of the Arabia-Eurasia collision and the comparison of short-term and long-term deformation rates. *Tectonics* **23**, TC2008, doi:10.1029/2003TC001530.
- ARAI, S. 1994. Characterization of spinel peridotites by olivine-spinel compositional relationships: review and interpretation. *Chemical Geology* **113**, 191–204.
- ARAI, S. & ISHIMARU, S. 2008. Insight into petrological characteristics of the lithosphere of mantle wedge beneath arcs through peridotite xenoliths: a review. *Journal of Petrology* **49**, 665–95.
- ARCULUS, R. J. 2003. Use and abuse of the term calcalkaline and calcalkalic. *Journal of Petrology* **44**, 929–35.
- ARCULUS, R. J., PEARCE, J. A., MURTON, B. J., & VAN DER LAAN, S. R. 1992. Igneous stratigraphy and major-element geochemistry of Holes 786 A and 786B. In *Proceedings of the Ocean Drilling Program, Scientific Results, vol. 125* (eds P. Fryer, J. A. Pearce, L. B. Stocking, et al.), pp. 143–69. College Station, Texas.
- ARVIN, M. & ROBINSON, P. T. 1994. The petrogenesis and tectonic setting of lavas from the Baft ophiolitic mélange, southwest of Kerman, Iran. *Canadian Journal of Earth Science* **31**, 824–34.
- ARVIN, M. & SHOKRI, E. 1997. Genesis and eruptive environment of basalts from the Gogher ophiolitic mélange, southwest of Kerman, Iran. *Ophioliti* **22**, 175–82.
- ASATRYAN, G., DANELIAN, T., SOSSON, M., SAHAKYAN, L., PERSON, A., AVAGYAN, A. & GALOYAN, G. 2010. Radiolarian ages for the sedimentary cover of Sevan ophiolite (Armenia, Lesser Caucasus). *Ophioliti* **35**, 91–101.
- AZIZI, H., CHUNG, S. L., TANAKA, T. & ASAHARA, Y. 2011. Isotopic dating of the Khoy metamorphic complex (KMC), northwestern Iran: a significant revision of the formation age and magma source. *Precambrian Research* **185**, 87–94.
- BABAEI, A., BABAIE, H. A. & ARVIN, M. 2005. Tectonic evolution of the Neyriz ophiolite, Iran: an accretionary model. *Ophioliti* **30**, 65–74.
- BABAIE, H. A., BABAEI, A., GHAZI, A. M. & ARVIN, M. 2006. Geochemical,  $^{40}\text{Ar}/^{39}\text{Ar}$  age, and isotopic data for crustal rocks of the Neyriz ophiolite, Iran. *Canadian Journal of Earth Sciences* **43**, 57–70.
- BABAIE, H. A., GHAZI, A. M., BABAEI, A., LA TOUR, T. E. & HASSANIPAK, A. A. 2001. Geochemistry of arc volcanic rocks of the Zagros Crush Zone, Neyriz, Iran. *Journal of Asian Earth Sciences* **19**, 61–76.
- BAGCI, U., PARLAK, O. & HOCK, V. 2008. Geochemistry and tectonic environment of diverse magma generations forming the crustal units of the Kizildag (Hatay) ophiolite, southern Turkey. *Turkish Journal of Earth Sciences* **17**, 43–71.
- BÉDARD, J. H., LAUZIÈRE, K., TREMBLAY, A. & SANGSTER, A. 1998. Evidence from Betts Cove ophiolite boninites for forearc seafloor-spreading. *Tectonophysics* **285**, 233–45.
- BERBERIAN, M. 1995. Master blind thrust faults hidden under the Zagros folds: active basement tectonics and surface morphotectonics. *Tectonophysics*, **241**, 193–224.
- BERBERIAN, F. & BERBERIAN, M. 1981. Tectono-plutonic episodes in Iran. In *Zagros-Hindu Kush-Himalaya Geodynamic Evolution*, vol. 3 (eds H. K. Gupta & F. M. Delany), pp. 5–32. Washington, D.C.: American Geophysical Union.
- BERBERIAN, M. & KING, G. C. P. 1981. Towards a paleogeography and tectonic evolution of Iran. *Canadian Journal of Earth Sciences* **18**, 210–65.
- BERBERIAN, F., MUIR, I. D., PANKHURST, R. J. & BERBERIAN, M. 1982. Late Cretaceous and early Miocene Andean type plutonic activity in northern Makran and Central Iran. *Journal of Geological Society, London* **139**, 605–14.
- BLOME, C. D. & IRWIN, W. P. 1985. Equivalent radiolarian ages from ophiolitic terranes of Cyprus and Oman. *Geology* **13**, 401–4.
- BLOOMER, S. H. & HAWKINS, J. W. 1983. Gabbroic and ultramafic rocks from the Mariana Trench: an island arc ophiolite. In *The Tectonic and Geologic Evolution of Southeast Asian Seas and Islands Part 2* (ed. D. E. Hayes), pp. 94–317. American Geophysical Union, Geophysical Monograph vol. 27. Washington, DC, USA.
- BONATTI, E. & MICHAEL, P. J. 1989. Mantle peridotites from continental rifts to ocean basins to subduction zones. *Earth and Planetary Science Letters* **91**, 297–311.
- BRAUD, J. 1970. Les formations du Zagros dans la région de Kermanshah (Iran) et leurs rapports structuraux. *Comptes Rendus l'Academie des Sciences* **271**, 1241–4.
- BRAUD, J. 1978. *Geological Map of Kermanshah, 1/250000 scale*. Tehran: Geological Survey of Iran.
- CANNAT, M., CHATIN, F., WHITECHURCH, H. & CEULENEER, G. 1997. Gabbroic rocks trapped in the upper mantle at the Mid-Atlantic Ridge. In *Proceedings of the Ocean Drilling Program, Scientific Results, vol. 153* (eds J. A. Karson, M. Cannat, D. J. Miller & D. Elthon), pp. 243–64. College Station, Texas.
- CASEY, J. F. 1997. Comparison of major- and trace element geochemistry of abyssal peridotites and mafic plutonic rocks with basalts from the MARK region of the Mid-Atlantic ridge. In *Proceedings of the Ocean Drilling Program, Scientific Results, vol. 153* (eds J. A. Karson, M. Cannat, D. J. Miller & D. Elthon), pp. 181–241. College Station, Texas.
- CRAWFORD, A. J., FALLOON, T. J. & GREEN, D. H. 1989. Classification, petrogenesis and tectonic setting of boninites. In *Boninites and Related Rocks* (ed. A. J. Crawford), pp. 1–49. London: Unwin Hyman.
- DAVOUDIAN, A. R., GENSER, J., DACHSE, E. & SHABANIAN, N. 2007. Petrology of eclogites from north of Shahrekord, Sanandaj-Sirjan Zone, Iran. *Mineralogy and Petrology* **92**, 393–413.
- DAVOUDIAN, A. R., KHALILI, M., NOORBEHESHT, I., DACHSE, E., GENSER, J. & SHABANIAN, N. 2006. Geochemistry of metabasites in the north of the Shahrekord, Sanandaj-Sirjan Zone, Iran. *Neues Jahrbuch für Mineralogie-Abhandlungen* **182**, 291–8.
- DAVOUDZADEH, M. 1972. *Geology and petrography of the area north of Nain, Central Iran*. Geological Survey of Iran, report No.14.
- DAVOUDZADEH, M. & SCHMIDT, K. 1984. Contribution to the paleogeography and stratigraphy of the Upper Triassic to Middle Jurassic of Iran. *Neues Jahrbuch für Geologie und Paleontologie* **162**, 137–63.
- DELALOYE, M. & DESMONS, J. 1980. Ophiolites and mélange terranes in Iran: a geochronological study and its paleotectonic implications. *Tectonophysics* **68**, 83–111.

- DERCOURT, J., ZONENSHAIN, L. P. RICOU, L.-E., KAZMIN, V. G., LE PICHON, X., KNIPPER, A. L., GRANDJACQUET, C., SBORTSHIKOV, I. M., GEYSSANT, J., LEPVRIER, C., PECHERSKY, D. H., BOULIN, J., SIBUET, J.-C., SAVOSTIN, L. A., SOROKHTIN, O., WESTPHAL, M., BAZHENOV, M. L., LAUER, J. P. & BIJU-DUVAL, B. 1986. Geological evolution of the Tethys belt from the Atlantic to the Pamirs since the Lias. *Tectonophysics* **123**, 241–315.
- DESMONS, J. & BECCALUVA, L. 1983. Mid-ocean ridge and island arc affinities in ophiolites from Iran: palaeographic implications. *Chemical Geology* **39**, 39–63.
- DICK, H. J. B. & BULLEN, T. 1984. Chromian spinel as a petrogenetic indicator in abyssal and Alpine-type peridotites and spatially associated lavas. *Contributions to Mineralogy and Petrology* **86**, 54–76.
- DILEK, Y. & FURNES, H. 2009. Structure and geochemistry of Tethyan ophiolites and their petrogenesis in subduction rollback systems. *Lithos* **113**, 1–20.
- DILEK, Y., FURNES, H. & SHALLO, M. 2007. Suprasubduction zone ophiolite formation along the periphery of Mesozoic Gondwana. *Gondwana Research* **11**, 453–75.
- DILEK, Y. & THY, P. 2009. Island arc tholeiite to boninitic melt evolution of the Cretaceous Kizildag (Turkey) ophiolite: model for multi-stage early arc–forearc magmatism in Tethyan subduction factories. *Lithos* **113**, 68–87.
- DIMITRIJEVIC, M. D. 1973. *Geology of Kerman Region*. Geological Survey of Iran, report No. 72.
- EDGE, H. S. 1996. Salt tectonism in the Persian Gulf Basin. In *Salt Tectonics* (eds G. I. Alsop, D. J. Blundell & I. Davison), pp. 129–51. Geological Society of London, Special Publication no. 100.
- EFTKHARNEJAD, J. 1981. Tectonic division of Iran with respect to sedimentary basins. *Journal of Iranian Petroleum Society* **82**, 19–28 (in Farsi).
- ERNEWEIN, M., PFLUMINO, C. & WHITECHURCH, H. 1988. The death of an accretion zone as evidenced by the magmatic history of the Sumail ophiolite (Oman). *Tectonophysics* **151**, 247–74.
- FALCON, N. L. 1969. Problems of the relationship between surface structure and deep displacements illustrated by the Zagros range. In *Time and Place in Orogeny* (ed. P. E. Kent), pp. 9–22. Geological Society of London, Special Publication no. 3.
- FALCON, N. L. 1974. An outline of the geology of the Iranian Makran. *Geographical Journal* **140**, 283–91.
- FALLOON, T. J. & CRAWFORD, A. J. 1991. The petrogenesis of high-Ca boninite lavas dredged from the northern Tonga ridge. *Earth and Planetary Science Letters* **102**, 375–94.
- FARHOUDI, G. & KARIG, D. E. 1977. Makran of Iran and Pakistan as an active arc system. *Geology* **5**, 664–8.
- FAZLNI, A., SCHENK, V., VAN DER STRAATEN, F. & MIRMOHAMMADI, M. 2009. Petrology, geochemistry and geochronology of trondhjemites from the Qori complex, Neyriz, Iran. *Lithos* **112**, 413–33.
- FLOYD, P. A., YALINIZ, M. K. & GONCUOGLU, M. C. 1998. Geochemistry and petrogenesis of intrusive and extrusive ophiolitic plagiogranites, Central Anatolian Crystalline Complex, Turkey. *Lithos* **42**, 225–41.
- GALOYAN, G., ROLLAND, Y., SOSSON, M., CORSINI, M., BILLO, S., VERATI, C. & MELKONYAN, R. 2009. Geology, geochemistry and  $^{40}\text{Ar}/^{39}\text{Ar}$  dating of Sevan ophiolites (Lesser Caucasus, Armenia): evidence for Jurassic back-arc opening and hot spot event between the South Armenian Block and Eurasia. *Journal of Asian Earth Sciences* **34**, 135–53.
- GARFUNKEL, Z. 2006. Neotethyan ophiolites: formation and obduction within the life cycle of the host basins. In *Tectonic Development of the Eastern Mediterranean Region* (ed. A. H. F. Robertson), pp. 301–26. Geological Society of London, Special Publication no. 260.
- GHASEMI, H., JUTEAU, T., BELLON, H., SABZEHI, M., WHITECHURCH, H. & RICOU, L. E. 2002. The mafic-ultramafic complex of Sikhoran (central Iran): a poly-genetic ophiolite complex. *Comptes Rendus Geoscience* **334**, 431–8.
- GHASEMI, A. & TALBOT, C. J. 2006. A new tectonic scenario for the Sanandaj-Sirjan zone (Iran). *Journal of Asian Earth Sciences* **26**, 683–93.
- GHAZI, A. M. & HASSANIPAK, A. A. 1999. Geochemistry of subalkaline and alkaline extrusives from the Kermanshah ophiolite, Zagros Suture Zone, western Iran: implications on Tethyan plate tectonics. *Journal of Asian Earth Sciences* **17**, 319–32.
- GHAZI, A. M. & HASSANIPAK, A. A. 2000. Petrology and geochemistry of the Shahr-Babak ophiolite, Central Iran. *Geological Society of America Bulletin*, Special paper **349**, 485–97.
- GIRARDEAU, J., MONNIER, C., LEMEE, L. & QUATREVAUX, F. 2002. The Wuqbah peridotite, central Oman ophiolite: petrological characteristics of the mantle in a fossil overlapping ridge setting. *Marine Geophysical Research* **23**, 43–56.
- GLENNIE, K. W. 2000. Cretaceous tectonic evolution of Arabia's eastern plate margin: a tale of two oceans. In *Middle East Models of Jurassic/Cretaceous Carbonate Systems* (eds A. S. Alsharan & R. W. Scott), pp. 9–20. Society of Economic Paleontologists and Mineralogists (SEPM), Special Publication no. 69.
- GODARD, M., BOSCH, D. & EINAUDI, F. 2006. A MORB source for low-Ti magmatism in the Semail ophiolite. *Chemical Geology* **234**, 58–78.
- GODARD, M., DAUTRIA, J. M. & PERRIN, M. 2003. Geochemical variability of the Oman ophiolite lavas: relationship with spatial distribution and paleomagnetic directions. *Geochemistry, Geophysics, Geosystems (G<sup>3</sup>)* **4**, 8609, doi:10.1029/2002GC000452, 15 pp.
- GODARD, M., JOUSSELIN, D. & BODINIER, J. L. 2000. Relationships between geochemistry and structure beneath a palaeo-spreading centre: a study of the mantle section in the Oman ophiolite. *Earth and Planetary Science Letters* **180**, 133–48.
- GOLONKA, J. 2004. Plate tectonic evolution of the southern margin of Eurasia in the Mesozoic and Cenozoic. *Tectonophysics* **381**, 235–73.
- HACKER, B. R., MOSENFELDER, J. L. & GNOS, E. 1996. Rapid emplacement of the Oman ophiolite: thermal and geochronologic constraints. *Tectonics* **15**, 1230–47.
- HALL, R. 1980. Contact metamorphism by an ophiolite peridotite from Neyriz, Iran. *Science* **208**, 1259–62.
- HATZFELD, D., TATAR, M., PRIESTLY, K. & GHAFOR-ASHTIANY, M. 2003. Seismological constraints on the crustal structure beneath the Zagros Mountains (Iran). *Geophysical Journal International* **155**, 403–10.
- HAYNES, S. J. & REYNOLDS, P. H. 1980. Early development of Tethys and Jurassic ophiolite displacement. *Nature* **283**, 561–3.
- HÉBERT, R., ADAMSON, A. C. & KOMOR, S. C. 1990. Metamorphic petrology of ODP 109, Hole 670A serpentinized peridotites: serpentinization processes at a slow spreading ridge environment. In *Proceedings of the Ocean Drilling Program, Scientific Results vol. 106/109* (eds R. Detrick, J. Honnorez, W. B. Bryan, et al.), pp.103–15. College Station, Texas.

- HELLEBRAND, E., SNOW, J. E., DICK, H. J. B. & HOFMANN, A. W. 2001. Coupled major and trace elements as indicators of the extent of melting in mid-ocean ridge peridotites. *Nature* **410**, 677–81.
- HELLEBRAND, E., SNOW, J. E. & MUHE, R. 2002. Mantle melting beneath Gakkel Ridge (Arctic Ocean): abyssal peridotite spinel compositions. *Chemical Geology* **182**, 227–35.
- HOMKE, S., VERGES, J., SERRA-KIEL, J., BERNAOLA, G., SHARP, I., GARCES, M., MONTERO-VERDO, I., KARPUSZ, R. & GOODARZI, M. 2009. Late Cretaceous–Paleocene formation of the proto-Zagros foreland basin, Lurestan Province, SW Iran. *Geological Society of America Bulletin* **121**, 963–78.
- ISHII, T., ROBINSON, P. T., MAEKAWA, H. & FISKE, R. 1992. Petrological studies of peridotites from diapiric serpentinite seamments in the Izu-Ogazawara-Mariana forearc, Leg 125. In *Proceedings of the Ocean Drilling Program, Scientific Results vol. 125* (eds P. Fryer, J. A. Pearce, L. B. Stocking, et al.), pp.445–85. College Station, Texas.
- ISHIZUKA, O., KIMURA, J. I., LI, Y. B., STERN, R. J., REAGAN, M. K., TAYLOR, R. N., OHARA, Y., BLOOMER, S. H., ISHII, T., HARGROVE, U. S. & HARAGUCHI, S. 2006. Early stages in the evolution of Izu-Bonin arc volcanism: new age, chemical and isotopic constraints. *Earth and Planetary Science Letters* **250**, 385–401.
- JAMES, G. A. & WYND, J. G. 1965. Stratigraphic nomenclature of Iranian Oil Consortium agreement area. *Bulletin of American Association of Petroleum Geology* **49**, 2182–245.
- JOHNSON, K. T. M., DICK, H. J. B. & SHIMIZU, N. 1990. Melting in the oceanic upper mantle: an ion microprobe study of diopsides in abyssal peridotites. *Journal of Geophysical Research* **95**, 2661–78.
- KHALATBARI-JAFARI, M., JUTEAU, T., BELLON, H., WHITECHURCH, H., COTTEN, J. & EMAMI, H. 2004. New geological, geochronological and geochemical investigations on the Khoys ophiolites and related formations, NW Iran. *Journal of Asian Earth Sciences* **23**, 507–35.
- LANPHERE, M. A. & PAMIC, T. 1983.  $^{40}\text{Ar}/^{39}\text{Ar}$  ages and tectonic setting of ophiolites from Neyriz area, south-east Zagros range, Iran. *Tectonophysics* **96**, 245–56.
- LEAT, P. T., PEARCE, J. A., BARKER, P. F., MILLAR, I. L., BARRY, T. L. & LARTER, R. D. 2004. Magma genesis and mantle flow at a subducting slab edge: the South Sandwich arc-basin system. *Earth and Planetary Science Letters* **227**, 17–35.
- LE MÉE, L., GIRARDEAU, J. & MONNIER, C. 2004. Mantle segmentation along the Oman ophiolite fossil mid-ocean ridge. *Nature* **432**, 167–72.
- LETERRIER, J. 1985. Mineralogical, geochemical and isotopic evolution of two Miocene mafic intrusions from the Zagros (Iran). *Lithos* **18**, 311–29.
- MACKENZIE, G. D., MAGUIRE, P. K. H., COOGAN, L. A., KHAN, M. A., EATON, M. & PETRIDES, G. 2006. Geophysical constraints on the crustal architecture of the Troodos ophiolite: results from the IANGASS project. *Geophysical Journal International* **167**, 1385–401.
- MACPHERSON, C. G. & HALL, R. 2001. Tectonic setting of Eocene boninite magmatism in the Izu-Bonin-Mariana forearc. *Earth and Planetary Science Letters* **186**, 215–30.
- MCCLAY, K. R., WHITEHOUSE, P. S., DOOLEY, T. & RICHARDS, M. 2004. 3D evolution of fold and thrust belts formed by oblique convergence. *Marine and Petroleum Geology* **21**, 857–77.
- MCCLUSKY, S., BALASSANIAN, S., BARKA, A., DEMIR, C., ERGINTAV, S., GEORGIEV, I., GURKAN, O., HAMBURGER, M., HURST, K., KAHLE, H., KASTENS, K., KEKELIDZE, G., KING, R., KOTZEV, V., LENK, O., MAHMOUD, S., MISHAIN, A., HADARIYA, M., OUZOUNIS, A., PARADISSIS, D., PETER, Y., PRILEPIN, M., REILINGER, R., SANLI, I., SEEGET, H., TEALEB, A., TOKSÖZ, M. H. & VEIS, G. 2000. Global positioning system constraints on plate kinematics and dynamics in the eastern Mediterranean and Caucasus. *Journal of Geophysical Research* **105**, 5695–719.
- MCDONOUGH, W. F. & SUN, S. S. 1995. The composition of the Earth. *Chemical Geology* **120**, 223–53.
- MCQUARRIE, N., STOCK, J. M., VERDEL, C. & WERNICKE, B. P. 2003. Cenozoic evolution of Neotethys and implications for the causes of plate motions. *Geophysical Research Letters* **30**, 2036, doi:10.1029/2003GL017992, 4 pp.
- MICHAEL, P. J., ESCRIG, S., RUBIN, K. H., COOPER, L. B., LANGMUIR, C. H., CLAGUE, D. A., KELLER, N. S. & PLANK, T. 2009. Major and trace elements and volatiles in glasses from the 2009 rapid response expedition to West Mata Volcano and Northeast Lau Spreading Center (NELSC). American Geophysical Union, Fall Meeting 2009, abstract #V51D-1720.
- MIJALKOVIC, N., CVETIC, S. & DIMITRIJEVIC, M. D. 1972. *Geological Map of Balvard. 1/100000 Series, Sheet 7248*. Tehran: Geological Survey of Iran.
- MIYASHIRO, A. 1973. The Troodos ophiolitic complex was probably formed in an island arc. *Earth and Planetary Science Letters* **19**, 218–24.
- MIYASHIRO, A. 1974. Volcanic rock series in island arcs and active continental margins. *American Journal of Science* **274**, 321–55.
- MOHAJEL, M. & FERGUSON, C. L. 2000. Dextral transpression in Late Cretaceous continental collision, Sanandaj-Sirjan zone, western Iran. *Journal of Structural Geology* **22**, 1125–39.
- MOHAJEL, M., FERGUSON, C. L. & SAHANDI, M. R. 2003. Cretaceous-Tertiary convergence and continental collision, Sanandaj-Sirjan Zone, western Iran. *Journal of Asian Earth Sciences* **21**, 397–412.
- MOLINARO, M., GUEZOU, J. C., LETURMY, P., ESHRAGHI, S. A. & FRIZON DE LAMOTTE, D. 2004. The origin of changes in structural style across the Bandar Abbas syntaxis, SE Zagros (Iran). *Marine and Petroleum Geology* **21**, 735–52.
- MORITZ, R., GHAZBAN, F. & SINGER, B. S. 2006. Eocene gold ore formation at Muteh, Sanandaj-Sirjan Tectonic Zone, Western Iran: a result of Late-stage extension and exhumation of metamorphic basement rocks within the Zagros Orogen. *Economic Geology* **101**, 1–28.
- MUKASA, S. & LUDDEN, J. N. 1987. Uranium-lead isotopic ages of plagiogranites from the Troodos Ophiolite, Cyprus, and their tectonic significance. *Geology* **15**, 825–28.
- NEUMANN, E. -R. & SIMON, N. S. C. 2009. Ultra-refractory mantle xenoliths from ocean islands: how do they compare to peridotites retrieved from oceanic sub-arc mantle? *Lithos* **107**, 1–16.
- OHARA, Y. 2006. Mantle process beneath Philippine Sea back-arc spreading ridges: a synthesis of peridotite petrology and tectonics. *Island Arc* **15**, 119–29.
- OHARA, Y., STERN, R. J., ISHII, T., YURIMOTO, H. & YAMAZAKI, T. 2002. Peridotites from the Mariana Trough: first look at the mantle beneath an active back-arc basin. *Contributions to Mineralogy and Petrology* **143**, 1–18.

- PAMIĆ, J. & ADIB, D. 1982. High-grade amphibolites and granulites at the base of the Neyriz peridotites in southeastern Iran. *Neues Jahrbuch für Mineralogie* **143**, 113–21.
- PARKINSON, I. J. & PEARCE, J. A. 1998. Peridotites from the Izu-Bonin-Mariana Forearc (ODP Leg 125): evidence for mantle melting and melt-mantle interaction in a supra-subduction zone setting. *Journal of Petrology* **39**, 1577–618.
- PEARCE, J. A., BAKER, P. E., HARVEY, P. K. & LUFF, I. W. 1995. Geochemical evidence for subduction fluxes, mantle melting and fractional crystallization beneath the South Sandwich arc. *Journal of Petrology* **36**, 1073–109.
- PEARCE, J. A., BARKER, P. F., EDWARDS, S. J., PARKINSON, I. J. & LEAT, P. T. 2000. Geochemistry and tectonic significance of peridotites from the South Sandwich arc-basin system, South Atlantic. *Contributions to Mineralogy and Petrology* **139**, 36–53.
- PEARCE, J. A. & PARKINSON, I. J. 1993. Trace element models for mantle melting: application to volcanic arc petrogenesis. In *Magmatic Processes and Plate Tectonics* (eds H. M. Prichard, T. Alabaster, N. B. Harris & C. R. Neary), pp. 373–403. Geological Society of London, Special publication no. 76.
- PEARCE, J. A. & PEATE, D. W. 1995. Tectonic implications of the composition of volcanic arc magmas. *Annual Review of Earth and Planetary Sciences* **23**, 251–85.
- PEARCE, J. A. & ROBINSON, P. T. 2010. The Troodos ophiolitic complex probably formed in a subduction initiation, slab edge setting. *Gondwana Research* **18**, 60–81.
- PEARCE, J. A., VANDER LAAN, S. R., ARCULUS, R. J., MURTON, B. J., ISHII, T., PEATE, D. W. & PARKINSON, I. J. 1992. Boninite and harzburgite from Leg 125 (Bonin-Mariana forearc): a case study of magma genesis during the initial stages of subduction. In *Proceedings of the Ocean Drilling Program, scientific results vol. 125* (eds P. Fryer, J. A. Pearce, L. B. Stocking, *et al.*), pp. 623–59. College Station, Texas.
- PICCARDO, G. B., ZANETTI, A., SPAGNOLO, G. & POGGI, E. 2005. Recent researches on melt-rock interaction in the Lanzo South peridotites. *Ophioliti* **30**, 135–60.
- RACHIDNEJAD, N., EMAMI, M. H., SABZEHEI, M., RASTAD, E., BELLON, H. & PIQUÉ, A. 2002. Lithostratigraphie et histoire Paléozoïque de la région de Muteh, zone de Sanandaj–Sirjan (Iran méridional). *Comptes Rendus Geoscience* **334**, 1185–91.
- RAHMANI, F., NOGHREYAN, M. & KHALILI, M. 2007. Geochemistry of sheeted dikes in the Nain ophiolite (Central Iran). *Ophioliti* **32**, 119–29.
- RASTAD, E., MIRALIPOUR, A. M. & MOMENZADEH, M. 2002. Sheikh-Ali copper deposit: a Cyprus-type VMS deposit in southeast Iran. *Journal of Sciences, Islamic Republic of Iran* **13**, 51–63.
- REAGAN, M. K., ISHIZUKA, O., STERN, R. J., KELLEY, K. A., OHARA, Y., Blichert-Toft, J., Bloomer, S. H., Cash, J., Fryer, P., Hanan, B. B., Hickey-Vargas, R., Ishii, T., Kimura, J. I., Peate, D. W., Rowe, M. C. & Woods, M. 2010. Fore-arc basalts and subduction initiation in the Izu-Bonin-Mariana system. *Geochemistry, Geophysics, Geosystems* (*G<sup>3</sup>*) **11**, Q03X12, doi: 10.1029/2009GC002871, 17 pp.
- REILINGER, R., MCCLUSKY, S., VERNANT, P., LAWRENCE, S., ERGINTAV, S., CAKMAK, R., OZENER, H., KADIROV, F., GUILÉV, I., STEPANYAN, R., HADARIYA, M., HAHUBIA, G., MAHMOUD, S., SAKR, K., ARRAJEHI, A., PARADISSIS, D., AL-AYDRUS, A. PRILEPIN, M., GUSEVA, T., EVREN, E., DMITROSTA, A., FILIKOV, S. V., GOMEZ, F., AL-GHAZZI, R. & KARAM, G. 2006. GPS constraints on continental deformation in the Africa-Arabia-Eurasia continental collision zone and implications for the dynamics of plate interactions. *Journal of Geophysical Research* **111**, B05411, doi:10.1029/2005JB004051, 26 pp.
- RICOU, L. E. 1968. Une coupe à travers les séries à radiolarite des monts Pichakun (Zagros, Iran). *Société Géologique de France* **7**, 478–85.
- RICOU, L. E. 1971. Le croissant ophiolitique peri-Arabe une ceinture de nappes mise en place au Crétacé supérieur. *Review Géographie Physique Géologie Dynamique* **13**, 327–50.
- RICOU, L. E. 1976. Evolution structurale des Zagrides. La région clef de Neyriz (Zagros Iranien). *Mémoire Société Géologie de la France*, **125**, 140 pp, (Thèse Orsay, 1974).
- RICOU, L. E., BRAUD, J. & BRUNN, J. H. 1977. Le Zagros. *Mémoire Société Géologie de la France* **8**, 33–52.
- ROBERTSON, A. H. F. 1998. Mesozoic-Tertiary tectonic evolution of the easternmost Mediterranean area: integration of marine and land evidence. In *Proceedings of the Ocean Drilling Program, vol. 160* (eds A. H. F. Robertson, K. C. Emeis, C. Richetr & A. Camerlenghi), pp. 723–82. College Station, Texas.
- ROBERTSON, A. H. F. 2000. Mesozoic-Tertiary tectonic-sedimentary evolution of a south Tethyan oceanic basin and its margins in southern Turkey. In *Tectonics and Magmatism in Turkey and the Surrounding Area* (eds E. Bozkurt, J. A. Winchester & J. D. A. Piper), pp. 97–138. Geological Society of London, Special Publication no. 173.
- ROBERTSON, A. H. F. 2002. Overview of the genesis and emplacement of Mesozoic ophiolites in the Eastern Mediterranean Tethyan region. *Lithos* **65**, 10–67.
- ROBERTSON, A. H. F. 2007. Overview of tectonic settings related to the rifting and opening of Mesozoic ocean basins in the Eastern Tethys: Oman, Himalayas and Eastern Mediterranean regions. In *Imaging, Mapping and Modeling Continental Lithosphere Extension and Breakup* (eds G. D. Karner, G. Manatschal & L. M. Pinheiro), pp. 325–88. Geological Society of London, Special Publication no. 282.
- ROBERTSON, A. H. F. & MOUNTRAKIS, D. 2006. Tectonic development of the Eastern Mediterranean region: an introduction. In *Tectonic Development of the Eastern Mediterranean Region* (ed. A. H. F. Robertson), pp. 1–9. Geological Society of London, Special Publication no. 260.
- ROBIN, C., GORICAN, S., GUILLOCHEAU, F., RAZIN, P., DROMART, G. & MOSAFFA, H. 2010. Mesozoic deep-water carbonate deposits from the southern Tethyan passive margin in Iran (Pichakun nappes, Neyriz area): biostratigraphy, facies sedimentology and sequence stratigraphy. In: *Tectonic and Stratigraphic Evolution of Zagros and Makran During the Mesozoic–Cenozoic* (eds P. Leturmy & C. Robin), pp. 179–210. Geological Society of London, Special Publication no. 330.
- SABZEHEI, M. 1996. *Geological Map of Neyriz. 1/100000 Series, Sheet 6848*. Tehran: Geological Survey of Iran.
- SABZEHEI, M. 1997. *Geological Map of Dehshir. 1/100000 Series, Sheet 6752*. Tehran: Geological Survey of Iran.
- SELLA, G. F., DIXON, T. H. & MAO, A. 2002. REVEL: a model for recent plate velocities from space geodesy. *Journal of Geophysical Research* **107**, B4, 2081, doi: 10.1029/2000B000033.
- SENGOR, A. M. C. 1990. A new model for the late Palaeozoic–Mesozoic tectonic evolution of Iran and

- implications for Oman. In *The Geology and Tectonics of the Oman Region* (eds A. H. F. Robertson, M. P. Searle & A. C. Ries), pp. 797–831. Geological Society of London, Special Publication no. 49.
- SHAHABPOUR, J. 2007. Island-arc affinity of the Central Iranian Volcanic Belt. *Journal of Asian Earth Sciences* **30**, 652–65.
- SHAFARI MOGHADAM, H., STERN, R. J. & RAHGOSHAY, M. 2010. The Dehshir ophiolite (Central Iran): geochemical constraints on the origin and evolution of the Inner Zagros Ophiolitic Belt. *Geological Society of America Bulletin* **122**, 1516–47.
- SHAFARI MOGHADAM, H., WHITECHURCH, H., RAHGOSHAY, M. & MONSEF, I. 2009. Significance of Nain-Baft ophiolitic belt (Iran): short-lived, transtensional Cretaceous back-arc oceanic basins over the Tethyan subduction zone. *Comptes Rendus Geosciences* **341**, 1016–28.
- SHEIKHOLESLAMI, M. R., PIQUE, A., MOBAYEN, P., SABZEHEI, M., BELLON, H. & EMAMI, M. H. 2008. Tectono-metamorphic evolution of the Neyriz metamorphic complex, Quri-Kor-e-Sefid area (Sanandaj-Sirjan Zone, SW Iran). *Journal of Asian Earth Sciences* **31**, 504–21.
- SHERVAIS, J. W. 1982. Ti-V plots and the petrogenesis of modern ophiolitic lavas. *Earth and Planetary Science Letters* **59**, 101–18.
- SHERVAIS, J. W. 2001. Birth, death, and reconstruction: the life cycle of suprasubduction zone ophiolites. *Geochemistry, Geophysics, Geosystems (G<sup>3</sup>)* **2**, 1010, doi:10.1029/2000GC000080, 45 pp.
- SRDIC, A., DIMITRIJEVIC, M. N., CVETIC, S. & DIMITRIJEVIC, M. D. 1972. *Geological Map of Baft. 1/100000 Series, Sheet 7348* Tehran: Geological Survey of Iran
- STAMPFLI, G. M. & BOREL, G. D. 2002. A plate tectonic model for the Paleozoic and Mesozoic constrained by dynamic plate boundaries and restored synthetic oceanic isochrons. *Earth and Planetary Science Letters* **196**, 17–33.
- STAMPFLI, G. M., MOSAR, J., FAVRE, P., PILLEVUIT, A. & VANNAY, J.-C. 2001. Permo-Mesozoic evolution of the western Tethyan realm: the Neotethys/East-Mediterranean connection. In *Peri-Tethys Memoir 6: Peri-Tethyan rift/wrench basins and passive margins, IGCP 369* (eds P. A. Ziegler, W. Cavazza, A. H. F. Robertson & S. Crasquin-Soleau). *Mémoires du Muséum National D'Histoire Naturelle* **186**, 51–108.
- STERN, R. J. 2004. Subduction initiation: spontaneous and induced. *Earth and Planetary Science Letters* **226**, 275–92.
- STERN, R. J. 2010. The anatomy and ontogeny of modern intra-oceanic arc systems. In *The Evolving Continents: Understanding Processes of Continental Growth* (eds T. M. Kusky, M. G. Zhai & W. Xiao), pp. 7–34. Geological Society of London, Special Publication no. 338.
- STERN, R. J. & BLOOMER, S. H. 1992. Subduction zone infancy; examples from the Eocene Izu-Bonin-Mariana and Jurassic California arcs. *Geological Society of America Bulletin* **104**, 1621–36.
- STERN, R. J. & SCHOLL, D. 2010. Yin and yang of continental crust creation and destruction by plate tectonics. *International Geology Review* **52**, 1–31.
- STOCKLIN, J. 1968. Structural history and tectonics of Iran: a review. *American Association of Petroleum Geologist Bulletin* **52**, 1229–58.
- STOCKLIN, J. 1977. Structural correlation of the Alpine range between Iran and Central Asia. *Mémoire Hors-Serie, Société Géologique de France* **8**, 333–53.
- STOCKLIN, J., EFTEKHAR-NEZHAD, J. & HUSHMANDZADEH, A. 1972. *Central Lut Reconnaissance, East Iran*. Geological Survey of Iran, report No.22.
- SUN, S. S. & MCDONOUGH, W. F. 1989. Chemical and isotopic systematics of oceanic basalts: implications for mantle composition and processes. In *Magmatism in Ocean Basins* (eds A. D. Saunders & M. J. Norry), pp. 313–45. Geological Society of London, Special Publication no. 42.
- TAMURA, A. & ARAI, S. 2005. Unmixed spinel in chromitite from the Iwanai-dake peridotite complex, Hokkaido, Japan: a reaction between peridotite and highly oxidized magma in the mantle wedge. *American Mineralogist* **90**, 473–80.
- TAMURA, A. & ARAI, S. 2006. Harzburgite–dunite–orthopyroxenite suite as a record of supra-subduction zone setting for the Oman ophiolite mantle. *Lithos* **90**, 43–56.
- TAYLOR, R. N., LAPIERRE, H., VIDAL, P., NESBITT, R. W. & CROUDACE, I. W. 1992. Igneous geochemistry and petrogenesis of the Izu-Bonin forearc basin. In *Proceedings of the Ocean Drilling Program, vol. 126* (eds B. Taylor, K. Fujika, et al.), pp. 405–30. College Station, Texas.
- THY, P. & XENOPHONTOS, C. 1991. Crystallization orders and phase chemistry of glassy lavas from the pillow sequences, Troodos ophiolite, Cyprus. *Journal of Petrology* **32**, 4030–428.
- VERNANT, P. & CHERY, J. 2006. Mechanical modeling of oblique convergence in the Zagros, Iran. *Geophysical Journal International* **165**, 991–1002.
- VERNANT, P., NILFOROUSHAN, F., HATZFELD, D., ABBASSI, M., VIGNY, C., MASSON, F., NANKALI, H., MARTINOD, J., ASHTIANI, A., BAYER, R., TAVAKOLI, F. & CHERY, J. 2004. Contemporary crustal deformation and plate kinematics in Middle East constrained by GPS measurement in Iran and northern Oman. *Geophysical Journal International* **157**, 381–98.
- WHATTAM, S. A. & STERN, R. J. 2009. The “Ophiolite Rule”, chemostratigraphy of Tethyan-type ophiolites, and subduction initiation, AGU Fall meeting abstract #T21 A-1783.
- WORKMAN, R. & HART, S. R. 2005. Major and trace element composition of the depleted MORB mantle (DMM). *Earth and Planetary Science Letters*, **231**, 53–72.
- WROBEL-DAVEAU, J.-C., RINGENBACH, J.C., TAVAKOLI, S., RUIZ, G.M.H., MASSE, P., & FRIZON DE LAMOTTE, F. 2010. Evidence for mantle exhumation along the Arabian margin in the Zagros (Kermanshah area, Iran). *Arabian Journal of Geoscience* **3**, 499–513.
- YILMAZ, Y., TUYSUZ, O., YIGITBAS, E., GENÇ, S. C. & SENGOR, A. M. C. 1997. Geology and tectonic evolution of the Pontides. In *Regional and Petroleum Geology of the Black Sea and Surrounding Region* (ed. A. G. Robinson), American Association of Petroleum Geologists Memoir **68**, 183–226.